

**REGULATION OF IMMUNE TOLERANCE AND ALLERGIC
PREDISPOSITION
BY THE INTESTINAL MICROBIOME**

Luisa Alexandra Kreft

Vollständiger Abdruck der von der Fakultät für Medizin
der Technischen Universität München zur Erlangung des akademischen Grades
einer Doktorin der Naturwissenschaften (Dr. rer. nat.)
genehmigten Dissertation.

Vorsitz: Prof. Dr. Carsten Schmidt-Weber

Prüfende der Dissertation:

1. Priv.-Doz. Dr. Caspar Ohnmacht
2. Hon.-Prof. Dr. Michael Schloter

Die Dissertation wurde am 15.12.2022 bei der Technischen Universität München
eingereicht und durch die Fakultät für Medizin am 21.03.2023 angenommen.

**...to kill an error is as good a service as, and sometimes even better than,
the establishing of a new truth or fact.**

Charles Darwin

More Letters of Charles Darwin, Volume II by Charles Darwin, Francis Darwin (ed.)
Letter 752, Darwin to Wilson, March 5, 1879 (p. 292)
a public domain book (online version)
first published at
D. Appleton & Company. New York, New York, USA, 1903

ACKNOWLEDGMENTS

Caspar Ohnmacht

Thank you for the opportunity and your trust to develop my own research ideas in your lab which have culminated in this thesis. Thank you for your supervision and guidance and always having an open door. Your deep scientific expertise has greatly helped me throughout this doctoral journey.

Michael Schloter, Tilo Biedermann

Thank you for your advice and evaluations and being an active part in my thesis committee.

Anna-Lena Geiselhöringer

Thank you for being such a supportive colleague and friend and for the helpful scientific and non-scientific discussions.

To the further current and past members of the Ohnmacht Lab

Maria Szente-Pasztoi, Daphne Kolland, Amelie Köhler, Anela Arifovic,

Ann-Marie Maier, Renske de Jong, Maria Potthast, Wenjing Chen, Karsten Huth

Thank you for all your experi-/mental support, expertise and scientific discussions that I greatly benefitted from. I could not have done some experiments without your assistance.

To the further current and past members of the IAF/ZAUM

Carsten Schmidt-Weber, Simon Blank, Francesca Alessandrini, the Esser-von Bieren Lab,

Sonja Heine, Michael Dittmar, Maximilian Schiener, Dennis Russkamp,

Benjamin Schnautz, Johanna Grosch

Thank you for your expertise, input and assistance.

To my collaborators

Miriam Hils, Aloys Schepers, Andrew Flatley, Regina Feederle, Christiane Hilger, Kyra Swiontek, Neera

Chakrapani, Robert Janowski, Dierk Niessing, Konrad Fischer, Mohammadali Khan Mirzaei, Li Deng,

Marijana Basic, Silvia Bolsega, Anna Smoczek, Saib Hussain, Bärbel Stecher-Letsch,

Chen Meng, Karin Kleigrew, Benedikt Bächler

Thank you all for your (experimental) input and expertise. Thank you for providing me with material and methods that were vital for this thesis.

To my family

Christine, Michael and Theresa Kreft, Mathilde Vilgertshofer

Thank you for all your support throughout my whole education and believing in me.

Brendan Voss

Thank you for your academic and non-academic advice, endless support and uplifting mood.

Lastly, I would like to express my appreciation towards Helmut Böker who sparked my interest in biomedical sciences in school. Further, I would like to express my deepest gratitude to Julia Neugebauer and Carola Vinuesa for being such important role models. Your positive evaluations of my previous work has helped me gain the confidence to fight through the difficult times.

PUBLICATIONS STATEMENT

Journal articles

Parts of the presented work have been published in the following original research article:

A novel monoclonal IgG1 antibody specific for Galactose-alpha-1,3-galactose questions alpha-Gal epitope expression by bacteria

Kreft L, Schepers A, Hils M, Swiontek K, Flatley A, Janowski R, Mirzaei M. K, Dittmar M, Chakrapani N, Desai M, Eyerich S, Deng L, Niessing D, Fischer K, Feederle R, Blank S, Schmidt-Weber C, Hilger C, Biedermann T, Ohnmacht C

Frontiers in Immunology. (2022); 13:958952. doi: 10.3389/fimmu.2022.958952

Reference [1]

Parts of this thesis have been published in the following review article:

Therapeutic Potential of the Intestinal Microbiota for Immunomodulation of Food Allergies

Kreft L, Hoffmann C, Ohnmacht C

Frontiers in Immunology. (2020); 11:1853. doi:10.3389/fimmu.2020.01853

Reference [2]

Conferences

Partial results of the conducted studies have been presented at the following international conferences:

Revealing a microbial impact on intestinal immune tolerance by using gnotobiotic mice

Kreft L, Meng C, Bächler B, Kleigrewe K, Basic M, Stecher B, Bleich A, Ohnmacht C

12th Seeon Conference "Microbiota, Probiotics and Host", Seeon, Germany, June 2019

(selected for oral presentation)

Use of gnotobiotic mouse models to reveal a microbial impact on intestinal immune tolerance

Kreft L, Meng C, Bächler B, Kleigrewe K, Basic M, Stecher B, Bleich A, Ohnmacht C

II Joint Meeting of the German Society for Immunology (DGfI) and the Italian Society of Immunology, Clinical Immunology and Allergology (SIICA), Munich, Germany, September 2019

(poster presentation)

ABSTRACT

The increased prevalence of allergic diseases has been attributed to changed lifestyle factors affecting intestinal microbiota composition. Intestinal bacteria have a profound impact on human physiology by nutrient provision and maturation of the immune system. Microbial metabolites are able to induce peripherally induced regulatory T cells (pTregs) capable of counteracting T helper 2 cell (Th2) driven diseases such as food allergies. These pTregs characterized by ROR γ t expression are diminished in germ-free mice and induced by bacterial colonization. To assess whether different complexities of microbiotas impact pTregs to a variable extent, gnotobiotic mice were used in this study to identify pTreg frequencies in the intestine. Mice exhibiting lower microbial complexities colonized with strains from the Altered Schaedler flora and Oligo-Mouse-Microbiota 12 showed significantly lower frequencies of pTregs in the lamina propria of the small intestine than conventional specific pathogen free mice. The observed inverse correlation of pTregs with Th2 cells hinted towards a greater susceptibility of gnotobiotic mice for food allergies. Untargeted and targeted metabolomic analysis for the identification of pTreg inducing molecules revealed bile acid metabolism to be correlated with a changed microbial status. Both primary and secondary bile acids were diminished in gnotobiotic groups. Ratio changes in conventional dendritic cells (cDC1s vs cDC2s) suggested an involvement of antigen presenting cells for pTreg induction. Gnotobiotic animals were tested in a food allergy model to identify whether they displayed an increased susceptibility for sensitization against chicken ovalbumin compared to specific pathogen-free mice. An enhanced susceptibility could not be seen. Microbial metabolites and structures can lead to a humoral response responsible for the generation of antibodies against certain foreign molecules. One molecule that has been hypothesized to be expressed by bacteria is the α -Gal epitope with the structure: Galactose- α 1,3-Galactose- β 1,4-N-acetylglucosamine. Humans display α -Gal-binding serum IgGs of unknown source, but can become sensitized against this molecule *via* tick bites developing α -Gal-specific IgE antibodies that may be fatal upon ingestion of α -Gal-rich foods or treatment with α -Gal-containing medicines. Detection of α -Gal has been mostly limited to a low-affine IgM antibody and lectins that exhibit considerable cross-reactivity. This study describes the development of a novel α -Gal specific IgG antibody (27H8) displaying high affinity and showing wide applicability in ELISA, histology, and flow cytometry. This tool was then used to decipher α -Gal expression by intestinal bacteria. While cross-reactive lectin bound to intestinal bacteria and isolates, the 27H8 monoclonal antibody did not. Bacterial expression of the α -Gal epitope should therefore be questioned and highlights that a related epitope could lead to cross-reactive human IgG antibodies. Further studies will be needed to identify other possible sources of the α -Gal epitope in the human intestine.

ZUSAMMENFASSUNG

Die steigende Prävalenz allergischer Erkrankungen wird auf veränderte Lebensgewohnheiten zurückgeführt, die das intestinale Mikrobiom beeinflussen. Intestinale Bakterien haben einen wesentlichen Einfluss auf die menschliche Physiologie, unter anderem in der Toleranzentstehung des Immunsystems. Mikrobielle Metabolite induzieren peripher induzierbare regulatorische T-Zellen (pTregs), die T-Helferzellen des Typs 2 (TH2) inhibieren können. TH2 spielen eine zentrale Rolle in Lebensmittelallergien. pTregs, die anhand ihrer ROR γ t-Expression charakterisiert werden, sind in keimfreien Mäusen vermindert vorhanden und können durch bakterielle Kolonialisierung in ihrer Frequenz vermehrt werden. Zur Modulation des Mikrobioms wurden in dieser Arbeit gnotobiotische Tiere verwendet. Dies erlaubt unterschiedliche mikrobielle Komplexitäten mit der relativen Häufigkeit von pTregs in Zusammenhang zu bringen. Mäuse, die mit einer geringeren Anzahl an Bakterienstämmen besiedelt wurden als spezifisch pathogenfrei gehaltene Mäuse (Besiedelung mit Stämmen der ‚Altered-Schaedler-Flora‘ oder ‚Oligo-Mouse-Microbiota 12‘), zeigten eine signifikant niedrigere Frequenz an pTregs in der Lamina Propria des Dünndarms. Die beobachtete inverse Korrelation von pTregs und TH2 deutete auf eine erhöhte Suszeptibilität von gnotobiotischen Mäusen für die Sensibilisierung mit Lebensmittelallergenen hin. Die Analyse des Metaboloms zeichnete einen Zusammenhang der mikrobiellen Besiedelung mit Metaboliten des Gallensäurenstoffwechsels auf. Die Konzentration von primären und sekundären Gallensäuren waren in den gnotobiotischen Gruppen im Intestinum (Ileum) verringert. Beobachtete Unterschiede in dendritischen Zellpopulationen könnten mit der Induktion von pTregs zusammenhängen. Gnotobiotische Mäuse wurden auf eine erhöhte Suszeptibilität für die Sensibilisierung mit dem Allergen Ovalbumin in einem Lebensmittelallergiemodel getestet. Diese konnte jedoch nicht festgestellt werden.

Mikrobielle Metabolite und Strukturen können zu einer humoralen Immunantwort führen. Ein Molekül, das vermutlich von Bakterien exprimiert wird, ist das α -Gal-Epitop (Galaktose- α 1,3-Galaktose- β 1,4-N-acetylglucosamin). Menschen weisen anti- α -Gal-spezifische IgG-Antikörper im Serum auf, können jedoch gegen α -Gal durch Zeckenstiche sensibilisiert werden (anti- α -Gal-IgE). Bakterien werden als Induktionsquelle für anti- α -Gal-IgG vermutet. Anti- α -Gal-IgE kann zu schweren allergischen Reaktionen führen, wenn α -Gal-haltige Lebensmittel oder Medikamente eingenommen bzw. verabreicht werden. Diese Arbeit beschreibt die Entwicklung eines neuen α -Gal-spezifischen IgG-Antikörpers (27H8), der eine hohe Affinität besitzt und in verschiedenen Assay-Formen Anwendung finden kann (ELISA, Histologie, Durchflusszytometrie). Durch die Verwendung des 27H8 Antikörpers konnte gezeigt werden, dass intestinale Bakterien das α -Gal-Epitop nicht exprimieren. Weitere Studien sollten andere α -Gal-Epitop-Quellen als Bakterien in Betracht ziehen.

TABLE OF CONTENTS

ACKNOWLEDGMENTS	3
PUBLICATIONS STATEMENT	5
ABSTRACT	6
ZUSAMMENFASSUNG	7
TABLE OF CONTENTS	8
LIST OF FIGURES	12
LIST OF TABLES	13
ABBREVIATIONS	14
1 INTRODUCTION	17
1.1 Basic concepts in immunology	17
1.2 The humoral immune response	18
1.3 The cell-mediated immune response	19
1.3.1 T helper cells	20
1.3.2 Dendritic cells	20
1.3.3 Innate lymphoid cells	21
1.4 The regulators of the immune system	21
1.5 The microbiota and its impact on host physiology and pTregs	22
1.6 The rise of atopic diseases in the industrialized world	23
1.6.1 Classification of hypersensitivity reactions	23
1.6.2 Hallmarks of type I or IgE-mediated allergic diseases	24
1.7 Nature of IgE-inducing allergens	24
1.8 Food allergies	25
1.8.1 Linking (food-)allergies, microbiota and (p)Tregs	25
1.8.2 Red meat allergy	27
1.9 Aim of the study	28
1.9.1 Identifying a microbial impact for immune tolerance by using gnotobiotic mice	28
1.9.2 Development of a monoclonal IgG antibody specific for the α -Gal epitope to investigate the microbial impact of tolerance induction in red meat allergy	29
2 MATERIAL AND METHODS	30
2.1 Material	30
2.1.1 Instruments	30
2.1.2 Expendable materials	30
2.1.3 Preparation of common buffers and solutions	31
2.1.4 Antibodies and staining reagents for flow cytometric analysis	32
2.1.5 Human samples	33

2.1.6	Mouse lines	33
2.1.6.1	<i>Ggta1</i> KO animals	33
2.1.6.2	Wildtype animals	33
2.1.6.2.1	SPF housing	34
2.1.6.2.2	Gnotobiotic animals colonized with ASF	34
2.1.6.2.3	Gnotobiotic animals colonized with Oligo-MM ¹²	34
2.1.6.2.4	GF animals	35
2.1.7	Pig samples	35
2.1.8	Screening material for monoclonal antibody development against α -Gal	35
2.1.8.1	Purchased and purified material	35
2.1.8.2	Tissue and cell lysates	36
2.1.8.3	Bacterial strains and lysates	36
2.1.9	Websites and software	37
2.2	Methods	38
2.2.1	General mouse protocols	38
2.2.1.1	Maintenance	38
2.2.1.2	Organ withdrawal	38
2.2.2	Food allergy model	38
2.2.3	Cell preparations from mouse organs	39
2.2.3.1	Isolation of lamina propria small intestinal immune cells and from colon	39
2.2.3.1.1	Spatial distribution of T cells and ILCs along the intestine and from food allergic mice and isolation of intestinal immune cells for assessment of DCs	39
2.2.3.1.2	Isolation of immune cells from the intestine from whole small intestine for steady state frequencies of T cells and ILCs	40
2.2.3.2	Isolation of splenocytes	40
2.2.3.3	Preparation of single cell suspension from mesenteric lymph nodes	40
2.2.4	Monoclonal antibody development against α -Gal via hybridoma technology	41
2.2.4.1	Immunization of <i>Ggta1</i> KO mice and screening of hybridoma supernatants	41
2.2.4.2	Purification of the monoclonal antibody	41
2.2.5	Immunoassays	41
2.2.5.1	Immunostaining for flow cytometric analysis of isolated cells from murine organs 41	
2.2.5.2	Dot blot screening of monoclonal antibodies against α -Gal	42
2.2.5.3	Immunohistochemistry for detection of α -Gal in tissue slides	43
2.2.5.4	Flow cytometry with 27H8 antibody	44
2.2.5.4.1	Eukaryotic flow cytometry for 27H8 monoclonal antibody screening	44
2.2.5.4.2	Bacterial flow cytometry for 27H8 monoclonal antibody screening	44

2.2.5.5	Surface Plasmon Resonance (SPR) analysis	45
2.2.5.6	Enzyme-linked Immunosorbent Assay (ELISA)	46
2.2.5.6.1	27H8 and M86 titration on glycoproteins	46
2.2.5.6.2	Epitope blocking experiments with 27H8 and M86 monoclonal antibodies	46
2.2.5.6.3	Human serum immunoglobulin against α -Gal.....	47
2.2.5.6.4	Murine Mast cell protease-1 (mMCPT-1) ELISA.....	47
2.2.5.6.5	OVA-specific IgE ELISA	47
2.2.6	Biochemical assays	47
2.2.6.1	Enzymatic digestion and cleavage of the α -Gal epitope.....	47
2.2.6.2	Periodic acid treatment of blotted samples in dot blot.....	48
2.2.6.3	Biotinylation of 27H8 antibody	48
2.2.7	Metabolomics analysis of ileum content	49
2.2.7.1	Untargeted metabolomics	49
2.2.7.2	Targeted metabolomics	50
2.2.8	Statistical analysis	51
3	RESULTS	52
3.1	Microbial impact on immune tolerance using gnotobiotic mice	52
3.1.1	Preamble.....	52
3.1.2	Gnotobiotic animals display changed frequencies in T cell populations compared to SPF mice particularly in the small intestine	52
3.1.3	Gnotobiotic animals display an increase in cDC2s in mLNs and SI.....	56
3.1.4	Spatial distribution of pTregs reveals highest frequency in colon and representative frequency in ileum SI segment.....	59
3.1.5	Metabolomic analysis of ileum content samples reveal changes in bile acid metabolism comparing mouse groups of differential microbial complexity	62
3.1.6	Reduced microbial complexity, reduced pTregs numbers and enhanced Th2 in steady state does not correlate with enhanced food allergy sensitization	67
3.1.7	Summary.....	69
3.2	Development of a novel monoclonal antibody specific for Galactose- α 1,3-Galactose questions alpha-Gal epitope expression by bacteria.....	71
3.2.1	Preamble.....	71
3.2.2	Generation and screening of an α -Gal epitope-specific IgG antibody with wide applicability.....	71
3.2.2.1	The novel 27H8 monoclonal antibody specifically binds to Gal- α 1,3-Gal	71
3.2.2.2	27H8 monoclonal antibody detects α -Gal epitopes of natural origin and offers a wide range of possible applications	74
3.2.3	Monoclonal anti- α -Gal antibody 27H8 is superior to other α -Gal binding moieties binding with high affinity	77
3.2.4	Application of 27H8 antibody questions α -Gal expression by bacteria.....	80

3.2.4.1	<i>Staphylococcus aureus</i> does not express the α -Gal epitope.....	80
3.2.4.2	27H8 and M86 antibodies do not bind to <i>E. coli</i> O86:B7 nor to other members of the intestinal microbiota.....	83
3.2.5	Summary.....	84
4	DISCUSSION	86
4.1	Use of gnotobiotic animals to reveal an impact of the intestinal microbiome on immune tolerance	86
4.1.1	Immune cell changes correlating with microbial complexity	86
4.1.2	Untargeted and targeted metabolomics reveal increased primary and secondary bile acids in SPF compared to gnotobiotic animals.....	89
4.1.3	Food allergy model	92
4.1.4	Future directions of microbiota and host relationship	94
4.2	A novel IgG antibody for Gal- α 1,3-Gal detection questioning α -Gal epitope expression by bacteria.....	95
4.2.1	Development of an α -Gal specific IgG antibody	96
4.2.2	Do bacteria express the α -Gal epitope?	97
4.2.3	Future prospects of 27H8 antibody and implications of the α -Gal epitope	98
4.3	Concluding remarks	99
5	APPENDIX	100
6	REFERENCES	114

LIST OF FIGURES

Figure 1: Schematic structure of an IgG antibody.....	18
Figure 2: The impact of a reduced complexity of the intestinal microbiota on intestinal tolerance and food allergy sensitization.....	29
Figure 3: Sample generation for untargeted and targeted metabolomics.....	49
Figure 4: Decrease in ROR γ t ⁺ Helios ⁻ Tregs and increase in Th2 cells correlates with decreased microbial complexity.....	55
Figure 5: Increase in cDC2s in mLNs and SI correlates with reduced microbial complexity.....	58
Figure 6: Spatial distribution of ROR γ t ⁺ Helios ⁻ Tregs, Th2 and ILCs along the intestine.....	61
Figure 7: Untargeted and targeted metabolomic analysis of ileum content samples of gnotobiotic and SPF mouse groups.....	67
Figure 8: Oral sensitization of GF, ASF ⁷ , Oligo-MM ¹² and SPF mice in a model of food allergy.....	69
Figure 9: Generation, screening and biotinylation of a monoclonal IgG antibody recognizing galactose- α 1,3-galactose.....	74
Figure 10: Specificity of 27H8 monoclonal antibody.....	76
Figure 11: High affinity recognition of synthetic α -Gal epitopes.....	80
Figure 12: <i>Staphylococcus aureus</i> strains bind 27H8 independent of α -Gal expression.....	82
Figure 13: No binding of 27H8 and M86 to intestinal bacteria in contrast to BSI-B4.....	84
Figure 14: Graphical summary of results presented in chapter 3.1.....	95
Figure 15: Gating strategy for T cell and ILC panel.....	100
Figure 16: Gating strategy for DC subpopulations in SI and colon.....	101
Figure 17: Gating strategy for DC subpopulations in mLNs.....	102
Figure 18: Targeted metabolomics measurement of ileum content.....	112
Figure 19. Uncropped blots appearing in results chapter 3.2.....	112
Figure 20: Representative gating for live cells and bacteria.....	113

LIST OF TABLES

Table 1: Abbreviation list (alphabetical).....	14
Table 2: List of instruments.....	30
Table 3: List of expendables.....	30
Table 4: Common buffers.....	31
Table 5: Staining reagents used for flow cytometric analysis.....	32
Table 6: Websites and software.....	37
Table 7: Feature table untargeted metabolomics in ddH ₂ O negative mode correlating with RORyt+ Helios- Treg percentages	103
Table 8: Feature table untargeted metabolomics in ddH ₂ O positive mode correlating with RORyt+ Helios- Treg percentages	104
Table 9: Feature table untargeted metabolomics in methanol (MetOH) negative mode correlating with RORyt+ Helios- Treg percentages.....	105
Table 10: Feature table untargeted metabolomics in MetOH positive mode correlating with RORyt+ Helios- Treg percentages	106
Table 11: Feature table untargeted metabolomics in MetOH positive mode correlating with Th2 percentages	108

ABBREVIATIONS

Table 1: Abbreviation list (alphabetical)

Abbreviation	Term
%	Percentage or frequency
(c)DC	(Conventional) dendritic cell
~	Approximately
ΔT_{\max}	Maximum temperature difference
μ	Micro
12-DHCA	12-dehydrocholic acid
12-KLCA	5 β -cholic acid-3 α -ol-12-one / 12-ketolithocholic acid
3-DHCA	3-dehydrocholic acid
6,7-KLCA	5 β -cholic acid-3 α -ol-6,7-dione / 6,7-Diketolithocholic acid
7,12-DKLCA	5 β -cholic acid-3 α -ol-7,12-dione
7AAD	7-Amino-Actinomycin D
7-KLCA	5 β -cholic acid-3 α -ol-7-one / 7-ketolithocholic acid
7-SCA	Cholic acid-7-sulphate / 7-sulfocholic acid
ACA	Allocholic acid
AD	Atopic dermatitis
AF	Alexa Fluor
ALCA	Allolithocholic acid
AP	Alkaline phosphatase
APC (cell type)	Antigen-presenting cell
APC (fluorochrome)	Allophycocyanin
ApCA	5 β -cholen-24-oic acid-3,12-diol / apocholic acid
APN	Aminopeptidase N
ASF ^{3/7}	Altered Schaedler flora containing 3 or 7 different bacterial species
BA	Bile acid
BLG	β -lactoglobulin
BSA	Bovine serum albumin
BSI-B ₄	<i>Bandeiraea simplicifolia</i> isolectin B4
BV786	Brilliant Violet 786
CA	Cholic acid
Ca-7ol-3one	β -Cholic acid-7 α -ol-3-one
CD	Cluster of differentiation
CDCA	Chenodeoxycholic acid
CF-LAS	Core Facility Laboratory Animal Services
CFU	Colony forming unit
cm	Centimeter
CT	Choleratoxin
ctrl	Control
DB / HMDB	Database / Human Metabolome Database
DCA	Deoxycholic acid
DHLCA	Dehydrolithocholic acid

Dig	Digested
EDTA	Ethylenediaminetetraacetic acid
EGCase I	Endoglycoceramidase I
ELISA	Enzyme-linked Immunosorbent Assay
FCS	Fetal calf serum
FITC	Fluorescein isothiocyanate
FXR	Farnesoid X receptor
g	Gram
GCA	Glycocholic acid
GCDCA	Glycochenodeoxycholic acid
GDCA	Glycodeoxycholic acid
GF	Germ-free
Ggta1	α -galactosyltransferase
GHCA	Glycohyocholic acid
GHDCA	Glycohyodeoxycholic acid
GLCA	Glycolithocholic acid
GUDCA	Glycoursodeoxycholic acid
h	hour
H+L	Heavy and light chain (of an antibody)
HDCA	Hyodeoxycholic acid
HEK cells	Human embryonic kidney
HEPES	4-(2-hydroxyethyl)-1-piperazineethanesulfonic acid
HRP	Horseradish peroxidase
i.g.	Intragastral
i.p.	Intraperitoneal
i.v.	Intravenous
IDCA	Isodeoxycholic acid
Ig	Immunoglobulin
ILC	Innate lymphoid cell
ILCA	Isolithocholic acid
K _D	Dissociation constant
KO	Knockout
l	Liter
LCA	Lithocholic acid
LCenA	Lithocholenic acid
LC-MS/MS	liquid chromatography with tandem mass spectrometry
m	Milli
M	Molar
max	Maximum
MDCA	Murideoxycholic acid
MHC	Major histocompatibility complex
min	Minutes
ml	Milliliter
mLNs	Mesenteric lymph nodes
mMCPT-1	Murine mast cell protease 1
MSA	Mouse serum albumin
n	Nano

ns	Not significant
o.n.	overnight
OCA	Obeticholic acid
Oligo-MM ¹²	Oligo-Mouse-Microbiota 12
OVA	Ovalbumin / chicken albumin
PAMP	Pathogen associated molecular patterns
PB	Pacific Blue
PBS	Phosphate buffered saline
PE	Phycoerythrin
PerCP-Cy5.5	Peridinin chlorophyll protein-Cyanine 5.5
Perm Buffer	Permeabilization Buffer
PFA	Paraformaldehyde
pTreg	Peripherally induced regulatory T cell
ROR γ t	RAR-related orphan receptor gamma t
rpm	Revolutions per minute
RPMI	Roswell Park Memorial Institute
RT	Room temperature
s.c.	Subcutaneously
SAv	Streptavidin
SCFAs	Short-chain fatty acids
SDS	Sodium dodecyl sulfate
SPF	Specific pathogen-free
TBS	Tris buffered saline
TCA	Taurocholic acid
TCDCA	Taurochenodeoxycholic acid
TCR	T cell receptor
TDCA	Taurodeoxycholic acid
Th	T helper cell
THDCA	Taurohyodeoxycholic acid
TLCA	Taurolithocholic acid
TMB	3,3', 5,5"-tetramethylbenzidine
tTreg	Thymic derived regulatory T cell
TUDCA	Tauroursodeoxycholic acid
T- α -MCA	Tauro- α -muricholic acid
T- ω -MCA	Tauro- ω -muricholic acid
U	Units
UCA	Ursocholic acid
UDCA	Ursodeoxycholic acid
w/o	Without
WT	Wildtype
x	Multiplied by
xg	Relative centrifugal force
α -Gal-DI	Gal- α 1,3-Gal
α -Gal-TRI	Gal- α 1,3-Gal- β 1,4-GlcNAc
α -MCA	α -muricholic acid
β -MCA	β -muricholic acid
γ -MCA	γ -muricholic acid / hyocholic acid
ω -MCA	ω -muricholic acid

1 INTRODUCTION

1.1 Basic concepts in immunology

The immune system is a highly specialized system protecting the body from external harm, such as pathogenic bacteria, viruses or parasites and has developed mechanisms to detect internal harm such as cancerous cells. Its players and mechanisms can be classified into innate and adaptive immunity. Innate immunity is responsible for a very fast inflammatory response and host defense without long lasting memory formation, and the recognition of invaders is performed through detection of patterns rather than individual pathogens. Danger associated molecular patterns (DAMPs) or pathogen associated molecular patterns (PAMPs) are recognized by pattern-recognition receptors (PRRs) such as Toll-like receptors, nucleotide-binding oligomerization domain (NOD)-, leucine-rich repeat-containing receptors (NLRs), Retinoic acid-inducible gene I (RIG-I)-like receptors (RLRs), C-type lectin receptors (CLRs) and intracellular sensors of nucleic acids, such as AIM-2 like receptors (ALRs), oligoadenylate synthase (OAS) proteins and cyclic GMP-AMP synthase (cGAS) [3–5]. PAMP structures are highly variable and embody broad pathogen specificities, such as double stranded RNA, flagellin, CpG oligonucleotides, glycolipids and many more. White blood cells or leucocytes are central for the immune defense and can be characterized as rather innate or adaptive e.g. based on the absence or presence of specific antigen-recognition receptors allowing adaption and memory formation. The first line of defense regarding external threats are epithelial or mucosal tissues that prevent intrusion in the first place. If this line of defense is breached, tissues become inflamed and release chemokines to attract immune cells. Furthermore, structures of pathogens are transported by dendritic cells to secondary lymphoid organs for the initiation of the adaptive immune response mediating a coherent antigen specific counterattack to the pathogen. Lymphocytes, specifically T helper cells, enter these secondary lymphoid organs (lymph nodes, spleen, mucosa-associated lymphoid tissue) via lymphatic vessels, bind to antigens presented on major histocompatibility complex (MHC) II molecules by dendritic cells, mature and exit via the blood stream. The innate immune system hereby serves as an inducer of adaptive immunity since it recognizes the general type of intruder. However, not only pathogens can be seen as a threat for the immune system. Harmless substances or structures that are recognized as foreign and are not tolerized can act as immunogens. These can be allergens, but also transplanted tissues that result in an unwanted reaction of host immune system. Cellular structures such as HLA-antigens differ between individuals which pose a significant challenge in transplantation of tissues from one person to another (allograft transplantation). In xenotransplantation efforts, the immunogenicity of pig transplants suitable for transplantation is higher than human allografts due to

the phylogenetic distance of the species, but could help meet the high demand for organ transplants [6]. To solve xenograft rejection, knockout (KO) pigs have been generated to remove the most immunogenic molecules, such as the α -Gal epitope [7]. In first trials, kidneys of multiple KO pigs have been transplanted into two brain-dead humans [8] and a heart from these pigs was transplanted in January 2022 into a 57-year-old man with nonischemic cardiomyopathy [9]. While the transplants did not survive long term due organ failure (the transplanted heart e.g. was edematous and showed myocyte necrosis in histological analysis [9]), both procedures did not result in immediate rejection and can be seen as a step forward towards feasibility of xenotransplantation. The immune system can be further segregated into the humoral and cell-mediated immune response, both containing elements of the innate and adaptive immune system.

1.2 The humoral immune response

Next to the exertion of macromolecules such as complement factors or anti-microbial peptides, an integral part of the humoral immune response is the generation of antibodies, also known as immunoglobulins (Ig). These Y-shaped glycoproteins are either integral in the cell membrane of B-cells as part of the B-cell receptor or can be excreted from B-cell derived plasma cells. The basic structure of an antibody consists of two light

and two heavy chains connected via disulfide bridges (see Figure 1: Schematic structure of an IgG antibody). The variable domains are the antigen binding sites (also called paratopes) and each antibody sub-unit consists of two identical binding sites recognizing their respective epitopes. Light chains can be either κ or λ . An immunoglobulin can be cleaved into Fab and Fc domains by the enzyme papain. The crystallizable fragment region (Fc) is a binding region of Fc-receptors expressed on a number of immune cells, including macrophages, monocytes, granulocytes, NK

and B cells. Antigen binding to such Fc-bound antibodies can lead to signal transduction in the Fc-receptor expressing cell, antibody-dependent cell-mediated cytotoxicity by NK cells [10] or engulfment and killing of an antibody covered pathogen in phagocytes [11]. Fc-receptors are

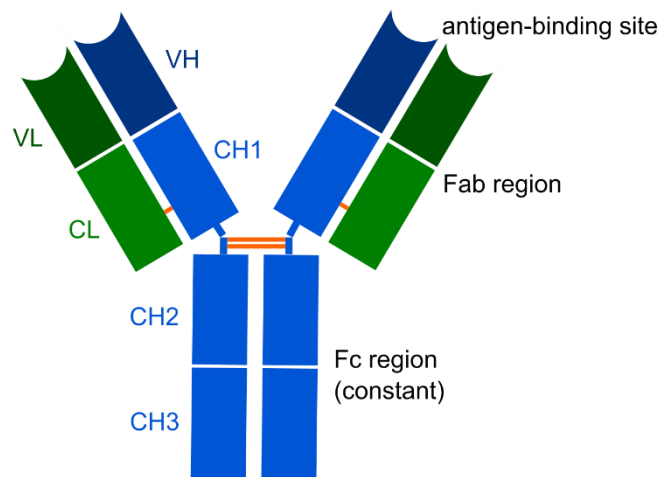


Figure 1: Schematic structure of an IgG antibody

An IgG antibody consists two heavy (H, blue) and two light chains (L, green) which form the variable antigen-binding domains (V) and the constant regions (C). H and L chains are connected via disulfide bonds (orange).

classified according to the immunoglobulin type they bind to and can also be inhibitory: FcγRIIB restricts immune responses by negatively regulating B cells, DCs and granulocytes [12]. Based on their heavy chain conformation, antibodies can be divided into different isotypes, such as IgG (γ, monomer), IgA (α, dimer), IgM (μ, pentamer), IgD (δ, monomer) and IgE (ε, monomer) with distinct biological properties. While IgM antibodies are produced rather early in the course of an infection and show lower affinity, the affinity of an antibody can be increased after class switch through somatic hypermutation. Purified and engineered antibodies are useful research tools in immunological detection methods: a specific molecule or structure can be visualized via enzymes or fluorophores coupled to a specific antibody. Monoclonality, which means an antibody is derived from one single clone is advantageous over a polyclonal antibody consisting of a pool of antibodies derived from different clones. Polyclonality enhances the risk of cross-reactivity to other epitopes due to multiple paratopes. Antibodies can also be used therapeutically for disease treatment, i.e. in cancer therapeutics as so called therapeutical monoclonal antibodies to enhance immune detection of cancerous cells either in a cancer-cell specific mode or as check-point inhibitors by generally enhancing the immune response towards cancerous cells.

1.3 The cell-mediated immune response

The cell-mediated immune response involves a plethora of immune cells interacting with each other and the tissue milieu through direct receptor binding or via soluble factors, such as cytokines, chemokines and other regulators such as lipid mediators. Immune cells derive from precursors in the bone marrow and lymphocytes mature in the bone marrow (B cells) or thymus (T cells) also referred to as primary lymphoid organs. The important players in antigen sampling, detection and presentation on major histocompatibility complex (MHC) molecules are professional antigen-presenting cells (APCs). The best-studied APCs involve B cells, dendritic cells (DCs) and macrophages. While B cells are also important for the humoral immune response, DCs represent the most professional antigen-presenting cell population. Monocytes are released into the blood stream from myeloid precursors in the bone marrow and can give rise to macrophage subsets and to some DC subsets [13]. Macrophages are very heterogeneous depending on the local tissue milieu [14]. They are important for the ingestion and destruction of microbes and inflammation, but are also implicated in tissue repair and integrity by removing dead cells and debris [14]. Granulocytes are primarily innate immune cells releasing a vast amount of pre-formed mediators, enzymes and signaling molecules in response to microbial and parasite infections. They can be divided into basophils, neutrophils, eosinophils and mast cells. Neutrophils are early responders in an acute inflammation after bacterial infection and are implicated in the immune response against helminths and are

important for debris clearing (phagocytosis), inflammation and neutrophil extracellular traps (NETs) formation, while eosinophils and basophils are important for parasite killing. T cells are an important cell type of the adaptive immune response that provide essential signals for other immune cells, but also act via direct killing of infected cells. CD8+ cytotoxic T cells are responsible for anti-viral immune defense, while CD4+ T helper cells coordinate a variety of anti-pathogenic immune defenses, tissue restoration and immune maintenance. The immune cells particularly discussed in the results section of this thesis are introduced in more detail below.

1.3.1 T helper cells

T helper cells (Ths) are characterized by CD4 co-receptor expression and bind to antigens presented on MHCII molecules by APCs via their individual T cell receptor (TCR). They provide B cell help for antibody production, provide help to CD8+ T cells and regulate macrophages. They orchestrate a variety of other immune responses, but also regulate immunity to suppress autoimmunity [15] and allergies. Upon TCR stimulation, together with additional cofactor and most importantly cytokine stimulation, naïve T cells can differentiate into different effector lineages that can be categorized by the specific transcription factors they express, the cytokines they release and their immune function. Th1 cells (Tbet+) produce IFN γ as their signature cytokine, Th2 cells (GATA3+) produce IL-4, IL-5 and IL-13, and Th17 cells (ROR γ t+) are characterized by the production of IL-17A, IL17F and IL-22 [15]. Recently, further Th cells were described, such as Th9 or Th22 cells [16]. Another CD4+ T cell population derived from naïve T cells are peripherally induced T regs (pTregs). T follicular helper cells (Tfh, characterized by expression of the transcription factor Bcl6) provide B cell help in germinal centers of secondary lymphoid organs. Other CD4+ T cell types that do not derive from naïve T cells in the periphery are thymus-derived T regs (tTregs) and NKT cells [15]. The differentiation into a distinct Th lineage in some cases counteracts the development of other Th types and therefore the immune response is driven into one direction for a specific orchestrated immune response against one type of pathogen. Th2 cytokines such as IL-4 for example suppresses Th1 development by upregulating GATA3 inhibiting a Th1 phenotype and IFN- γ production [17, 18]. Th1 cells are generally involved in antiviral defense, Th2 cells have been implicated in antiparasitic defense, but also play a distinct role in allergy development, Th17 cells defend against microbial infection such as extracellular bacteria and mucosal fungi, but also promote inflammatory diseases.

1.3.2 Dendritic cells

DCs display a heterogeneous cell population that can be divided into conventional dendritic cells (cDCs), plasmacytoid dendritic cells (pDCs) and monocyte-derived DCs [19]. Tissue DCs sample

antigens and migrate from the tissue to the lymph nodes for antigen presentation to T cells. CDCs prime naïve T cells and promote their differentiation [20] and are thus integrators of environmental signals for T cell priming [21], bridging the innate and adaptive immune response. CDCs express high levels of CD11c and MHCII and lack the expression of macrophage-associated markers CD64 and F4/80 and can be further subdivided into cDC1s (initiators of Th1 responses) and cDC2s (drive and maintain Th2, Th17 and Treg responses) [19]. In the gut, gut associated lymphoid tissue (GALT) such as gut-draining lymph nodes (mesenteric lymph nodes (mLNs)) are principal locations for adaptive immune cell priming [19]. In the mouse and human intestine, three main subsets of cDCs have been defined: CD103+CD11b- cDC1s, CD103+CD11b+ cDC2s, and CD103-CD11b+ cDC2s [19]. In the mLNs, the major antigen-presenting site draining the intestine, both migratory (MHC-II^{hi}, mature) and resident cDCs (MHCII+, immature) can be found [19].

1.3.3 Innate lymphoid cells

Innate lymphoid cells (ILCs) comprise cytotoxic natural killer (NK) cells, lymphoid tissue inducer (LTi) cells, but also very recently discovered non-cytotoxic ILC populations [22]. They are characterized by a classical lymphoid cell morphology, but lack antigen-specific receptors and do not express cell-surface molecules that identify other immune cells and are thus cell lineage marker-negative (LIN-) cells [22]. Like T helper cells they can be segregated into different subtypes based on the production of their cytokines: ILC1s (IFN γ producers, e.g. NK cell), ILC2s (produce Th2 cell-associated cytokines; GATA3+) and ILC3s (produce IL17A, IL-22; ROR γ t+) [23]. ILC2s are important for host resistance against nematodes, wound repair, but have also been implicated in allergic asthma exacerbation [23].

1.4 The regulators of the immune system

In order to dampen and prevent overshooting inflammation, the immune system developed negative regulators suppressing immune responses. Regulatory T cells (Tregs) are a subpopulation of CD4+ T cells that are responsible for controlling self-reactive T cells, tolerance induction, wound healing and tissue homeostasis in particular of barrier surfaces [24]. Regulatory T cells are identified via their transcription factor Foxp3 [25]. Another regulatory Th cell subset called Tr1 cells, characterized by expression of Interleukin-10 (IL-10) and transforming growth factor-beta (TGF- β) is independent from Foxp3 expression [26]. Tregs come in many flavors, and can upregulate certain transcription factors known from conventional Ths, such as GATA3+ tissue Tregs [27]. Among Foxp3 expressing Tregs, Foxp3 expression can be either already upregulated in the thymus in which T cells are educated and checked for self-recognition as thymic derived Tregs (tTregs or natural Tregs) or Foxp3 is

upregulated in the periphery after stimulation of naïve CD4⁺ T cells [28]. These latter Tregs are called peripherally induced Tregs (pTregs or iTregs). In the intestine, microbial colonization is able to induce the differentiation of pTregs [29]. Preventing pTreg differentiation by knocking out the CNS1 (conserved non-coding sequence 1) region next to the Foxp3 promoter revealed that these immune cells prevent a spontaneous type 2 immune bias at mucosal sites [30]. Dietary antigens from solid foods are also tolerized by inducing a population of short-lived pTregs in the small intestine where uptake of nutrients including food allergens most likely takes place [31]. Intestinal Tregs are distinct from Tregs in other organs, as their T cell receptors (TCRs) are partially specific for intestinal antigens and thereby play a distinct role for suppression of immune responses against harmless dietary antigens and commensal microorganisms [32]. Microbiota-induced pTregs share features with intestinal Th17 cells, such as the expression of the transcription factor RAR-related orphan receptor gamma t (ROR γ t) and have an enhanced suppressive function compared to Foxp3⁺ ROR γ t⁻ Tregs [33, 34]. ROR γ t seems to also play an essential role in maintaining Foxp3 expression by suppressing other transcription factors such as T-bet [35]. The transcription factor Helios can be used to distinguish tTregs from pTregs [36] as it is specifically expressed in tTregs. Peripherally induced Tregs can thus be distinguished by lack of Helios expression. The induction of ROR γ t⁺ Tregs for dietary antigens has been found to be mediated by cDCs [37]. Lyu *et al.*, however, found that ROR γ t⁺ ILC3s in the intestine-draining lymph nodes are necessary for microbiota-specific ROR γ t⁺ Treg selection while preventing the development of inflammatory Th17 cells [38]. Kedmi *et al.* also report that ROR γ t⁺ APCs which are not cDCs (they suggest Janus cells, ILC3s or a new cell type) and express CCD7, MHCII and $\alpha\beta$ 8 integrins are important for microbiota-specific pTreg induction [39]. Another study implied that a subgroup of Thetis cells (TC IV) expressing ROR γ t is crucial for pTreg differentiation in early life with dispensable functions of ILC3s and DCs [40]. Important for this induction is the expression of MHCII on Thetis cells in the intestine [40]. This reflects that the induction of pTregs by APCs might be differentially regulated in early and adult life and various cell types are implicated in the induction or development of pTregs specific for different antigens.

1.5 The microbiota and its impact on host physiology and pTregs

Next to the pathogenicity of certain microbes, microbial colonization also has beneficial functions in human physiology. The collection of microorganisms living as commensals within and on a host, is commonly referred to as the microbiota. Microbiota-host relationships have profound effects on the availability of nutrients and metabolism, but are also vital for immune homeostasis [41]. The intestinal microbiota has profound effects on regulatory T cell populations in the intestine. Mice that are housed under germ-free conditions, lack colonic ROR γ t⁺ Tregs which can be re-induced via

recolonization [33]. Certain microbial metabolites, such as short chain acids (SCFAs) [42, 43] and cell surface polysaccharides from *Bifidobacterium bifidum* [44] have been shown to induce pTregs. Secondary bile acids (BAs) are also inducers of pTregs and result in Foxp3 upregulation either directly or indirectly via DCs [45–47]. Isodeoxycholic acid producing bacteria induce colonic ROR γ t⁺ Tregs *in vivo*, which was not seen when transplanting bacteria unable to produce this secondary BA [47]. Furthermore, different bacterial species induce pTregs to a variable extent independent of their phylum [34]. In recent years it was hypothesized that the Western lifestyle has a profound effect on the microbiota, making individuals more susceptible for atopic diseases but whether this observation can be linked to reduced pTreg induction remains to be investigated.

1.6 The rise of atopic diseases in the industrialized world

Allergic diseases have been increasing in the past half-century which include allergic rhinitis, asthma, atopic dermatitis and food allergies [48]. Factors for this incline include the impact of air pollution on asthma and climate change being responsible for an increased duration and intensity of pollen seasons [49]. Further factors that may influence allergic susceptibility by changing the intestinal microbiota include antibiotic use, high-fat diet, elimination of enteric pathogens and reduced exposure to infection (hygiene hypothesis), Cesarean birth and formula feeding [50]. The skin and mucosal tissues are vital for tissue homeostasis by protecting from infections, environmental toxins, pollutants and allergens [51]. A disrupted epithelial barrier (skin, gut) allowing intrusion of these substances and pathogens may also be the result of industrialization, urbanization and modern life [51].

1.6.1 Classification of hypersensitivity reactions

Hypersensitivity reactions were classified according to their physiopathologic mechanisms by Gell and Coombs in 1963 into four different categories, however they have since been extended to contain the following categories [52]: Firstly, type I or immediate hypersensitivity reactions which are further characterized below. Secondly, type II hypersensitivity reactions, which comprise self-antigen recognition via IgG or IgM antibodies leading to cytolytic destruction of targeted cells. This either happens through complement activating antigen-antibody complexes, antibody-dependent cell-mediated cytotoxicity mediated by NK cells and macrophages or initiating phagocytosis by binding Fc receptors (type IIa) and autoantibodies directly stimulating target cells resulting for example in chronic urticaria (type IIb). In type III responses, immune complexes are formed by antigen and IgG/IgM antibodies leading to organ damage at complex deposition sites and resulting in glomerulonephritis and arthritis. Type IV hypersensitivities are delayed reactions involving T cells as

the major mediators. They are classified according to the effector cells, whereby either Th1 cell-mediated macrophage activation (IVa, allergic contact dermatitis), Th2 cell-mediated eosinophilic inflammation (IVb, chronic asthma), cytotoxic T cell-mediated reactions (IVc, allergic contact dermatitis (with IVa), graft rejections) or T cell-mediated neutrophilic inflammation (IVd, e.g. acute generalized exanthematous pustulosis) takes place [52].

1.6.2 Hallmarks of type I or IgE-mediated allergic diseases

The classical allergies to food, medications and insect stings follow the characteristic of type I or immediate hypersensitivity reactions [52]. Reactions can occur locally, e.g. sneezing in hay fever or systemically if the antigen is taken up orally or intravenously. Anaphylaxis is a potential life-threatening systemic type I allergic response. Type I hypersensitivity reactions are mediated by allergen-specific IgE molecules, mostly bound to high-affinity FcεR1. High-affinity FcεR1 can be found on mast cells and basophils in the 'classical' tetrameric form or in a trimeric form on human monocytes, blood DCs and Langerhans cells of the skin [53]. A prerequisite for allergen sensitization is the class-switch of the B cell to produce allergen-specific IgE. Tfh13 cells have been found to help B cells produce allergen-reactive high-affinity IgE inducing anaphylaxis [54]. These allergen-specific IgE molecules can lead to an allergic response upon re-exposure to the allergen by IgE cross-linking bound to FcεR1 and results in immediate histamine, protease (tryptase and chymase), lysosomal enzyme and lipid mediator release immediately after mast cell degranulation [52]. More generally, a type 2 immune response is characterized by Th2 cells and involves further cellular and cytokines such as eosinophils, mast cells, basophils, ILC2s, IL-4 and/or IL-13 exposed macrophages (termed alternatively as activated macrophages, AAM), IgE and the cytokines IL-5, IL-9 and IL-13 [55]. Despite the pathogenic role of dysregulated type 2 immune responses, type 2 immunity also promotes antihelminth immunity via facilitated parasite expulsion, suppresses type 1-driven autoimmune disease, neutralizes toxins, maintains metabolic homeostasis and regulates wound repair and tissue regeneration [55, 56]. Allergen-specific IgE molecules are furthermore used as diagnostic marker by clinicians in allergic patients to determine sensitization patterns [57].

1.7 Nature of IgE-inducing allergens

Traditionally, mostly protein antigens have been described for triggering type I hypersensitivity reactions to pollen, venom or food. However, also carbohydrates including glycolipids have been shown to be involved in sensitization and elicitation of hypersensitivity reactions [58]. In particular, IgE cross-reactive to carbohydrate determinants (CCDs) linked via asparagine present on plants and insect venoms have been identified [59]. These CCDs may pose problems in allergy diagnosis for

correct allergen identification. About 20% of allergic patients display anti-glycan IgE, but CCDs do not appear to cause clinical symptoms in most patients [60].

1.8 Food allergies

The most common food allergies can be classified as type I allergic reactions, whereby after ingestion of food allergens an immediate allergic response occurs. This can result in swelling, urticaria but also life-threatening anaphylactic shock. Treatment options are sparse and mostly include strict avoidance of the allergen. The most common food allergies comprise reactions to milk, eggs, peanuts, tree nuts, soy, wheat, fish and shellfish [61]. Exact numbers of people affected by food allergies are difficult to pinpoint as the rates differ vastly between populations of different geographic areas [62]. However, the overall prevalence in children is estimated to reach 3.9-8% in Western societies [63–65]. The prevalence of food allergies is not only increasing in Western societies but also in developing countries and correlates with economic growth and adoption of Westernized lifestyle in these countries [66]. Different theories try to explain the rising prevalence of food allergies correlating with this changed lifestyle. The hygiene hypothesis is based on the negative effect of a reduced exposure to microbes [67]. The balanced microbiota and microbial stimulation hypotheses sees antibiotic use and dietary changes as a cause for commensal microbial community perturbations [68, 69]. The biodiversity hypothesis implies that changed environmental, diet and lifestyle factors lead to reduced complexity of the intestinal microbiota [70]. Furthermore, explanations for the decrease or lack of tolerance to dietary antigens include the dual-allergen hypothesis whereby low-dose cutaneous exposures predispose for allergic sensitization in contrast to the preventive effect of high dose food protein intake at an early age [71]. The barrier regulation hypothesis implies that allergy-protective bacterial populations important for tissue homeostasis in the intestinal mucosa have been depleted which eventually leads to reduced epithelial barrier integrity [61, 72] and increased allergen take-up and inflammation. Further factors disturbing mucosal intestinal barriers could be environmental toxins and particularities of the diet, i.e. low consumption of fibers [73].

1.8.1 Linking (food-)allergies, microbiota and (p)Tregs

Evidence from large human cohort studies has shown that a more traditional farming environment is beneficial for preventing the development of atopic diseases and these environments have been linked with a more diverse microbial environment [74–77]. Evidence from mice housed under germ-free conditions or treated with broad-spectrum antibiotics gave the first direct hints that the microbiota is essential to maintain a balanced (and thus a non-type 2 immunity prone) immune system. Such mice typically show elevated serum Immunoglobulin E (IgE) levels while all other

immunoglobulins are downregulated [78–80]. The microbiota maintains IgE at basal levels which requires microbial exposure during early life [81]. In the absence of microbial colonization during this time window, Th2-skewed follicular helper T cells (Tfh) may develop that support class-switching to IgE in B cells which is directed against food antigens [82]. In patients and mice with food allergy it has been found that IgE is specific for both bacteria and food antigens [83]. Antibiotic treatment in mice can also result in exaggerated basophil-mediated Th2 cell responses and allergic inflammation, indicating that the microbiota directly restrains the size of circulating basophil populations by limiting the proliferation of bone marrow resident precursor populations [78]. Recolonization of germ-free mice with specific bacterial strains (such as *Clostridia* mixtures) leads to decreased allergen-specific IgE and reduced susceptibility to anaphylactic reactions in a model of peanut allergy [83]. Recolonization with *Clostridia* in this model also reduced the uptake of the allergen by affecting the intestinal barrier permeability. Furthermore, transplantation of gut microbiota samples from children with food allergy into germ-free animals led to more severe anaphylactic reactions when such xenotransplanted mice were challenged with the allergen in a food allergy model [83, 84]. Since the induction of ROR γ t⁺ Tregs can be mediated by a diverse range of bacterial metabolites (see 1.5 The microbiota and its impact on host physiology and peripheral Tregs) and bacterial species [85] and the lack of ROR γ t⁺ Tregs leads to exacerbated Th2 and Th17 pathology in the intestine [86, 87], ROR γ t⁺ Tregs could be crucial in preventing food allergic type 2 immune responses. Indeed, ROR γ t⁺ Tregs have been shown to have a protective role in a model of food allergy, and the expression of ROR γ t is indispensable for this function [83]. This study relied on a murine model of enhanced signaling via the interleukin 4 receptor (IL-4R), which is based on a point mutation within the intracellular domain of the IL-4R that has also been found in a subset of patients with food allergy [88]. Transplantation of fecal samples from IL-4R mutated mice subjected to food allergy can confer the enhanced Th2 skewing and allergic reactions to wildtype animals suggesting that excessive IL-4R signaling also has a strong impact on the microbiota [89]. Bacterial therapy of these food allergic mice with *Clostridiales*, suppressed disease and induced ROR γ t⁺ Tregs in a MyD88-dependent way [83], further supporting the importance of this cell type in the counteraction of food allergy. In these IL-4R-mice intestinal Tregs start to (over-) express the transcription factor Gata3 and secrete the cytokine IL-4, making this Treg population rather a pathogenic driver of food allergy than an immune regulator [90]. Such type 2 prone Tregs are less stable but most likely their differentiation is independent from microbiota effects, as Gata3⁺ Tregs can be found in germ-free animals and Gata3 and ROR γ t expression are usually mutually exclusive [33, 91]. In other contexts, Gata3 expression in Tregs has been proposed as a general hallmark of Tregs residing within different tissues [27]. Altogether, the discovery of different Tregs subsets with unique functions offers a cellular and

molecular link to how microbial compositions may modulate the risk for allergic inflammation.

1.8.2 Red meat allergy

One particular food allergy whereby the intestinal microbiota is believed to play a major role is the allergy against mammalian (red) meat. This allergy is based on the formation of IgE molecules against the carbohydrate epitope α -Gal. The determining structure of the epitope is the disaccharide galactose- α 1,3-galactose (Gal- α 1,3-Gal), which naturally occurs as the trisaccharide galactose- α 1,3-galactose- β 1,4-N-acetylglucosamine (Gal- α 1,3-Gal- β 1,4-GlcNAc) on glycosylated proteins or lipids [92]. The immunogenic property of the α -Gal epitope in humans is based on the loss of the enzyme α -1,3-galactosyltransferase (GGTA1) in Catarrhines, including apes and humans, which catalyzes the reaction of Gal- β 1,4-GlcNAc-R + UDP-Gal to Gal- α 1,3-Gal- β 1,4-GlcNAc-R + UDP [93]. Humans therefore do not express the α -Gal epitope in contrast to most other mammals. This absence eventually allows for the sensitization of humans and a subsequent development of the so-called ' α -Gal syndrome' or red meat allergy that is based on the formation of IgE molecules against α -Gal mostly via tick bites [58, 94, 95]. These IgE molecules may lead to allergic reactions including fatal anaphylaxis following ingestion of red meat or related products which are major sources of allergen in α -Gal-induced meat allergy [96–99]. The allergic reaction is characterized by a delayed onset typically occurring 2 to 6 hours after ingestion, attributed to the oral ingestion and digestion of α -Gal rich glycolipids or glycoproteins and depends on further cofactors such as alcohol, physical exercise or drugs [100]. Moreover, sensitization to α -Gal can also result in severe allergic reactions in cancer patients who receive Cetuximab, a chimeric human-murine monoclonal antibody that contains α -Gal on the Fab fragment resulting in a rapid allergic reaction onset within minutes [101]. Interestingly, antibodies of different isotypes against the α -Gal epitope are quite abundant in humans with IgG levels estimated to range between 1% [102] to 0.1 % of total plasma IgG with high variability between subjects and lowest abundance in individuals carrying the blood type B antigen [103]. The latter observation is likely due to the structural similarity between the α -Gal epitope and blood type B antigen, which contains an additional fucose molecule on the second last galactose molecule [92]. The microbiota is believed to play a major role in tolerance induction and anti- α -Gal-IgG formation, since intestinal bacteria are recognized by anti- α -Gal binding molecules, such as purified polyclonal human anti- α -Gal antibodies [104, 105] or Isolectin B4 from *Bandeiraea simplicifolia* (BSI-B₄) [106–108].

1.9 Aim of the study

In this thesis the impact of the intestinal microbiota on immune tolerance and sensitization in particular in regard to food allergies, such as meat allergy, will be studied. The thesis can be divided into two sub-aims.

1.9.1 Identifying a microbial impact for immune tolerance by using gnotobiotic mice

Since pTregs seem to be central in establishing tolerance to microbial antigens, this cell type will be of central importance to investigate the impact of microbial complexity on immune tolerance induction towards dietary antigens. The reduction in microbial load (germ-free mice, antibiotics treated mice) has shown to lead to an increased susceptibility to food allergen sensitization [86]. The aim of this study was to use more physiological models of reduced microbial complexities to study the impact of dysbiosis of the intestinal microbiota on pTreg regulation and food allergen sensitization using reductionist and well-established bacterial consortiums.

The overview of the aim is displayed in Figure 2 and includes:

- use of gnotobiotic mouse models with reduced microbial complexities (Oligo-Mouse Microbiota 12 (Oligo-MM¹²), Altered Schaedler Flora (ASF) or germ-free (GF)) to study the effect of minimal microbial colonization on intestinal tolerance in particular on intestinal T cell populations, such as pTregs and Th2 cell distributions
- the investigation of intestinal immune cell differences in these models regarding DC and ILC populations
- the elaboration of spatial distributions of T cell populations along the intestine to study the effect of the local microbial milieu on local cell distributions
- the identification of molecules that could be implied in pTreg and/or Th2 cells induction or reduction
- lastly, the investigation of whether a reduced microbial complexity could prone for enhanced sensitization to food allergy in a food allergy model against chicken ovalbumin (OVA)

The results of this project are presented in the Results Chapter 3.1.

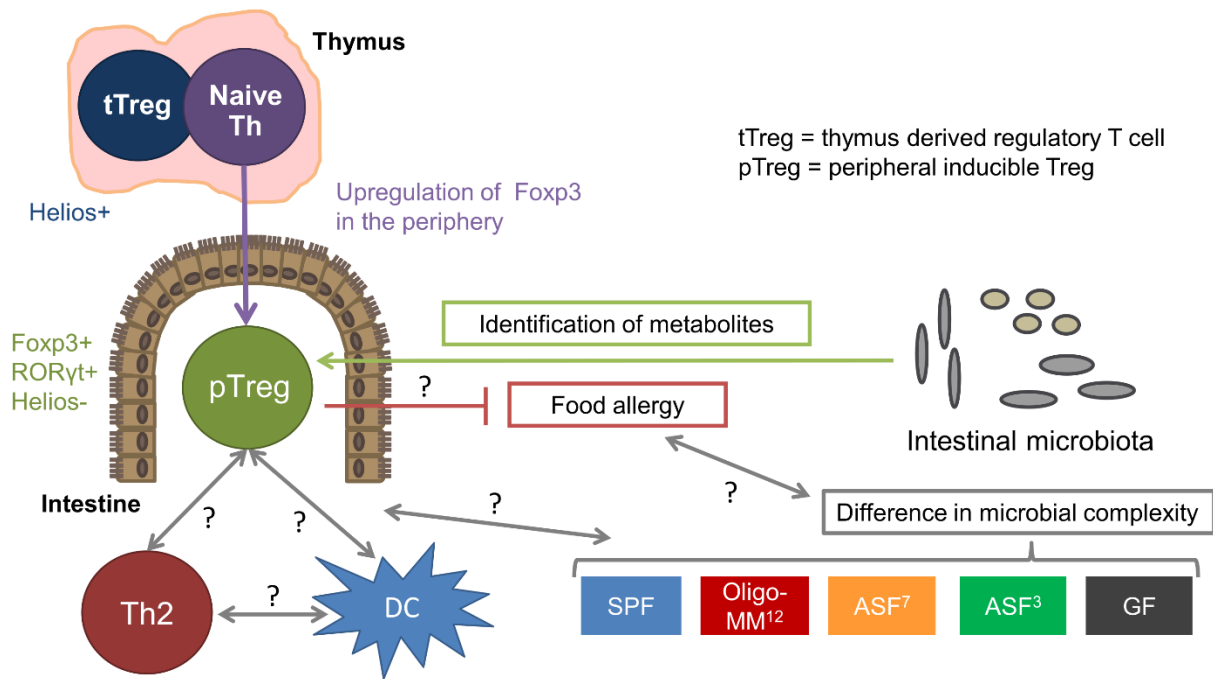


Figure 2: The impact of a reduced complexity of the intestinal microbiota on intestinal tolerance and food allergy sensitization

Gnotobiotic mouse models in comparison to SPF mice are used to investigate the impact of reduced microbial complexity on intestinal immune cell populations. Furthermore, metabolites that could be implicated in pTreg induction and possible immune cell changes should be identified. Lastly, the impact of a reduced microbial complexity on the sensitization of food allergy is examined. Further abbreviations: SPF, specific pathogen-free; ASF^{3/7}, ASF with 3 or 7 strains.

1.9.2 Development of a monoclonal IgG antibody specific for the α -Gal epitope to investigate the microbial impact of tolerance induction in red meat allergy

This sub-project aims to develop a novel IgG antibody against the carbohydrate epitope α -Gal, the glycoallergen implicated in red meat allergy. With this novel tool, the objective is to assess whether bacteria could potentially play a role in tolerance induction via expression of α -Gal that could explain differences in response of meat allergic subjects. First, a novel IgG monoclonal antibody should be established and rigorously screened for specificity. Second, advantages over current α -Gal binding moieties should be elaborated. Last, the potential antibody should be applied to verify α -Gal expression by bacteria as antigenic stimulation for anti- α -Gal antibody induction in humans was accredited to the intestinal microbiome [104]. The results of this project are presented in the Results Chapter 3.2.

2 MATERIAL AND METHODS

Elements of the material and methods section have been published elsewhere [1].

2.1 Material

2.1.1 Instruments

Table 2: List of instruments

Instrument	Manufacturer
ÄKTA	GE (Boston, MA, USA)
Analytic scales	Mettler (Columbus, OH, USA), Scaltec
Autoclave	H+P
Centrifuges	Eppendorf (Hamburg, Germany)
Dissecting tools	Fine Science Tools
Flow cytometer BD Accuri™ C6	BD (Franklin Lakes, NJ, USA)
Flow cytometer BD LSRFortessa™	BD
Fluorescence microscope Leica DM4B	Leica (Wetzlar, Germany)
Freezer -20 °C	Liebherr (Bulle, Germany)
Freezer -80 °C	New Brunswick, Eppendorf
Heating block Thermomixer C	Eppendorf
Ice machine	Manitowoc
Infrared lamp	Philips (Amsterdam, the Netherlands)
Magnetic stirrer RCT basic	IKA (Staufen im Breisgau, Germany)
Mouse restrainer	LabArt (Waldbüttelbrunn, Germany)
PH-Meter	VWR (Radnor, PA, USA)
Pipettes	Eppendorf
Plate reader	Epoch, Biotek, Thermo Fisher Scientific (Waltham, MA, USA)
Rectal probe	World Precision Instruments Germany GmbH, (Friedberg, Germany)
Refrigerator	Liebherr
Shaker for dot blots, IKA Rocker 2D basic	IKA
Shaking Incubator Innova 42	New Brunswick
Sonification instrument Sonopuls	Bandelin (Berlin, Germany)
Thermometer for rectal probe	World Precision Instruments Germany GmbH
TissueLyser LT	Quiagen (Hilden, Germany)
Ultrapure water system Milli-Q®	Merck (Darmstadt, Germany)
Vacuum collecting bottle	Carl Roth (Karlsruhe, Germany)
Vacuum pump	Gilson Inc. (Middleton, WI, USA)
Vortex Genie 2	Scientific industries (Bohemia, NY, USA)

2.1.2 Expendable materials

Table 3: List of expendables

Material	Company / Source
0.45 µm filter	Sarstedt (Nümbrecht, Germany)

II. Material and Methods

0.5 ml, 1 ml, 2 ml, 5 ml reaction tubes	Sarstedt
15 ml, 50 ml Falcon tubes	Sarstedt
2 ml, 5 ml, 10 ml, 25 ml, 50 ml serological pipets	Sarstedt
200 µl tube stripes	Starlab GmbH (Hamburg, Germany)
6-well plate	Thermo Fisher gScientific
96 well plate U-shaped bottom	Greiner (Kremsmünster, Austria)
Capillaries Na-Heparin, disposable	Hirschmann Laborgeräte (Eberstadt, Germany)
Cell strainer	Omnilab (Bremen, Germany), Greiner
FACS tubes small	Greiner
Flat bottom Maxi-Sorp 96-well plate	Thermo Fisher Scientific
Millex-GV syringe 0.22 µm Filter Unit	Merck
Pasteur pipettes	Carl Roth
Pipette tips	Sarstedt
Serum tubes with Ethylenediaminetetraacetic acid (EDTA), Monovette®	Sarstedt
Serum tubes with gel, Microvette®	Sarstedt
Surgical Disposable Scalpels	B. Braun (Melsungen, Germany)
Syringes 1 ml, 0.3x 12 mm, 30G	B. Braun

2.1.3 Preparation of common buffers and solutions

Table 4: Common buffers

Buffer	Preparation
PBS	Dilute 1:10 from 10x PBS (pH 7.4, Gibco by Life Technologies, Carlsbad, CA, USA)
Tris-buffered saline (TBS)	20 mM Tris (AppliChem, Darmstadt, Germany), 150 mM NaCl (AppliChem), pH 7.6
TBS/T or PBS/T	0.05% Tween20 (Calbiochem, Merck) in TBS or PBS
RIPA buffer	50 mM Tris buffer, pH 8.0 (AppliChem) 150 mM sodium chloride (AppliChem) 1% Nonidet P-40 (AppliChem) 0.5% sodium deoxycholate (Sigma-Aldrich, St. Louis, MO, USA) 0.1% sodium dodecyl sulfate (Sigma-Aldrich)
100 mM potassium phosphate buffer	Adjust 100 ml of 100 mM potassium phosphate monobasic solution (KH ₂ PO ₄ , Sigma) to a pH of 6.5 by adding potassium phosphate dibasic solution (K ₂ PO ₄ ·3H ₂ O)
ACK lysis buffer	155 mM NH ₄ , 10 mM KHCO ₃ , 0.1 mM EDTA-2Na-2H ₂ O; pH 7.2-7.4
Sodium carbonate-bicarbonate ELISA coating buffer	Add 4.2 g sodium hydrogencarbonate (NaHCO ₃ , Merck) and 1.78 g disodium carbonate (Na ₂ CO ₃ , Sigma-Aldrich), fill up with dH ₂ O to 500 ml, adjust to pH 9.5
BSA-buffer	1% BSA (Applichem) in PBS
BSA-SA-buffer	1% BSA, 0.05% sodium azide (Morphisto, Offenbach am Main, Germany)
FACS buffer	PBS, 1% fetal calf serum (FCS), 2.5 mM EDTA

2.1.4 Antibodies and staining reagents for flow cytometric analysis

Table 5: Staining reagents used for flow cytometric analysis

Reagent/ antigen (murine)	Fluorochrome	Clone	Endconcentration/dilution	Manufacturer
7-Amino-actinomycin D (7AAD)	n.a.	n.a.	5 µg/ml	Enzo Life Sciences (Farmingdale, NY, USA)
B220/CD45R	Alexa Fluor 488 (AF488)	RA3-6B2	1:200	BioLegend (San Diego, CA, USA)
BSI-B ₄ (<i>Griffonia simplicifolia</i> isolectin B4)	DyLight®594	n.a.	1:100	Vector Laboratories (Burlingame, CA, USA)
CD103	Biotin	2E7	1:400	eBioscience (Thermo Fisher Scientific)
CD11b	Brilliant Violet 711 (BV711)	M1/70	1:200	BioLegend
CD11c	BV785	N418	1:200	BioLegend
CD16/CD32 (Fc-block™)	unconjugated	2.4G2	1:100	BD
CD3e	Fluorescein isothiocyanate (FITC)	145-2C11	1:100	BD
CD4	AF700	RM4-5	1:200	eBioscience
CD4	Phycoerythrin (PE)	RM4-5	1:600	BD
CD4	eFluor 660 (eF660)	GK1.5	1:1000	eBioscience
CD4	Pacific Blue (PB)	GK1.5	1:200	BioLegend
CD45	Allophycocyanin - eF780 (APC-eF780)	30-F11	1:200	eBioscience
CD45	PB	104	1:200	BioLegend
CD64	APC	X54-5/7.1	1:100	BioLegend
CD8α	PE	53.6.7	1:100	BD
Fixable viability dye	Zombie Aqua™	n.a.	1:800	BioLegend
FoxP3	Peridinin chlorophyll protein-Cyanine 5.5 (PerCP-Cy5.5)	FJK-16s	1:100	eBioscience
GATA3	eF660	TWAI	1:20	eBioscience
Helios	PB	22F6	1:33	BioLegend
IgG1	PE	A85-1	1:100	BD
IgM	AF488	1B4B1	1:500	Southern Biotech

II. Material and Methods

Lineage cell detection cocktail (anti-CD5, anti-CD11b, anti-CD45R/B220, anti-7-4, anti-Gr-1 (Ly-6G/C), and anti-Ter-119)	biotinylated	multiple	1:30	Miltenyi Biotec, Bergisch Gladbach, Germany
MHCII	APC-eF780	M5/114.15.2	1:200	eBio
RORyt	PE	AFKJS-9	1:100	eBioscience
SIRP α /CD172a	PerCP-eF710	P84	1:100	eBioscience
Streptavidin	PE	n.a.	1:500	BD
Streptavidin	BV786	n.a.	1:250	BioLegend
Streptavidin	BV650	n.a.	1:500	BioLegend
SYBR green	SYBR green	n.a.	1:100,000	Sigma-Aldrich

2.1.5 Human samples

Serum samples were retrieved from atopic dermatitis patients (male n=13, female n= 6) with a mean SCORAD of 63 ± 14.2 , α -Gal allergic patients with α -Gal-syndrome confirmed by α -Gal specific IgE, medical history or oral provocation test (n=7) or healthy controls (n=17). All individuals gave written consent and the study collection was approved by the local ethics committee. The α -Gal allergic patients and healthy controls were part of the BioBank of the Department of Dermatology and Allergy Biederstein, School of Medicine, Technical University of Munich, Munich, Germany and approved by ethical vote 419/18 S-KK. The atopic dermatitis patient collection was approved by ethical vote 5590/12.

2.1.6 Mouse lines

2.1.6.1 *Ggta1* KO animals

Ggta1 knockout (KO) animals [109] were kept under SPF conditions and were provided by the Biedermann lab, Department of Dermatology and Allergy Biederstein, School of Medicine, Technical University of Munich, Munich, Germany. Mice had been kindly provided to the Biedermann lab by the group of Florian Kreppel, University of Ulm, Germany. All interventions were performed in accordance with the European Convention for Animal Care and Use of Laboratory Animals and were approved by the local ethics committee and appropriate government authorities (ROB-55.2-2532.Vet_03-17-68).

2.1.6.2 Wildtype animals

All wildtype (WT) animals were of C57BL/6 background. Interventions were performed in accordance with the European Convention for Animal Care and Use of Laboratory Animals and

approved by the local ethics committee and appropriate government authorities (Lower Saxony: 33.12-42502-04-20/3406, Upper Bavaria ROB-55.2-2532.Vet_02-20-162).

2.1.6.2.1 *SPF housing*

WT animals were housed under SPF conditions unless otherwise stated. WT animals were housed and bred at the Core Facility Laboratory Animal Services (CF-LAS), Area E, at the Helmholtz Center Munich. For microbiome studies, WT SPF-housed animals were provided by the Stecher lab, Max von Pettenkofer Institute for Hygiene and Medical Microbiology, Ludwig-Maximilians University Munich, Charles River Germany and by the Hannover Medical School (MHH), in particular for food allergy experiments. WT animals were matched with age and gender to gnotobiotic animals.

2.1.6.2.2 *Gnotobiotic animals colonized with ASF*

Mice colonized with strains from the ASF [110] were inoculated with the following 3 strains and termed ASF³: ASF356 (*Clostridium* species), ASF361 (*Lactobacillus murinus*) and ASF519 (closely related to *Parabacteroides distasonis*) and were provided by the Stecher lab, Max von Pettenkofer Institute for Hygiene and Medical Microbiology, Ludwig-Maximilians University Munich. A second ASF mouse group was derived from mice colonized with all 8 Altered Schaedler strains: ASF356, ASF360 (*Lactobacillus* sp.), ASF361, ASF457 (*Mucispirillum schaedleri*), ASF492 (*Eubacterium plexicaudatum*), ASF500 (*Pseudoflavonifactor* species), ASF502 (*Clostridium* sp.) and ASF519. As ASF360 was not detectable due to either loss of the bacterium in the mouse colony or due to abundance below detection level, the mouse group was termed ASF⁷ as only the occurrence of 7 strains could be assured. All ASF³ animals were born from ASF³ colonized mothers. ASF⁷ animals were born from germ-free mothers and colonized after weaning (~3.5 weeks of age) by cohousing with ASF⁷ mice of another genetic background for 4 weeks for steady state experiments. For food allergy experiments ASF⁷ animals were born from ASF⁷ mothers and were thus colonized from birth.

2.1.6.2.3 *Gnotobiotic animals colonized with Oligo-MM¹²*

Gnotobiotic mice housed with Oligo-MM¹² strains [111, 112] were provided by the Stecher lab, Max von Pettenkofer Institute for Hygiene and Medical Microbiology, Ludwig-Maximilians University Munich and for some experiments maintained at the gnotobiotic core facility of the Hannover Medical School (MHH). The following strains were contained in the Oligo-MM¹² strains: *Acutalibacter muris* KB18, *Flavonifactor plautii* YL31, *Clostridium clostridioforme* YL32, *Blautia coccoides* YL58, *Clostridium innocuum* I46, *Lactobacillus reuteri* I49, *Enterococcus faecalis* KB1, *Bacteroides caecimuris* I48, *Muribaculum intestinale* YL27, *Bifidobacterium longum subsp. animalis* YL2, *Turicimonas muris* YL45 and *Akkermansia muciniphila* YL44. All animals in this study were born from Oligo-MM¹²-colonized mothers. For food allergy experiments, Oligo-MM¹²-housed animals were provided by the

Hannover Medical School (MHH).

2.1.6.2.4 *GF animals*

GF mice were housed at and provided by the Hannover Medical School (MHH). Germ-free status was regularly controlled.

2.1.7 Pig samples

Pig WT kidney was derived from a local butcher, kindly provided by Maximilian Schiener. *GGTA1* KO pigs were developed and maintained according to ROB-55.2-2532.Vet_02-18-56. Knockout of α -Galactosyltransferase gene in pigs was achieved according to [113] and kidney samples of KO pigs provided by Konrad Fischer, Chair of Livestock Biotechnology, School of Life Sciences Weihenstephan, Technische Universität München, Freising, Germany.

2.1.8 Screening material for monoclonal antibody development against α -Gal

2.1.8.1 Purchased and purified material

Mouse serum albumin (MSA) was purchased from Sigma-Aldrich, OVA EndoFit from InvivoGen (San Diego, CA, USA) and Bovine Serum Albumin (BSA) from AppliChem (Albumin Fraction V). Proteins coupled to the α -Gal epitopes Gal- α 1,3-Gal- β 1,4-GlcNAc (referred to as “TRI”-saccharide) and the “DI”-saccharide Gal- α 1,3-Gal were purchased from Dextra, Reading, UK. These are Gal- α 1,3-Gal- β 1,4-GlcNAc-MSA (α -Gal-MSA, 3 atom spacer), BSA-coupled to Gal- α 1,3-Gal (α -Gal-DI-BSA, 3-atom spacer, Dextra), Gal- α 1,3-Gal- β 1,4-GlcNAc-BSA (α -Gal-TRI-BSA, 3 atom spacer) and Gal- α 1,3-Gal- β 1,4-GlcNAc-OVA (α -Gal-OVA, 14-atom spacer, Dextra, Reading, UK). α -Gal-rich glycolipids were extracted from rabbit erythrocytes (Innovative Research, Novi, MI, USA) as described previously [114], modified from [115, 116] by Neera Chakrapani, Department of Infection and Immunity, Luxembourg Institute of Health (LIH), Esch-sur-Alzette, Luxembourg. Bovine thyroglobulin was purchased from Merck. His-tagged porcine aminopeptidase N (APN) was recombinantly produced in human embryonic kidney (HEK) 293 cells (APN control without α -Gal) [114] as well as in HEK293 cells stably expressing murine GGTA1 (α -Gal-APN) [117]. The cells were cultured in DMEM supplemented with 10% fetal calf serum (FCS), penicillin and streptomycin. After reaching 70% confluency, FCS-containing medium was removed and cells were gently washed once with PBS. Fresh DMEM (Sigma-Aldrich) containing PeproGrow-1 (serum-free cell culture supplement, PeproTech) was added and cells were cultured for further 4 - 6 days without medium exchange until cell viability showed the first signs of deterioration. Medium supernatant was harvested and passed through a 0.45 μ m filter to remove residual cell debris. The recombinant proteins were purified from the filtrate using Ni-NTA affinity chromatography and subsequent gradient elution with imidazole (AppliChem). Protein-

containing fractions were screened for purity via SDS-PAGE and subsequent staining with Coomassie blue. Suitable fractions were pooled. Proteins were concentrated using centrifugal filter units (Amicon Ultra-15, Merck), including a final washing step with PBS to reduce the imidazole concentration to ≤ 20 mM. After sterile filtration (Millex-GV syringe 0.22 μ m Filter Unit) and shock freezing in liquid N₂, proteins were stored at -80°C until use. APN (w/ and w/o α -Gal) was produced and purified by Michael Dittmar, Center of Allergy and Environment (ZAUM) and Institute of Allergy Research, Technical University of Munich, School of Medicine and Helmholtz Center Munich, German Research Center for Environmental Health, Neuherberg, Germany.

2.1.8.2 Tissue and cell lysates

Cultivated *GGTA1* KO and WT pig kidney cells were lysed with Cytobuster (Merck) and were provided by Konrad Fischer, Chair of Livestock Biotechnology, School of Life Sciences Weihenstephan, Technische Universität München, Freising, Germany. 0.5 cm x 0.25 cm pieces of pig kidneys (WT/KO) were lysed in 1 ml RIPA buffer. 10 ml RIPA buffer contained 1 tablet Protease Inhibitor Cocktail (Roche, Basel, Switzerland) and 1 tablet PhosSTOP (Roche). Tissue samples were homogenized using metal balls with the TissueLyser LT at 50 Hz 3 minutes (min), sonicated for 10 seconds and centrifuged at 16,000xg for 30 min at 4°C. Protein amounts in the collected supernatants were measured with a Pierce BCA Protein Assay Kit (Thermo Fisher Scientific) using bovine serum albumin (BSA) as standard.

500 μ l of whole blood from a donor with blood group B was centrifuged at 2000xg for 10 min and the cell pellet frozen at -80°C before adding 1 ml RIPA buffer containing protease and phosphatase inhibitor as described above. Cells were sheared by massive pipetting and vortexing steps and then incubated on ice for 30 min before centrifuging at 16,000xg for 30 min at 4°C. The supernatant was collected and stored at -80°C until usage.

2.1.8.3 Bacterial strains and lysates

Staphylococcus aureus strains Mu50, SA113, COL, 20231, RN1, SH1000, MW2, RN4220, Newman, USA300, *Escherichia coli* strains (K12, DH5 α), *Helicobacter pylori* (J99), *Pseudomonas aeruginosa* (DSM 50071), *Haemophilus influenza* (Hi375), *Acinetobacter baumannii* (ATCC 17978), *Salmonella typhimurium* (ATCC 14028) were purchased from ATCC Manassas, VA, USA and DSMZ, Leibniz Institute, Germany. *Akkermansia muciniphila* was obtained from Willem De Vos at Wageningen University. The bacteria were grown overnight at 37 °C to a density of 10⁹ CFU/ml. All bacteria were grown in Luria Bertani (L.B.) broth (tryptone 10g, NaCl 10g, yeast extract 5g in 1L H₂O, adjust pH to 7.0 with 5 N NaOH, sterilize), except for *H. pylori* in Brain Heart Infusion (BHI) (beef heart, 5 g/L, calf brains, 12.5 g/L, disodium hydrogen phosphate, 2.5 g/L, D(+)-glucose, 2 g/L, peptone, 10 g/L, sodium

chloride, 5 g/L) plus 20% FCS, *H. influenza* in BHI 37g, NAD 15mg, and Hemine 15mg in 1L H₂O, and *Akkermansia muciniphila* (ATCC BAA-835) in reduced BHI. Pelleted bacteria (approximately 3x10⁹ bacterial cells) were washed with PBS and resuspended in 1 ml RIPA buffer as described for mammalian samples above, and added to glass beads and beat for one hour (max speed 2800 rpm using a Vortex shaker) and transferred to new tubes for storage at -80°C. Cultivation and preparation of before-mentioned bacteria was performed by Mohammadali Khan Mirzaei, Institute of Virology, Technical University of Munich and Helmholtz Center Munich, German Research Center for Environmental Health, Neuherberg, Germany.

E. coli HS was originally isolated from a human fecal sample of a healthy adult [118] and provided by Mahesh S. Desai, Department of Infection and Immunity, Luxembourg Institute of Health (LIH), Esch-sur-Alzette, Luxembourg. *E. coli* O86:B7 and *Lactobacillus rhamnosus* were purchased from the American Type Culture Collection (ATCC 12701 and 53103), *E. coli* BL21 from Thermo Fisher Scientific (EC0114). *E. coli* strains were grown overnight at 37°C in LB medium, *L. rhamnosus* was grown overnight at 37°C in Lactobacilli MRS broth (proteose peptone #3 10 g, beef extract 10g, yeast extract 5g, dextrose 20g, sorbitan monooleate 1g, ammonium citrate 2g, sodium acetate 5g, MnSO₄ x H₂O 0.05g, Na₂HPO₄ 2g in 1L H₂O, adjust pH to 6.5). RIPA buffer was added to cell pellet of 5 ml culture and cells were lysed for 30min at 30Hz with glass beads. Cultivation and lysate preparation of bacteria was performed by Desai and Hilger laboratories, Department of Infection and Immunity, Luxembourg Institute of Health (LIH), Esch-sur-Alzette, Luxembourg.

2.1.9 Websites and software

Table 6: Websites and software

Name and Application	Website/Source
Pubmed Database for literature research	https://pubmed.ncbi.nlm.nih.gov/
Mendeley Desktop for referencing	Version 1.19.8, Mendeley Ltd
xcmsViewer for untargeted metabolomics analysis	Version 0.5.3, provided by BayBioMS, Freising, Germany
Flow jo for flow cytometric data analysis	FlowJo (Version 10.7.1)
Graphpad Prism 7 for graphs and statistical analysis	Version 7.04, GraphPad Software, Inc., www.graphpad.com
LAS X software for immunofluorescence imaging	Leica, Wetzlar, Germany
ImageJ software for immunofluorescence imaging	https://imagej.nih.gov/ij/ , Rasband, W.S., U. S. National Institutes of Health, Bethesda, MD, USA
Inkscape for figure design	Inkscape 1.1, GNU General Public License, version 3, www.inkscape.org

2.2 Methods

2.2.1 General mouse protocols

2.2.1.1 Maintenance

Mice received food and water *ad libitum*. For location of housing see Materials, 2.1.6 Mouse lines.

2.2.1.2 Organ withdrawal

Mice were sacrificed via cervical dislocation shortly before organs were removed.

2.2.2 Food allergy model

Mice from the groups GF, ASF⁷, Oligo-MM¹² and SPF were sensitized at an age of 6 weeks for four weeks with 5 mg chicken albumin (Albumin chicken egg grade III, Sigma) and 10 µg Cholera toxin (List Biological Laboratories, Campbell, CA, USA) in 300 µl PBS via oral gavage intragastrically (i.g.). Control animals (not sensitized; mouse groups GF and SPF) received 10 µg Cholera toxin diluted in PBS (300 µl) only. Oral gavage was performed on days 0, 2, 7, 14, 21 and 28. 7 days after the last sensitization, mice were analyzed for an anaphylactic reaction to chicken albumin (OVA) on day 35. To elicit anaphylaxis, 10 µg OVA (EndoFit Ovalbumin, InvivoGen) diluted in 150 µl PBS was applied intravenously (i.v.) to sensitized and control animals with a 1 ml syringe and G30 0.3x12 mm needle. Mice were fixed in a restrainer for i.v. injection and shortly warmed up under an infrared lamp for visibility of the vein. After OVA injection, the core body temperature of all mice was measured intrarectally for approximately 30-60 min every 5 min with a rectal probe (1.6 mm ball tip, World precision instruments Germany GmbH) until mice reached their initial body temperature. The rectal probe was covered with Vaseline (Carl Roth) to avoid rectal ruptures. The initial body temperature was measured before i.v. injection. The day before sensitization (day -1) and at day 35 after the anaphylaxis readout, blood was collected from mice via retrobulbar bleeding from the venous plexus with a capillary after anesthetizing the mice with 2% isoflurane (Zoetis Inc, Parsippany, NJ, USA) in O₂. On day 36, mice were sacrificed for organ withdrawal. For graphic summary of the model see Figure 8A. Sensitization of all mouse groups was performed by Marijana Basic, Silvia Bolsega, Anna Smoczek at the Hannover Medical School in isolators. After Day 28 mice were transferred to the Institute of Allergy Research, Helmholtz Center Munich for anaphylaxis readout and further processing of mouse organs. For ethical approval details see Materials, 2.1.6 Mouse lines.

2.2.3 Cell preparations from mouse organs

2.2.3.1 Isolation of lamina propria small intestinal immune cells and from colon

2.2.3.1.1 *Spatial distribution of T cells and ILCs along the intestine and from food allergic mice and isolation of intestinal immune cells for assessment of DCs*

For organ analysis animals ranged between 5 to 12 weeks of age. Specifics are indicated in figure captions. GF, ASF³, Oligo-MM¹² or SPF mice were sacrificed and mouse groups processed on different days for analysis of spatial distribution of intestinal cells. For DC stain ASF³, Oligo-MM¹² or SPF were processed on the same day and small intestine (SI) was processed as a whole. For analysis of lamina propria lymphocytes from the mouse groups GF, ASF⁷, Oligo-MM¹² and SPF that underwent the food allergy model, the SI was also processed as a whole. SI and colon were excised quickly and Peyer's patches were removed. For spatial distribution of lymphocytes, the SI was cut into three parts of equal length corresponding to the three parts (in descending order) duodenum, jejunum and ileum. Colon was removed as a whole. The gut parts were cut longitudinally, and washed with ice-cold PBS to remove gut content. The tissue was cut into 1-2 cm pieces and placed in 50 ml falcons containing 20 ml RPMI 1640 medium (Gibco), 3% FCS, 5 mM EDTA (pH 8.0, AppliChem), 25 mM 4-(2-hydroxyethyl)-1-piperazineethanesulfonic acid (HEPES, Gibco). Afterwards DL-Dithiotreitol (DTT, Sigma-Aldrich, stock diluted in ddH₂O) was added to each tube at 0.145 mg/ml and the tubes incubated horizontally for 20 min at 37°C shaking at 80 rpm. Tubes were vortexed highest speed for 30 s. To remove the mucus, the tube content was transferred to Petri dishes and the tissue pieces collected with forceps in a 50 ml tube containing 10 ml RPMI, 2 mM EDTA, 25 mM HEPES. Tubes were vortexed again and procedure repeated three times. After the last washing step, tissue pieces were transferred into 6 well plates and minced well with scissors. Then 5 ml digestion medium (5 ml RPMI medium containing 200 U/ml Collagenase IV (Worthington, Biochemical Corporation, Lakewood, NJ, USA), 10 µg/ml DNase (Sigma-Aldrich), 25mM HEPES) was added to each well of SI tissue pieces; the colon was transferred to 50 ml tube and digested in 10 ml digestion medium. Tubes were incubated shaking for 110 rpm at 37°C for 20 min, tissue pieces pipetted up and down with a cut-tip 1000 µl pipet for 45 s and the supernatant containing lymphocytes transferred to a new canonical tube through a 100 µm filter. The digestion procedure was repeated two times. Ice-cold FACS buffer (PBS, 1% FCS, 2.5 mM EDTA) was added to cell containing supernatants to stop digestion (on ice). Collected supernatants were centrifuged for 8 min, 550xg, 4°C. The cell suspensions were resuspended in 40% Percoll in RPMI (Percoll, GE Healthcare), placed into a 15 ml falcon and underplayed with 80% Percoll in RPMI using a glass Pasteur pipette. Percoll solutions were warmed up to room temperature (RT). Tubes were centrifuged at RT, 1600xg, 15 min without breaks. Cells were collected on 10 ml PBS in 15 ml

falcons, centrifuged for 8 min, 450xg, 4°C and the complete cell suspension was seeded out for flow cytometric cell staining in round-bottom 96 well-plates. For staining specifics of single cell suspension refer to 2.2.5.1 Immunostaining for flow cytometric analysis of isolated cells from murine organs.

2.2.3.1.2 Isolation of immune cells from the intestine from whole small intestine for steady state frequencies of T cells and ILCs

The isolation of immune cells in Figure 4 of the mouse groups ASF³, ASF⁷, Oligo-MM¹² and SPF-housed mice to assess T cell and ILC populations at steady state were processed on the same day. The SI was excised, Peyer's patches removed and the gut parts washed as described before. The tissue was cut into 2-3 cm pieces and incubated in 30 mM EDTA (pH 8.0) in PBS (Ca²⁺ and Mg²⁺ free) in a 50 ml tube at 4°C for 30 min. After vigorously shaking the tube for 20 s, the suspension was poured into a Petri dish and tissue pieces collected with forceps in 25 ml fresh PBS. This washing process was repeated several times until buffer solution was clear. Afterwards, tissues were cut into 1-2 mm pieces and digested in 5 ml RPMI containing 25 mM HEPES, 0.5 mg/ml Collagenase D (Roche) and 10 µg/ml DNase I (Sigma) and incubated for 10-12 min at 37°C as described before. Cells were collected as described before. Digestion step was repeated two to three times incubating another 20 to 30 min until tissue was fully digested. Cells were further processed with a Percoll as described before. This protocol yielded similar T cell amounts and population percentages compared to the protocol described under spatial distribution of intestinal cells and dendritic cell isolation.

2.2.3.2 Isolation of splenocytes

Spleen was excised and meshed through a 70-100 µm filter for generating a single cell suspension. After washing splenocytes twice with PBS, erythrocytes were lysed with ACK lysis buffer in 1 ml for 2 min. Cells were washed with FACS buffer twice before staining. Approximately 1/10 of the whole splenocyte suspension was stained in 50 µl per sample. Protocol was performed on ice and centrifuging 450xg.

2.2.3.3 Preparation of single cell suspension from mesenteric lymph nodes

All mLNs of one mouse were excised, meshed together on a 70-100 µm filter for generating a single cell suspension and washed twice with PBS in a 15 ml falcon. Half of the sample was used for immunostaining for flow cytometric analysis. Single color controls for fluorochrome compensation were generated from this cell suspension.

2.2.4 Monoclonal antibody development against α -Gal via hybridoma technology

2.2.4.1 Immunization of *Ggta1* KO mice and screening of hybridoma supernatants

Ggta1 KO mice [109] were immunized subcutaneously (s.c.) and intraperitoneally (i.p.) with a mixture of 50 μ g OVA-coupled Gal- α 1,3-Gal- β 1,4-GlcNAc trisaccharide (α -Gal-OVA) in 200 μ l PBS, 5 nmol CpG2006 (TIB MOLBIOL, Berlin, Germany), and 200 μ l Incomplete Freund's adjuvant (Sigma-Aldrich). After 11 weeks, a boost without Freund's adjuvant was given i.p. and s.c. 3 days before hybridoma fusion. Fusion of the myeloma cell line P3X63-Ag8.653 with mouse splenic B cells was performed using polyethylene glycol 1500 according to standard procedure [119]. After fusion, hybridoma cells were plated in 96-well plates using RPMI 1640 supplemented with 15% FCS, 1% glutamine, 1% pyruvate, 1% non-essential amino acids and 2% HAT media supplement (Hybri-Max, Sigma-Aldrich). Hybridoma supernatants were screened 10 days later in a flow cytometry assay (iQue, Intellicyt; Sartorius, Göttingen, Germany) using BSA-coupled Gal- α 1,3-Gal (α -Gal-DI-BSA) captured on 3D-aldehyde beads (PolyAN, Berlin, Germany). Beads were incubated for 90 min with hybridoma supernatant and Atto-488-coupled isotype-specific monoclonal rat anti-mouse IgG secondary antibodies. Antibody binding was analyzed using ForeCyt software (Sartorius). Positive supernatants were further validated by dot blot and cells from clone 27H8 were sub-cloned by five rounds of limiting dilution to obtain stable monoclonal hybridoma cell lines (mouse IgG1/ κ). Immunization and antibody generation was performed by Monoclonal Antibodies Core Facility, Helmholtz Center Munich, German Research Center for Environmental Health, Neuherberg, Germany. For ethical approval details of mouse interventions see Materials, 2.1.6 Mouse lines.

2.2.4.2 Purification of the monoclonal antibody

Hybridoma supernatant from subcloned 27H8 was purified on an ÄKTA Pure chromatography system (Cytiva) using Cytiva HiTrap Protein A HP column (Fisher Scientific). Monoclonal antibody purification was performed by Monoclonal Antibodies Core Facility, Helmholtz Center Munich.

2.2.5 Immunoassays

2.2.5.1 Immunostaining for flow cytometric analysis of isolated cells from murine organs

After cell isolation and plating, cells were washed once with PBS and stained in 50 μ l live dead stain for 15 min (diluted in PBS) for 15-20 min, 4°C. Cells were washed two times with FACS Buffer, Fc-block was added (5 μ l, shortly) and cells were extracellularly stained for 30 min (diluted in FACS Buffer, 50 μ l staining volume, 4°C). Cells were washed again two times with FACS buffer and stained

with streptavidin (if applicable) for 10 min, 4°C, and washed again. Cells were fixed overnight (o.n.) with Foxp3/Transcription Factor Staining Buffer Set (eBioscience) according to manufacturer's instructions at 4°C. The next day, cells were washed two times with Permeabilization (Perm) Buffer (diluted 1:10 in MilliQ) and stained for 1 h intracellularly (diluted in Perm Buffer, 50 µl reaction volume, RT). Before taking cells up in either 70 µl PBS for samples or 150 µl for single color controls, cells were washed with Perm Buffer two times. Centrifugation steps were carried out at 450xg before fixation and 550xg after fixation, washing was performed with 150 µl buffer, staining solutions incubated in the dark. Details about antibodies and dilutions can be found in Table 5: Staining reagents used for flow cytometric analysis in section 2.1.4. Acquisition was performed at Flow cytometer LSRFortessa™ System (BD). For gating strategy of either T cell and ILC populations or DC subpopulations see Appendix.

2.2.5.2 Dot blot screening of monoclonal antibodies against α -Gal

Nitrocellulose membranes (Carl Roth) were cut into length of 10 cm x 0.5 cm and 1 µl of sample was applied 1 cm apart to a maximum of 10 samples per membrane strip, except for horseradish peroxidase (HRP) detection for which 2 µl were spotted (Figure 9C). The amount of blotted α -Gal conjugated glycoproteins and proteins devoid of α -Gal was 0.1 µg (Figure 9E, Figure 12A,F, Figure 13B), 1 µg (Figure 9B,D, Figure 10A) or 2 µg (Figure 9C) per dot. 0.125 µg of glycolipids (with or without prior EGCase I digestion) and 1 µl of the whole blood lysate from a blood type B donor were spotted per dot. Pig kidney and cell lysates of cultured pig cells (pre-digested or not), α -Gal-APN, APN and thyroglobulin were spotted at an amount of 1 µg. Whole bacterial lysates were spotted at 1 µl without protein amount normalization. After a drying time of 15 min, the membrane was transferred to a chamber of mini-incubation trays (Bio-Rad Laboratories, Hercules, CA, USA) and blocked with 1.5 ml 2% BSA (Albumin Fraction V, AppliChem) in TBS for 1 hour at RT. Primary antibodies and lectin were incubated over night at 4°C and diluted in 1 ml TBS supplemented with 1 % BSA. Primary hybridoma supernatants from clones 27H8 and 25G8 were used at a 1:5 dilution, purified and biotinylated 27H8 antibody at 0.6 µg/ml, M86 hybridoma supernatant (Enzo Life Sciences) in a 1:5 dilution and biotinylated lectin from *Bandeiraea simplicifolia* (BSI-B4, Sigma-Aldrich) at 25 µg/ml. IgG isotype control (Invitrogen, Carlsbad, USA; polyclonal, Figure 4) and IgG1 isotype control (Clone P3.4.2.8.1., Thermo Fisher Scientific, Figure 13B) for bacterial samples were used at 0.6 µg/ml. After primary detection, membranes were washed three times for 5 min with 1 ml TBS/T. Secondary detection antibodies were incubated for 90 min at RT in 1 ml TBS/1%BSA. 27H8 primary hybridoma supernatant was detected by a monoclonal rat anti-mouse IgG1 (2E6, in house), 25G8 primary hybridoma supernatant was detected by a monoclonal rat anti-mouse IgG2b (7B8, in house) and in a

tertiary incubation step with alkaline phosphatase (AP)-conjugated anti-rat IgG with minimal cross-reactivity (Jackson ImmunoResearch, Philadelphia, PA, USA) at a dilution of 1:5000. Both, supernatant from subcloned 27H8 and purified 27H8 antibody was detected by AP-conjugated anti-mouse IgG, Fc-specific (Sigma-Aldrich) at a dilution of 1:10,000. M86 was detected by AP-conjugated μ -chain specific anti-mouse IgM (Sigma-Aldrich) at a dilution of 1:30,000; BSI-B₄ and biotinylated 27H8 by AP-conjugated Extravidin (Sigma-Aldrich) at 1:10,000. Membranes were washed three times in TBS/T for 5 min and immersed in 0.01 % nitro blue tetrazolium (AppliChem) and 0.005% 5-bromo-4-chloro-3-indolyl phosphate (AppliChem) in detection buffer (100mM Tris, 10 mM MgCl₂*6H₂O, 100 mM NaCl, pH 9.5) until dots were stained. After immersing membranes with distilled water, membranes were dried, aligned on a black paper and acquired with a photo camera at 15 cm height. For direct detection with HRP-labeled secondary antibodies, glyco-/proteins or glycolipids were spotted on a membrane strip pre-wet in transfer buffer containing 25 mM Tris, 19.2 mM glycine and 20 % isopropanol, pH 8.3. Rat anti-mouse-IgG1 (2E6, in house) labeled with HRP (for 27H8 primary supernatant) and rat anti-mouse-anti-IgG2b-HRP (for 25G8 primary supernatant). Uncropped dot blots from all figures are displayed in Appendix Figure 19.

2.2.5.3 Immunohistochemistry for detection of α -Gal in tissue slides

0.25 cm x 1 cm sections of WT and *GGTA1* KO pig kidneys were fixed in 3.6% buffered formaldehyde (Fischer, Saarbrücken, Germany) for 24 hours and embedded in paraffin. Sections of 4 μ m were cut and transferred to slides. Slides were washed twice with Xylo (Carl Roth, Karlsruhe, Germany) for 10 min. For rehydration, slides were transferred into a graded series of ethanol in distilled water: 100% (twice, 5 min), 96% (5 min), 70% (5 min), 50% (1 min), H₂O (30 seconds) and washed for 5 min in PBS (Sigma-Aldrich). Antigen was retrieved by transferring slides into nearly boiling citrate buffer, incubating at 90°C (10 min) and slowly cooling to RT (~30 min). Slides were washed 5 min in PBS and blocked with 2% BSA in PBS for 1 hour. Tissue sections were incubated with primary antibody solutions in 1% BSA at the following concentrations/dilutions: 1 μ g/ml 27H8 or IgG1 κ isotype control (Clone: P3.6.2.8.1, unconjugated, eBioscience) or 1:5 dilution of M86 supernatant (IgM) for 16 hours at 4°C. Slides were washed three times with PBS for 5 min and incubated for 30 min at RT with fluorochrome labeled secondary antibody diluted in 1% BSA in PBS at the following concentrations: goat anti-mouse IgG (H+L) conjugated to AF647 (polyclonal, Thermo Fisher Scientific) at 2 μ g/ml and goat anti-mouse IgM (heavy chain) conjugated to AF488 (polyclonal, Thermo Fisher Scientific) at 10 μ g/ml. Slides were washed in PBS (three times, 5 min) and 1 drop of ProLong Diamond Antifade mounting medium with DAPI (Life Technologies by Thermo Fisher) was added. Images were acquired on a Leica DM4B fluorescence microscope and processed using LAS X software with a 20X objective.

Contrast and brightness were adjusted simultaneously on all images per channel with ImageJ software. All antibody solutions were centrifuged to remove antibody complexes before use.

2.2.5.4 Flow cytometry with 27H8 antibody

2.2.5.4.1 Eukaryotic flow cytometry for 27H8 monoclonal antibody screening

HEK cells expressing α -Gal glycosylated APN and APN devoid of α -Gal (see description in screening material above) were washed with BSA-Buffer containing 1% BSA in PBS. 5×10^5 cells were seeded and stained with either 27H8 purified antibody or IgG1 κ isotype control (clone: B3102E8, Southern Biotech) at 1 μ g/ml, a 1:10 dilution of M86 supernatant, a 1:10 dilution (40 μ g/ml) of mouse IgM isotype control (clone: MOPC 104E, Sigma-Aldrich) or a 1:100 dilution of BSI-B₄ conjugated to DyLight®594 (*Griffonia simplicifolia* isolectin B₄, Vector Laboratories) in BSA-buffer. Cells were washed twice and stained with respective secondary antibodies: anti-mouse IgG1-PE at a 1:100 dilution or anti-mouse IgM-AF488 (clone: 1B4B1, Southern Biotech) at a 1:500 dilution. Staining was performed in 100 μ l for both primary and secondary antibody incubation steps for 45 min. Cells were washed twice and resuspended in 150 μ l BSA-buffer before acquisition at a Novocyte Quanteon Flow Cytometer. This experiment was performed by Kyra Swiontek, Department of Infection and Immunity, Luxembourg Institute of Health (LIH), Esch-sur-Alzette, Luxembourg.

For murine splenocyte staining, spleen was excised and meshed on a 70 μ M filter for generating a single cell suspension. After washing splenocytes twice with PBS, erythrocytes were lysed with an ACK lysis buffer in 1 ml for 2 min. Cells were washed with BSA-SA-buffer containing 1% BSA, 0.05% sodium azide twice before staining. Staining and acquisition were performed as described for intestinal bacterial staining (see protocol below), except that splenocytes were stained with 5 μ g/ml 7AAD instead of SYBR green identification of living cells (Appendix Figure 20B).

2.2.5.4.2 Bacterial flow cytometry for 27H8 monoclonal antibody screening

Bacteria were grown to a density of 10^9 CFU/ml. *S. aureus* 20231 and *E. coli* K12 were grown overnight at 37°C in L.B. medium. 100 μ l of the culture was seeded into a 96-well U-bottom plate and washed with BSA-SA-buffer at 4000xg for 5 min. Cells were stained with 1 μ g/ml 27H8 and washed twice and stained with anti-IgG1-PE antibody at a 1:100 dilution in a total volume of 50 μ l. Bacteria were washed twice and fixed for 30 min with 3.7% formaldehyde (AppliChem, 37% diluted 1:10 in PBS) and washed again twice before acquisition in 100 μ l PBS at an Acurri™ Flow Cytometer. *E. coli* O86:B7, BL21, HS and *L. rhamnosus* were cultivated o.n. at 37°C in 5 ml L.B. medium shaking at 150 rpm. Cells were centrifuged (4000xg, 5 min) and washed twice with PBS before fixing cells in 4% PFA for 30 min. Bacteria were washed with PBS and then stained with primary and secondary antibody as described for HEK cells (see protocol above). Bacterial pellet was resuspended in 100 μ l in BSA-buffer

for acquisition on a Novocyte Quanteon Flow Cytometer. In general, at least 5×10^5 events were acquired. The before-mentioned experiment was performed by Kyra Swiontek, Department of Infection and Immunity, Luxembourg Institute of Health (LIH), Esch-sur-Alzette, Luxembourg.

For intestinal bacteria staining of *Ggta1* KO and WT mice, the entire SI, cecum and colon were removed. SI was cut longitudinally and whole content streaked out with a sterile pipette tip into a 1.5 ml tube. The cecum was cut on the tip and 2/3rds of the content streaked out. For the colon, the whole content was streaked out. 1 ml BSA-SA-buffer was added and slurry mixed by vortexing and pipetting. Intestinal debris was spun down at 900xg for 5 min, 4°C, and supernatant was transferred to a new tube for another centrifugation step at 450xg for 5 min, 4°C, to remove host cells. Bacterial pellets were washed twice in 1 ml BSA-SA-buffer at 8000xg 5 min, 4°C and filtered (70 µM) before seeding 100 µl of washed SI content, 25 µl of cecum content, 50 µl of colon content into U-bottom plates. Pellets were centrifuged, supernatant removed and stained with antibodies/lectin in 50 µl for 30 min. Concentrations and dilutions were: 1 µg/ml biotinylated 27H8 or IgG1κ isotype control (clone P3.6.2.8.1., biotinylated, eBioscience/Thermo Fisher Scientific) or 1:40 dilution of biotinylated BSI-B₄. Before staining with a 1:500 dilution of streptavidin-PE (SAv-PE) cells were washed twice by a centrifugation step at 3200xg for 5 min at 4°C. After two additional washing steps, bacteria were resuspended in 200 µl of a 1:100,000 dilution of SYBR green (SYBR green I nucleic acid gel stain, Sigma-Aldrich), incubated for 5 min and acquired at an Acurri™ Flow Cytometer. Data analysis of fcs-files was performed with FlowJo (Version 10.7.1) and SYBR green positive were considered as bacteria (Appendix Figure 20A) as described in [120].

2.2.5.5 Surface Plasmon Resonance (SPR) analysis

The binding measurements were performed on a BIACORE 3000 instrument (Biacore Inc., Piscataway, NJ, USA) and analyzed with Origin software version 9.0. 27H8 purified antibody was diluted to a final concentration of 50 nM in 10 mM sodium acetate, pH 4.0, and chemically immobilized (amine coupling, 850 RU bound) onto CM5 sensor chip (Cytiva). α-Gal-DI-BSA and α-Gal-TRI-BSA were diluted in the running buffer (PBS, 1 mM DTT and 0.005 % Tween 20) to the final concentration of 0.977 nM, 1.95 nM, 3.91 nM, 7.81 nM, 15.6 nM, 31.3 nM, 62.5 nM, 125 nM, 250 nM, 500 nM and injected over the sensor chip surface at 30 µL/min at 25°C. The protein samples were injected onto the sensor chip from the lowest to the highest concentration. Both glycoprotein samples were tested three times. Injection of 250 nM ligand was performed in duplicate within each experiment. In order to subtract background noise from each experiment, all samples were run over an unmodified CM5 sensor chip surface. After each ligand injection, the sensor chip was regenerated using 3 M MgCl₂ solution. For each measurement the equilibrium dissociation constant was calculated (K_D). The K_D s

from three experiments were used to calculate the mean values of these variables and the standard deviation. This assay was performed by Robert Janowski, Institute of Structural Biology, Helmholtz Center Munich, German Research Center for Environmental Health, Neuherberg, Germany.

2.2.5.6 Enzyme-linked Immunosorbent Assay (ELISA)

2.2.5.6.1 27H8 and M86 titration on glycoproteins

For comparing supernatant from subcloned 27H8 hybridoma and M86 hybridoma supernatant, both antibodies were titrated on glycoproteins coated to standard ELISA plates. α -Gal-DI-BSA, α -Gal-TRI-BSA, α -Gal-OVA, α -Gal-MSA and respective negative control proteins BSA, OVA and MSA were coated at a concentration of 5 $\mu\text{g/ml}$ in 50 μl per well on a flat bottom Maxi-Sorp 96-well plate for 12 hours at 4°C in sodium carbonate-bicarbonate buffer, pH 9.5. Plates were washed three times with PBS/T and blocked with BSA-buffer for 1 hour at RT and washed again three times with PBS/T. 27H8 supernatant and M86 were titrated in BSA-buffer starting from 1.12 $\mu\text{g/ml}$ in a serial 1:10 dilution to 1.12 ng/ml. The starting concentration was set according to the stock concentration of the M86 antibody in the hybridoma supernatant. The amount of 27H8 and M86 antibody in the hybridoma supernatants was measured with a Biotech Clonotyping System-HRP Kit and mouse Immunoglobulin Panel for Standards (both Southern Biotech) according to the manufacturer's instruction, yielding a concentration of 116.69 $\mu\text{g/ml}$ 27H8 antibody in the supernatant and 1.12 $\mu\text{g/ml}$ of M86. IgG1 and IgM Isotype controls (Southern Biotech) were used at the highest concentration at 1.12 $\mu\text{g/ml}$. Primary antibodies incubated for 1 h at RT and plates were washed five times with PBS/T. Polyclonal antibody conjugated to HRP detecting both mouse IgG and IgM heavy and light chains (Jackson ImmunoResearch) were incubated at a concentration of 80 pg/ml (1:10,000 dilution) in 1% BSA in PBS in 50 μl per well for 1 hour at RT shaking at 450 rpm. Plates were washed again 8 times with PBS/T and 50 μl TMB substrate (1-step Ultra 3,3',5,5'-tetramethylbenzidin (TMB), Thermo Fisher Scientific) was added before stopping the reaction with 25 μl 2M sulfuric acid (Merck). Emission was measured with a plate reader at 450 nm. ELISAs were repeated three times. Analysis, logarithmic transformation and curve fit (nonlinear variable slope, 4 parameters) was performed with GraphPad Prism 7.

2.2.5.6.2 Epitope blocking experiments with 27H8 and M86 monoclonal antibodies

For epitope blocking ELISAs, α -Gal MSA was coated onto plates at 0.5 $\mu\text{g/ml}$ in 50 μl per well as described before. Plates were washed with PBS/T, blocked with BSA-buffer and washed again as described before. Blocking antibody 27H8 supernatant was added in a serial dilution (1:10) from 100 $\mu\text{g/ml}$ to 0.01 $\mu\text{g/ml}$ in BSA-buffer. As the concentration of M86 was low compared to 27H8 in supernatant, a serial dilution of M86 was applied from 1 $\mu\text{g/ml}$ to 0.01 $\mu\text{g/ml}$. The blocking antibody

was incubated for 1 hour at RT with shaking at 500 rpm and plates were washed 5 times. Afterwards, the competing antibody (27H8 supernatant for M86 block and M86 for 27H8 supernatant block) was incubated for 1 hour at a concentration of 0.1 µg/ml at RT and shaking at 500 rpm and wells were washed 5 times. Detection was performed with either anti-IgG1-HRP for 27H8 competing antibody or anti-IgM-HRP for M86 competing antibody (both from Southern Biotech) at a 1:500 dilution. TMB substrate addition and acquisition were done as described before.

2.2.5.6.3 *Human serum immunoglobulin against α -Gal*

For measurement of human IgG, IgM and IgE antibodies from serum, bovine thyroglobulin (Sigma Aldrich) was coupled onto plates as described above. After washing, plates were blocked with chicken serum albumin (Sigma Aldrich). Diluted serum was added and incubated for 2 hours at RT. After washing, the biotinylated primary antibody specific for the indicated isotypes was incubated for 1 hour at RT. Detection was performed using streptavidin-HRP and acquisition was done as described before using TMB substrate. This ELISA was performed by the Biedermann lab, Department of Dermatology and Allergy Biederstein, School of Medicine, Technical University of Munich, Munich, Germany.

2.2.5.6.4 *Murine Mast cell protease-1 (mMCPT-1) ELISA*

Murine MCPT-1 concentration in serum samples of mice undergoing the food allergy model was measured by the MCPT-1 Mouse Uncoated ELISA Kit with plates (Invitrogen by Thermo Fisher Scientific) and was performed according to manufacturer's instruction. Serum samples were diluted 1:2 with assay buffer.

2.2.5.6.5 *OVA-specific IgE ELISA*

OVA-specific IgE in serum samples from mice undergoing the food allergy model was measured with the Legend MAX™ Mouse OVA Specific IgE ELISA Kit (Biolegend) according to manufacturer's instructions.

2.2.6 Biochemical assays

2.2.6.1 Enzymatic digestion and cleavage of the α -Gal epitope

Glycolipids were digested by Endoglycoceramidase I (EGCase I) using a ratio of 1 µg Glycolipids per 1 milliunit enzyme in 1x EGCase I Reaction buffer (New England Biolabs, MA, USA) in PBS for 37°C for 16 hours. Precipitated enzyme was removed after heat inactivation for 20 min at 65°C. 2 µg/ml pig kidney tissue lysates were digested with α -Galactosidase from green coffee beans (Sigma Aldrich) at 10 U/ml in 100 mM potassium phosphate buffer, pH 6.5 for 3 hours at RT. Ammonium sulfate was removed from α -Galactosidase preparation before digestion by pelleting the enzyme through a

centrifugation step at 15,000xg for 10 min at 4°C. The supernatant was collected and then the pellet resuspended in an equal volume of potassium phosphate buffer. *S. aureus* lysate was digested by adding 5 µl of whole lysate to 5 µl potassium phosphate buffer containing 20 U/ml α-Galactosidase (end concentration 10 U/ml) and further processed as described before. For EGCase I digestion, 10 µl bacterial lysate was digested in 1x EGCase I reaction buffer diluted with PBS and 1 µl EGCase I as described above (end volume 20 µl).

2.2.6.2 Periodic acid treatment of blotted samples in dot blot

Nitrocellulose membranes with blotted samples were incubated in 40 mM periodic acid (H₅IO₄, Merck) diluted from a stock concentration of 200 mM in 50 mM sodium acetate buffer (AppliChem, adjust to pH 4.5 with HCl) for 1 hour at RT.

2.2.6.3 Biotinylation of 27H8 antibody

Purified 27H8 antibody was labeled with biotin-7-NHS using a Biotin Protein Labeling Kit (Roche) at a molar ratio of 1:10. Excess biotin-7-NHS was removed by gel filtration according to manufacturer's instructions. To verify the biotinylation efficiency, biotinylated 27H8 and a random biotinylated IgG antibody (biotinylated rat anti-mouse IgM, clone R6-60.2, BD) and as controls 27H8 without biotinylation and IgG1 isotype control (Southern Biotech) were coated at 2 µg/ml on a flat bottom MaxiSorp 454 96-well plate in 50 µl/well in sodium carbonate-bicarbonate buffer (pH 9.5) for 16 hours. The plate was washed three times with PBS/T, blocked with 300 µl 1% BSA and washed again three times. 50 µl streptavidin-HRP (BD) diluted 1:250 was added for 1 hour. Plate was washed again eight times and 50 µl 1-step Ultra TMB (Thermo Fisher Scientific) was added. Reaction was stopped with 25 µl 2M H₂O₂ (Merck) and emission was measured at 450 nm using a plate reader.

2.2.7 Metabolomics analysis of ileum content

ASF³, ASF⁷, Oligo-MM¹² and SPF mice were sacrificed and samples for metabolomics analysis established simultaneously with the progressing of mLNs and SI for intestinal T cell flow cytometric staining (see protocol above). Excised SI was divided into three parts of equal length representing duodenum, jejunum and ileum (descending from the stomach). From the ileum three content samples were generated by squeezing out ileum content from 1 cm sections with a sterile pipette tip. All content samples were immediately snap frozen in 1.5 ml reaction tubes in liquid nitrogen. Samples were stored at -80°C until further processing. Two of the ileum content sample underwent untargeted metabolomics analysis, the third one for targeted metabolomics analysis (see Figure 3).

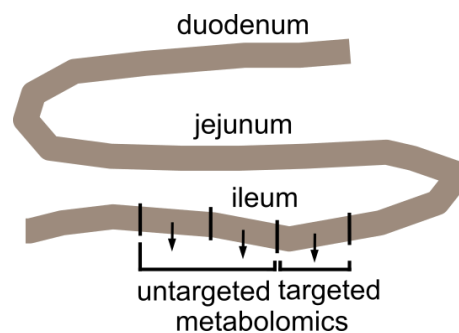


Figure 3: Sample generation for untargeted and targeted metabolomics

Ileum content was removed from tissue pieces for metabolomics analysis

2.2.7.1 Untargeted metabolomics

Two samples of ileum content per mouse of 4 mice per group (ASF³, Oligo-MM¹², SPF inhouse) were thawed on ice, weighed and double the volume of ddH₂O (autoclaved MilliQ) was added to one sample/mouse, to the other sample of the same mouse Methanol (Merck) was added. 1 mg corresponded to 1 µl volume. Debris was removed by three centrifugation steps, centrifuging once at 2000xg for 20 min and two times at 6000xg for 5 min. Afterwards quality control samples were set up by pooling 5 µl of each sample into one reaction tube. Supernatants were transferred to BayBioMS (Freising, Germany) for further liquid chromatography-mass spectrometry (LC-MS/MS) measurement and data processing. Each sample was measured in positive and negative ionization mode. The raw files were first converted to mzXML format via the ProteoWizard msConvert [121]. Peak-picking, alignment, correspondence was performed using the peak-density method and peak-grouping were performed using the previously published R-package “xcms” available via the Bioconductor website for bioinformatic processing [122–124]. The ion mass of the features was compared to different databases (MS1 annotation), including the MS-DIAL public datasets, Human Metabolome Database (HMDB) and in-house reference databases (DBs), allowing common modifications and a tolerance window of mass (15 ppm). The cosine distance between measured and reference spectra was calculated (MS2 annotation). The metabolite intensities were log transformed before statistical analysis. Detected metabolites were evaluated for correct annotation by reviewing

chromatographic characteristics between DB and measured metabolites or by availability of data of reference standards. For data analysis, a t-test with multiple testing correction was performed between ASF³, Oligo-MM¹² and SPF (fdr-value) and a fold change between the mean of each group was calculated for comparison by BayBioMS. Chromatograms of each compound of interest was checked for quality. Features that did not meet quality standard were discarded from analysis.

2.2.7.2 Targeted metabolomics

One ileum content sample per mouse of 4 mice per group from two experimental setups were used for targeted metabolomics analysis. One setup was derived from gnotobiotic mice derived from the AG Stecher from the Pettenkofer institute (ASF³, Oligo-MM¹², SPF inhouse) that were also used for untargeted metabolomics analysis and the other from gnotobiotic mice derived from the AG Bleich from the Hannover Medical School (ASF⁷, Oligo-MM¹², SPF from Charles River Germany). Frozen content samples were thawed on ice, weighed for later normalization and transferred to Precellys Lising Kit Tubes filled with ceramic beads (Bertin Technologies, Montigny-le-Bretonneux, France). Tubes were then sent on dry ice to BayBioMS for further processing to their internal protocol as follows: 1 ml methanol-based dehydrocholic acid extraction solvent (1.3 $\mu\text{mol/l}$) as an internal standard for work-up losses was added and homogenized by bead beating using a bead beater (Precellys Evolution, Bertin Technologies) supplied with a Cryolys cooling module (Bertin Technologies, cooled with liquid nitrogen) 3 times each for 20 seconds with 15 seconds breaks in between, at a speed of 10,000 rpm. After centrifugation of the suspension (10 min, 8000 rpm, 10 °C), using an Eppendorf Centrifuge 5415R (Eppendorf), 100 μL clear supernatant was mixed with 20 μL deuterated internal standard solution ($c=7 \mu\text{mol/L}$) for ionisation losses and injected into the LC-MS/MS system for targeted bile acid analysis. 40 μl clear supernatant was mixed with 15 μl internal standard solution, 20 μL EDC-solution and 20 μL 3-NPH-solution in a 1.5 ml Eppendorf-Cap. After shaking for 30 min at 40°C 905 μL ACN/H₂O (1/1, v/v) was added. After centrifugation for 2 min at 10,000 rpm the supernatant was transferred to a LC-MS/MS vial for short-chain fatty acid analysis. 0.5 ml clear supernatant was transferred to a LC-MS/MS vial for untargeted measurement. Depending on the sample size 10-100 μl of each sample was pooled to prepare a QC-sample. The leftover supernatant was transferred to a 2 ml Eppendorf-tube and stored at -80°C for potential further analysis.

The following bile acids (BAs) were measured:

- Primary BAs and their conjugates:
 - chenodeoxycholic acid, taurochenodeoxycholic acid, glycochenodeoxycholic acid
 - cholic acid, glycocholic acid, taurocholic acid

- α -muricholic acid, tauro- α -muricholic acid
- β -muricholic acid
- γ -muricholic acid / hyocholic acid, glycohyocholic acid
- ω -muricholic acid, tauro- ω -muricholic acid
- Unconjugated secondary BAs: deoxycholic acid, 5 β -cholic acid-3 α -ol-7-one / 7-ketolithocholic acid, 5 β -cholic acid-3 α -ol-12-one / 12-ketolithocholic acid, 5 β -cholen-24-oic acid-3,12-diol / apocholeic acid, lithocholic acid, ursodeoxycholic acid (in mice also a primary bile acid [125]), murideoxycholic acid, allolithocholic acid, isodeoxycholic acid, 3-dehydrocholic acid, 5 β -cholic acid-3 α -ol-6,7-dione / 6,7-diketolithocholic acid, 5 β -cholic acid-3 α -ol-6-one / 6-ketolithocholic acid, 7-dehydrocholic acid, isolithocholic acid, allocholic acid, ursocholic acid, cholic acid-7-sulphate / 7-sulfocholic acid, 12-dehydrocholic acid, β -cholic acid-7 α -ol-3-one, 5 β -cholic acid-3 α -ol-7,12-dione / 7,12 diketolithocholic acid, dehydrolithocholic acid, lithocholenic acid, obeticholic acid, hyodeoxycholic acid
- Secondary BAs conjugated to glycine: glycodeoxycholic acid, glycolithocholic acid, glycohyodeoxycholic acid, glycoursodeoxycholic acid
- Secondary BAs conjugated to taurine: taurodeoxycholic acid, tauroursodeoxycholic acid, taurohyodeoxycholic acid, tauroolithocholic acid

The following short-chain fatty acids (SCFAs) were measured: acetic acid, propionic acid, isobutyric acid, butyric acid, 2-methylbutyric acid, valeric acid, 4-methylvaleric acid, hexanoic acid, lactic acid, desaminotyrosine, indol-3-acetic acid, indol-3-carboxyaldehyd

2.2.8 Statistical analysis

For statistical analysis, a one-way ANOVA with Tukey's multiple comparisons test was performed with GraphPad Prism 7. A p value of $p < 0.05$ was considered statistically significant.

3 RESULTS

3.1 Microbial impact on immune tolerance using gnotobiotic mice

3.1.1 Preamble

A subpopulation of Tregs can be peripherally induced by microbial antigens and metabolites [43–47]. These pTregs can be characterized by the expression of transcription factor ROR γ t, are negative for Helios and can be induced by mono-colonizing mice with individual intestinal bacteria in the colon to a variable extent and independent of their phylum [34]. GF mice have a drastic decrease in ROR γ t+ Helios- Tregs compared to SPF mice in the SI and colon that can be replenished by recolonization with e.g. *clostridia* strains [33]. ROR γ t+ Tregs have been shown to be important to restrict Th2 cell associated pathologies [33] and are protective in a murine model of food allergy [83]. Gnotobiotic mouse models with reduced microbial complexities offer a more complex intestinal microbiome than mono-colonized or GF mice with a known and stable microbial community when regularly controlled [126].

The aim of this results chapter was to compare T cell, DC and ILC populations of mouse groups from different microbial complexities, investigate differences of their intestinal metabolomes for immune cell priming and determine whether a reduced intestinal microbial complexity segregates with enhanced susceptibility to food allergy. The most complex microbiota was represented by SPF mice. Gnotobiotic animals with a known microbial status were either colonized and maintained with the Oligo-MM¹² consortium [111, 112] or the ASF flora [110] with either 3 strains or compiled of all detectable 7 strains (ASF³, ASF⁷). The last mouse group was devoid of intestinal microbiota (GF). For further details see 2.1.6 Mouse lines. Inclusion and exclusion of mouse groups was due to availability of animals for experimentation.

3.1.2 Gnotobiotic animals display changed frequencies in T cell populations compared to SPF mice particularly in the small intestine

First, the lamina propria of the small intestine (LP-SI) was investigated in gnotobiotic animals with reduced complexities (ASF³, ASF⁷ and Oligo-MM¹²) and compared to SPF mice with the highest abundance of microbial species regarding frequencies of pTregs. These pTregs were characterized by the expression of ROR γ t and being negative for transcription factor Helios. SPF mice showed significantly higher frequencies of ROR γ t+ Helios- Tregs (referred to as pTregs) in the LP-SI than Oligo-MM¹², ASF⁷ and ASF³ animals (Figure 4A). Regarding ASF³ and Oligo-MM¹² animals, pTreg

frequency correlated with microbial complexity as pTregs in ASF³ animals were significantly less frequent than in Oligo-MM¹² mice. ASF⁷ animals displayed a higher relative abundance of pTregs than ASF³ and Oligo-MM¹² animals, but a lower abundance than SPF. While ASF³, Oligo-MM¹² and SPF animals were born from mothers with a similar microbial status, ASF⁷ mice had been born from GF mothers and were inoculated at 3 weeks of age with respective bacterial strains. The different time points of colonization could explain differences in pTreg frequency not correlating with microbial complexity.

Regarding Th2 cells in the LP-SI an inverse correlation with microbial complexity was visible. SPF animals had significantly less Th2 cells in the LP-SI than ASF³, while Oligo-MM¹² animals had significantly less Th2 cells than ASF³ animals but more than SPF (Figure 4B). The mean frequency of Th2 cells in the SI of ASF⁷ animals was similar to Oligo-MM¹² animals, however due to the low sample number the frequency of Th2 cells was not significantly different to ASF³, Oligo-MM¹² and SPF.

As the pTregs positively correlated with microbial complexity and Th2 cell frequency in the SI negatively correlated with microbial complexity, a ratio for each mouse was calculated (Th2 frequency divided by pTreg frequency in the SI per mouse) confirming the inverse correlation of pTregs and Th2 cells for each single mouse (Figure 4C).

The correlation between microbial complexity and pTreg frequencies was also observable in the mLNs with the highest abundance in SPF, followed by Oligo-MM¹² and ASF⁷ and ASF³ mice (Figure 4D). SPF mice significantly showed the highest frequency in pTregs compared to gnotobiotic groups, however the difference between SPF and Oligo-MM¹² did not reach significance ($p=0.063$). The correlation between reduced microbial complexity and a reduction in pTregs was therefore also visible in organs more distant from the SI. In the spleen, pTreg frequencies were highest in SPF mice with large variability, less frequent in Oligo-MM¹² than in SPF animals and least frequent in ASF³ mice (Figure 4E). The increase from ASF³ to SPF was statistically significant and was close to significance comparing Oligo-MM¹² and SPF mice ($p=0.059$).

The overall frequency of Treg abundance in the LP-SI was comparable between ASF³, Oligo-MM¹² and SPF mice, however ASF⁷ mice displayed a significantly enhanced frequency of Tregs compared to all other groups (Figure 4F).

Regarding other immune cells than pTregs and Th2 cells in the SI, Th17 cells were significantly more abundant in SPF mice than in ASF³, ASF⁷ and Oligo-MM¹² mice (Figure 4G). Segmented filamentous bacteria (SFB) were shown to induce Th17 cells in the intestine [127]. These SFBs were not contained in ASF³, ASF⁷ and Oligo-MM¹² microbial species, but could have been part of the SPF microbiome. The increased abundance in ASF⁷ could be explained by the later introduction of the microbiota (post-weaning) in ASF⁷ mice.

Tissue Tregs in the intestine are a regulatory cell type that are distinct from pTregs in their phenotype, epigenetic profile of differentially regulated Th2 associated loci and are important for tissue homeostasis [27, 128]. Tissue Tregs (defined here as GATA3⁺ Helios⁺ regulatory Tregs), were not correlated with microbial complexity. ASF⁷ and Oligo-MM¹² mice had the highest abundance compared to ASF³ and SPF animals (Figure 4H).

ILCs were defined here as CD45⁺, lineage negative lymphoid cells and the relative distributions of their subpopulations based on expression of GATA3 (ILC2s) or ROR γ t (ILC3s). ILC2s were decreased in ASF⁷ mice in comparison to ASF³, Oligo-MM¹² and SPF mice which displayed comparable frequencies of ILC2s in the LP-SI (Figure 4I). ILC3s (ROR γ t⁺ ILCs) were inversely correlated with ILC2 frequencies. ASF⁷ mice had the highest relative abundance of ILC3s while ASF³, Oligo-MM¹² and SPF mice had comparable numbers (Figure 4I). The variability of both ILC2s and ILC3s among the mouse groups was high, possibly also due to a high dependency of their percental abundance on the procedure of each experimental day. However, a difference in ILC2s to ILC3s ratio did not follow a pattern that segregated with microbial complexity.

In summary, a correlation of bacterial complexity with immune cell frequencies in the T cell and ILC compartments was most obvious for the relative abundance of pTregs (ROR γ t⁺ Helios⁻ Tregs). pTregs segregated with bacterial complexity most visibly in the LP-SI but also in other organs such as the mLNs and the spleen. Furthermore, there was an inverse correlation of Th2 cells and pTregs visible in the SI-LP that could prone mice with a low microbial complexity to Th2 cell mediated diseases in the intestine such as food allergies.

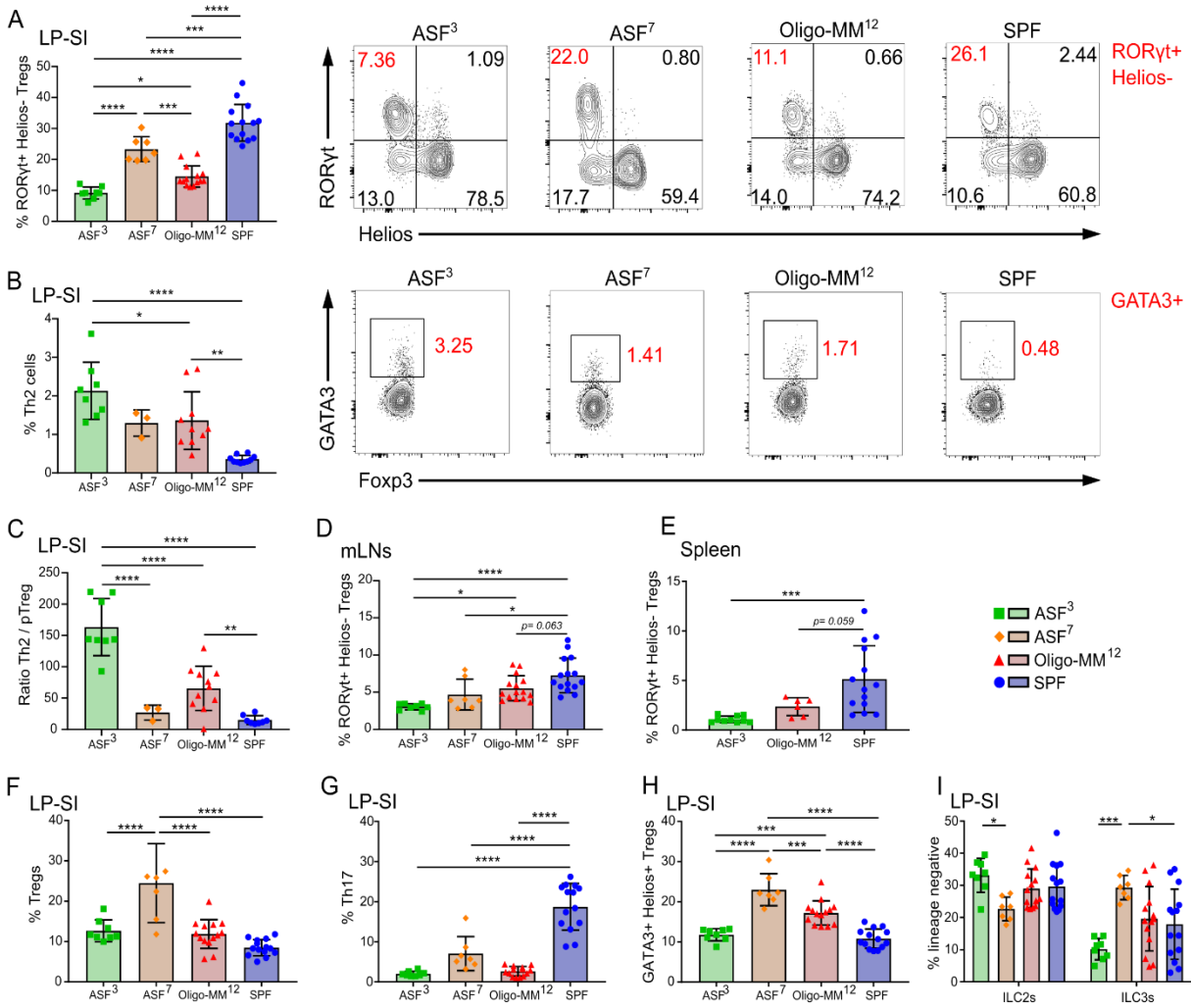


Figure 4: Decrease in RORγt+ Helios- Tregs and increase in Th2 cells correlates with decreased microbial complexity

(A) Frequency (%) of RORγt+ Helios- Tregs as determined by gating Foxp3+ CD3+ CD4+ cells for RORγt+ and Helios- in the LP-SI of ASF³, ASF⁷, Oligo-MM¹² and SPF mice (left). Representative flow cytometry plots of RORγt+ Helios- Tregs (right) in the LP-SI. **(B)** Th2 cell frequency of all Foxp3- CD3+ CD4+ T cells (pregated: CD45+, live) among gnotobiotic and SPF groups in LP-SI (left). Representative flow cytometry plots of % Th2 cells (right). **(C)** Ratio of % Th2 cells divided by % RORγt+ Helios- Tregs of all CD4+ T cells per mouse in LP-SI. **(D, E)** % of RORγt+ Helios- Tregs in other organs than SI: **(D)** mLN and **(E)** spleen. **(F-I)** Frequencies of further immune cell populations in the LP-SI: **(F)** % of all Tregs (Foxp3+ of CD4+ T cells), **(G)** Th17 cells (% RORγt+ of Foxp3- CD4+ CD3+), **(H)** GATA3+ Helios+ tissue Tregs (of Foxp3+ CD3+ CD4+), and **(I)** frequencies of ILC subpopulations, ILC2s (GATA3+) and ILC3s (RORγt+) pregated for CD3- lineage- CD45+ cells. **(A-D, F-I)** Age of mice: 7-10 weeks. Data merged from 4 different experiments. **(E)** Age of mice: 5-9 weeks. Data merged from 3 different experiments. **(A-I)** Mice were mixed-gender. Testing for significance was performed with one-way ANOVA with Tukey's multiple comparisons test. Multiple comparisons were performed within each cell population comparing different mouse colonization groups. Significance is indicated as *p<0.05, **p<0.01, ***p<0.001, ****p<0.0001. Complete gating depicted in Appendix Figure 15.

3.1.3 Gnotibiotic animals display an increase in cDC2s in mLNs and SI

DCs play an important role in priming T cell responses. CDCs are implicated in oral tolerance induction to dietary antigens as they are critical for pTreg cell induction [37]. In order to examine the effect of a reduced microbial complexity on the frequency of DCs, cDC subpopulations were assessed of the same mouse groups used for the evaluation of T cell and ILC populations (ASF³, Oligo-MM¹², SPF), except ASF⁷. The overall frequency of cDCs was compared between ASF³, Oligo-MM¹² and SPF animals and found to be comparable between groups (Figure 5A).

CDCs (CD11c⁺, MHCII⁺ CD64⁻) were first gated for expression of CD8 α (cDC1s) and SIRP α (cDC2s) [20]. An inverse correlation between microbial complexity and relative abundance of SIRP α ⁺ cDC2s was visible, as ASF³ mice displayed significantly higher frequencies of SIRP α ⁺ cDC2s than Oligo-MM¹² and SPF animals, while Oligo-MM¹² tended to display a higher frequency than SPF mice though not significantly (Figure 5B). The inverse trend was observed for cDC1s with the highest frequency visible in SPF mice (Figure 5B).

Another way of gating for cDC subpopulations is the use of CD11b and CD103 surface marker expression [19]. In the mouse intestinal LP, three cDC subpopulations have been described: CD103⁺ CD11b⁻ cDC1s, and cDC2s which are either CD11b⁺ CD103⁺ or CD11b⁺ CD103⁻ [19]. (DP) CD11b⁺ CD103⁺ DCs cDC2s inversely correlated with microbial complexity (Figure 5C). Single positive (SP) cDCs that were either CD103⁺ CD11b⁻ cDC1s or CD11b⁺ CD103⁻ cDC2s were more abundant in SPF mice than in ASF³ mice. Oligo-MM¹² animals aligned for SP CD103⁺ cDC1s with ASF³ mice, for SP CD11b⁺ cDC2s the results were variable, as three Oligo-MM¹² mice exceeded in their frequency all other groups (Figure 5C). If gating for cDC1s and cDC2s was performed with CD8 α and SIRP α first (as in Figure 5B) and the SIRP α ⁺ cDC2s were gated in a second step for CD11b and CD103 expression, it became apparent that specifically SP CD11b⁺ cDC2s were decreased in mouse groups with lower microbial complexity (ASF⁷, Oligo-MM¹²) that results in a frequency increase in CD11b⁺ CD103⁺ DP cDC2s (Figure 5D).

Regarding lymphoid tissues, the frequency of resident and migratory cDCs in the mLNs was comparable among mouse groups (Figure 5E). Among the resident cDCs in the mLNs the same trend as in the LP-SI was visible: while CD8 α ⁺ cDC1s increased with microbial complexity, SIRP α ⁺ cDC2s decreased, with the highest frequencies visible in ASF³ and Oligo-MM¹² compared to SPF mice (Figure 5F). Among the migratory cDCs in the mLNs, the frequency of CD8 α ⁺ cDC1s did not vary among the mouse groups of different microbial complexities (Figure 5G). In contrast, a higher frequency of SIRP α ⁺ migratory cDC2s was visible, inversely correlating with microbial complexity, even though only the increase in ASF³ in comparison to SPF mice for this cell population was significant. The difference of SPF vs Oligo-MM¹² and Oligo-MM¹² vs ASF³ was close to significance (p=0.055, p=0.051)

(Figure 5G). Lastly, if the migratory DCs were discriminated for CD11b or CD103 expression, trends observed in the SI could be recapitulated: the frequency of DP CD11b⁺ CD103⁺ cDC2s decreased with microbial complexity while SP CD103⁺ CD11b⁻ cDC1s increased with microbial complexity with the highest amount in SPF mice (Figure 5H). CDC subpopulations were also investigated in the colon, however changes were not consistent among two experiments (data not shown).

Overall, significant differences in DC populations in the SI and mLNs of ASF³, Oligo-MM¹², SPF were visible that were comparable in both organs. This included the significant relative increase in SIRP α ⁺ cDC2s inversely correlating with microbial complexity and simultaneously a tendency of decreased CD8 α ⁺cDC1s (LP-SI and resident mLNs). Furthermore, DP CD11b⁺ CD103⁺ cDCs were lowest in mice with microbial complexity (lower in SPF than ASF³ and Oligo-MM¹²), which could partly be explained by an increase in SP CD11b⁺ among the cDC2 population in the SI correlating with microbial complexity (higher in SPF than ASF³ and Oligo-MM¹²). SP CD11b⁺ cDC2s in the SI or SP CD103⁺ cDC1s whose reduction was visible both in the SI and mLNs could be important for Treg induction, as they were reduced in gnotobiotic animals. Changes in ratios of cDC subpopulations could thus drive the changes in pTreg vs Th2 ratios in the intestine.

III.1 Results

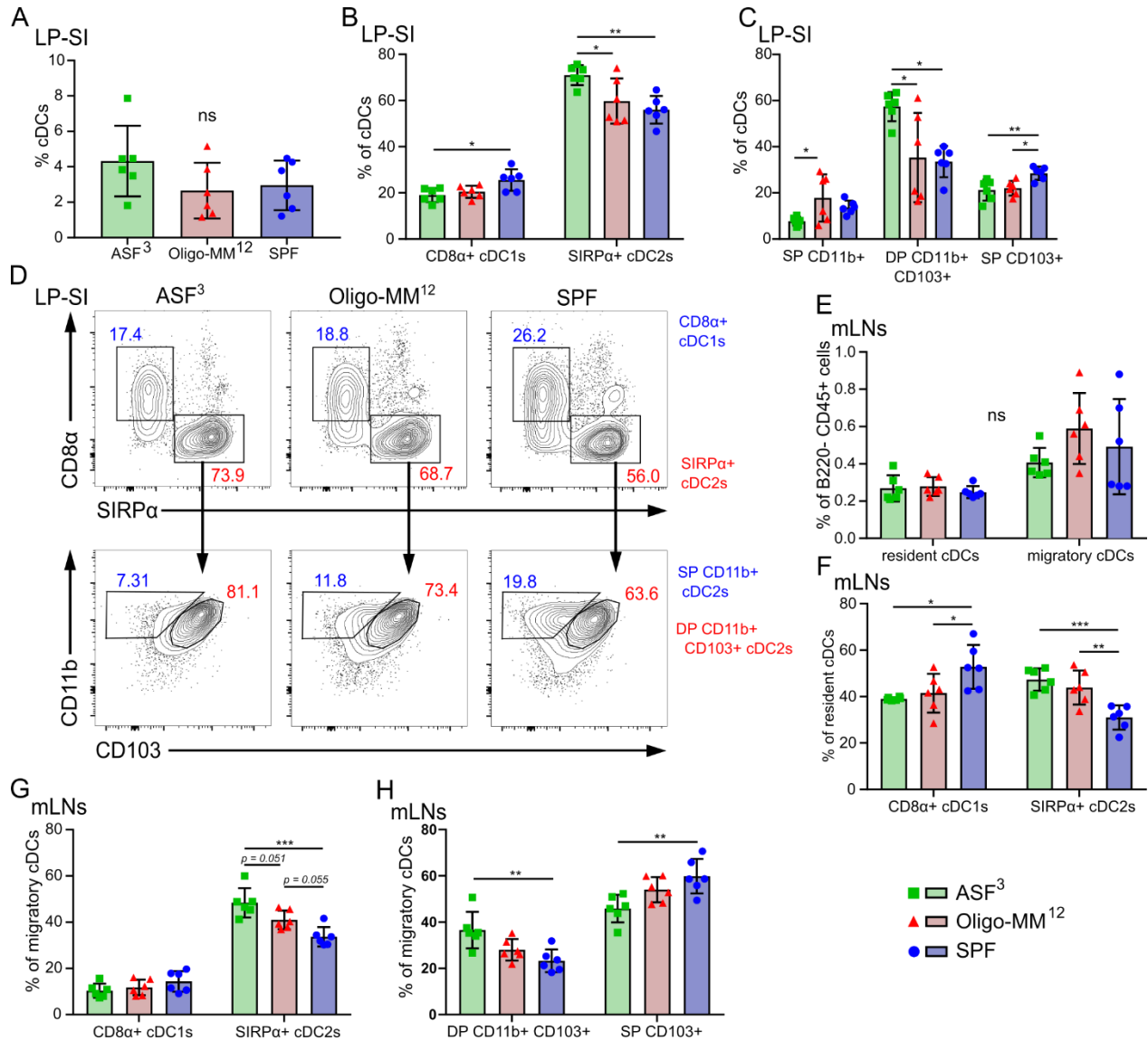


Figure 5: Increase in cDC2s in mLN and SI correlates with reduced microbial complexity

(A) Frequency of overall cDCs as determined by gating for non-monocyte (CD64⁻) CD11c⁺ MHCII⁺ CD45⁺ cells in the LP-SI of ASF³, Oligo-MM¹² and SPF mice. **(B)** % of cDC1s (CD8 α +) and cDC2s (SIRP α +) subpopulations gated on overall cDCs in the LP-SI. **(C)** Gating cDCs for the markers CD11b vs CD103 to determine frequencies of single positive (SP) CD11b+ cDC2s, double positive (DP) CD11b+ CD103+ cDC2s and SP CD103+ cDC1s in the LP-SI. **(D)** Representative flow cytometry plots of CD8 α + cDC1s and SIRP α + cDC2s in LP-SI of **(B)** and gating SIRP α + cDC2s for CD11b and CD103 expression. **(E)** Overall % of resident and migratory cDCs in mLN (based on CD11c and MHCII+ expression gated on B220- CD45+ cells). **(F)** % of CD8 α + cDC1s and SIRP α + cDC2s of resident cDCs in mLN. **(G)** % of CD8 α + cDC1s and SIRP α + cDC2s of migratory cDCs in mLN. **(H)** Frequencies of DP CD11b+ CD103+ cDC2s and SP CD103+ cDC1s of migratory cDCs in mLN. **(A-H)** Data merged from two experiments. Mice were mixed-gender and age ranged from 5-7 weeks. Testing for significance was performed with an one-way ANOVA with Tukey's multiple comparisons test. Multiple comparisons were performed within each cell population comparing different mouse colonization groups. Significance is indicated as *p<0.05, **p<0.01, ***p<0.001, ****p<0.0001. Only significant or close to significant bars are displayed. Gating strategy is displayed in Appendix Figure 16 and Figure 17.

3.1.4 Spatial distribution of pTregs reveals highest frequency in colon and representative frequency in ileum SI segment

To assess whether ileal content from the SI is a fair representative for metabolomics analysis of the whole SI and whether the distribution of different T cell or ILC populations varies among the gut segments, the small intestine was cut into the three segments duodenum, jejunum and ileum and immune cell frequencies in the LP-SI were compared to the colon lamina propria. The experiment for each mouse group (GF, ASF³, Oligo-MM¹² and SPF) was performed separately in contrast to experiments in Figure 4 and Figure 5 in which mouse groups were assessed simultaneously.

First, overall Treg frequencies were assessed. In Oligo-MM¹² mice, Treg numbers among the intestinal segments were comparable, however in GF the ileum displayed less Tregs than all other three segments and in ASF³ mice the jejunum had increased Treg frequencies (Figure 6A). All mouse groups (GF, ASF³, Oligo-MM¹² and SPF) displayed an increased frequency of Tregs in the colon compared to duodenum, jejunum and ileum with wide variability. However, only in SPF mice the frequency of Tregs was significantly increased, possibly due to the highest abundance of colonizing bacteria or microbial complexity (Figure 6A).

pTregs (ROR γ t⁺ Helios⁻) frequencies did not vary in relative abundance among the four gut segments in GF mice, in mice colonized with bacteria (ASF³, Oligo-MM¹², SPF) the colon consistently showed slightly enhanced frequencies of pTregs (Figure 6B). Furthermore, the frequency of pTregs in the ileum was comparable to the duodenum and ileum in GF and SPF mice. In ASF³ mice, the ileum showed comparable frequencies to the jejunum, however the highest frequency of pTregs in the SI was seen in the duodenum. In the jejunum of Oligo-MM¹² mice there was a lower frequency of pTregs than in the duodenum and ileum, which had a comparable frequency of pTregs (Figure 6B). This might have been due to the different bacterial strains in the gnotobiotic animals colonizing different gut segments. If the microbiota was very complex as in SPF mice or devoid of bacteria in GF mice, the duodenum, jejunum and ileum displayed equal frequencies of pTregs.

Th2 cells did not vary among the different SI segments in mouse groups colonized by bacteria (ASF³, Oligo-MM¹² and SPF) (Figure 6C). In GF mice there was a slight increase in the ileum, but only statistically significantly enhanced between duodenum to ileum. The frequency of Th2 cells in the colon varied greatly and was increased in the gnotobiotic mouse groups (GF, ASF³, Oligo-MM¹²), but not in SPF animals (Figure 6C). Overall, comparing pTreg and Th2 cell frequency distribution among mouse groups of different microbial complexities, nearly the same result as in Figure 4 could be obtained even if the different mouse groups were analyzed in separate experiments: pTregs followed the pattern GF<ASF³<Oligo-MM¹²<SPF (Figure 6B) and Th2 followed the pattern SPF<Oligo-MM¹², ASF³<GF (Figure 6C) with Oligo-MM¹² and ASF³ sharing approximately the same relative abundance

of Th2 among the gut segments.

The results for ILCs showed that there were indeed differences in ILC2 (GATA3 expressing ILCs) and ILC3 (ROR γ t expressing ILCs) ratios observable in relation to their localization along the intestine. These differences were independent of bacterial colonization as they were also observable in GF mice. ILC2s increased in frequency from proximal to distal with the lowest frequency visible in the duodenum and the highest frequency in the colon (Figure 6D). This pattern was most visible in GF mice, though tendencies were also visible in ASF³, Oligo-MM¹² and SPF mice. In particular, the colon showed the highest frequency of ILC2s in all mouse groups (Figure 6D). The frequency of ILC3s could be seen as inverse to ILC2s. The highest abundance was found in the duodenum, decreasing in the jejunum and ileum with the lowest abundance in the colon in GF mice (Figure 6E). The significantly lowest frequency of ILC3s in the colon compared to the SI segments was visible also for all other mouse groups (ASF3, Oligo-MM12 and SPF). The decrease of ILC3s from the duodenum to the jejunum and ileum was only slightly visible for the Oligo-MM12 mouse group, but not at all for ASF3 and SPF animals (Figure 6E).

Since for the intestinal compartment analysis the additional mouse group of GF was available, analysis of pTregs in the mLN and spleen was performed again including GF mice. As in Figure 4D, frequencies of pTregs in the mLN followed the pattern ASF3<Oligo-MM12<SPF while the frequency in the GF was comparable to ASF3, the mouse group displaying the lowest frequency of pTregs (Figure 6F). The same result could be obtained for the spleen. Additionally, the data of Figure 4E could be confirmed as the pTreg frequency in the spleen followed the pattern GF, ASF3<Oligo-MM12<SPF (Figure 6G).

Altogether, the results showed that the ileum is a fair representation of the overall SI regarding frequency of pTregs and Th2 cells to use in metabolomics analysis to identify factors implicated in the observed immune cell frequencies. The most significant difference in the gut segments was seen for the ILC ratios with a significant increase in ILC2s in the colon compared to the SI and an inverse dependency for ILC3s (colon<SI segments).

III.1 Results

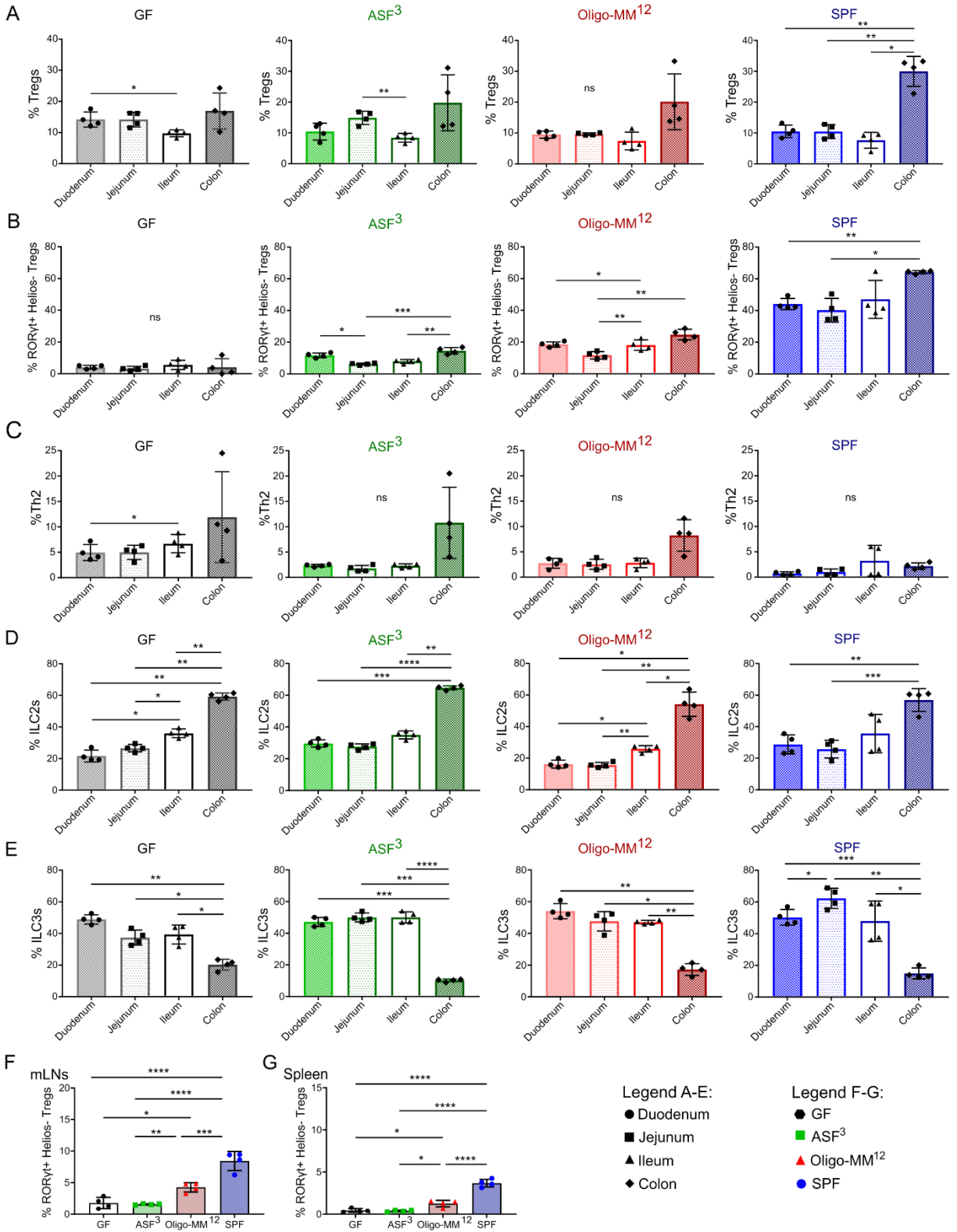


Figure 6: Spatial distribution of RORγt+ Helios- Tregs, Th2 and ILCs along the intestine
(A) Frequencies of regulatory T cells (% Foxp3 of CD4+ T cells) in the lamina propria of intestinal segments in descending order along the intestinal tract (duodenum, jejunum, ileum, colon) of GF,

ASF³, Oligo-MM¹², and SPF mice. **(B-E)** Mouse groups and organs as in **(A)**. **(B)** Frequencies of ROR γ ⁺ Helios⁻ Tregs (ROR γ ⁺ Helios⁻ % of Foxp3⁺). **(C)** Frequencies of Th2 cells (GATA3⁺ of Foxp3⁻ CD4⁺ T cells). **(D)** Frequencies of ILC2s (GATA3⁺ of CD3⁻ lineage⁻ CD45⁺ cells). **(E)** Frequencies of ILC3s (ROR γ ⁺ of CD3⁻ lineage⁻ CD45⁺ cells). **(F)** Frequencies of ROR γ ⁺ Helios⁻ Tregs (% of Foxp3⁺ CD4⁺ T cells) in mLNs of the mouse groups GF, ASF³, Oligo-MM¹² and SPF mice. **(E)** Frequencies of ROR γ ⁺ Helios⁻ Tregs (% of Foxp3⁺ CD4⁺ T cells) in spleen. Mouse groups as in **(F)**. **(A-G)** Data merged from four different experiments. Each mouse group was examined in a separate experiment. Mice were mixed-gender and age ranged from 10-12 weeks. Testing for significance was performed with an one-way ANOVA with Tukey's multiple comparisons test. Significance is indicated as *p<0.05, **p<0.01, ***p<0.001, ****p<0.0001. Only significant or close to significant bars are displayed. Gating strategy is displayed in Appendix Figure 15.

3.1.5 Metabolomic analysis of ileum content samples reveal changes in bile acid metabolism comparing mouse groups of differential microbial complexity

To investigate which metabolites correlated with microbial diversity and pTreg or Th2 cell frequency patterns in the intestine of the mouse groups in Figure 4 A,B, a metabolomics analysis was performed to identify possible inducers and repressors of pTreg induction. These metabolites could be either produced by the microbiota itself or by metabolizing host molecules. The ileum lamina propria frequencies of pTreg and Th2 cells had been determined as a fair representation of the whole SI for ASF³, Oligo-MM¹² and SPF mice (Figure 6B,C) used for immune cell frequency and metabolite correlation in this metabolomics experiment.

First, an unbiased approach to measure all metabolites contained in ileum content samples was performed by an untargeted metabolomics measurement that allowed relative comparison of feature intensities between mouse groups. Ileum content samples were either diluted in H₂O or Methanol (MetOH) as it was unknown in which solution more metabolites could be solved and identified in a LC-MS/MS measurement. After analysis of the untargeted metabolomics, an ileum content sample of the same mouse was used for targeted metabolomics of BAs and SCFAs. A scheme of the untargeted and targeted metabolomics approach and analysis procedure of untargeted metabolomics is depicted in Figure 7A. The untargeted metabolomics analysis was performed on ileum content samples derived from animals of mouse groups ASF³, Oligo-MM¹² and SPF (Figure 7B). Intensities of m/z spectra were correlated to the pTreg and Th2 frequencies stained from the whole SI of these mice. For statistical analysis a t-test was performed with multiple correction of the mean intensities per metabolite within a mouse group. Features that aligned with the pattern ASF³<Oligo-MM¹² and Oligo-MM¹²<SPF based on a negative mean difference ASF³ vs Oligo-MM¹² or Oligo-MM¹² vs SPF were selected as possible pTreg inducing metabolites (complete list depicted in Appendix Table 7 - Table 10). A false discovery rate (fdr) below 0.05 meant statistical significance between groups. The features resulting from two different modes (negative/positive) and solvents (ddH₂O, MetOH) were assessed separately. The

same analysis was performed for Th2 cells but in an inverse correlation: ASF³>Oligo-MM¹² and Oligo-MM¹²>SPF based on a positive mean difference ASF³ vs Oligo-MM¹² or Oligo-MM¹² vs SPF (only MetOH positive mode is shown as it resulted in the most features, see Appendix Table 11). More details regarding the analysis is described in 2.2.7 Metabolomics analysis of ileum content. The identification of metabolites from the measured features in the untargeted metabolomics analysis depended on how well features could be annotated. Most features were annotated from internal standards since annotation from the HMDB database resulted in fewer alignments (Appendix Table 7 - Table 11). None of the features displayed significant mean intensity differences within mouse groups for both cases ASF³ vs Oligo-MM¹² and Oligo-MM¹² vs SPF (fdr<0.05). The features were mostly significant for the latter case. While ASF³ and Oligo-MM¹² mice differed significantly in their pTreg frequencies in the SI, most metabolites that also differed between Oligo-MM¹² and SPF were not significantly different comparing ASF³ and Oligo-MM¹². Assessing the type of metabolites that correlated with pTreg frequencies in the SI, it became apparent that numerous annotations were part of the BA metabolism (see Appendix Table 7 - Table 10). Since BAs had been described as possible pTreg inducers [45–47] a targeted measurement of BAs was performed next (all measured BAs are listed in 2.2.7.2 Targeted metabolomics). Additionally, as certain SCFAs, such as butyrate, had been identified as pTreg inducers [43], a targeted analysis of SCFAs was included to assess if pTreg differences could be due to a difference in SCFAs abundance among the mouse groups. Targeted metabolomics allows the quantitative measurement of analytes with higher accuracy of metabolite identification than untargeted metabolomics. For the targeted metabolomics analysis, further mouse groups that were derived from a different facility than the ones used in untargeted metabolomics (Figure 7B) were included in the analysis. These mouse groups were ASF⁷, Oligo-MM¹² and SPF and their pTreg frequency is displayed in Figure 7C. As these two mouse cohorts were derived from different facilities and in particular the microbiota of SPF animals can differ quite distinctly between facilities, they were plotted separately and indicated as “B” and “C” referring to Figure 7B and Figure 7C.

BAs are synthesized in the liver either unconjugated or in a conjugated form to glycine or taurine [125]. BAs play an important role in lipid metabolisms [129]. Primary BAs can be metabolized by the intestinal microbiota into secondary BAs, but also enzymes for primary BA metabolism (and not just secondary BAs) can be influenced by the microbiota [125]. Regarding the primary BAs and their conjugates to glycine and taurine, it became apparent that there is an effect of microbial colonization visible in primary and secondary BAs abundance, however this depended on the conjugate. The concentration of chenodeoxycholic acid (CDCA) and its glycine conjugate glycochenodeoxycholic acid (GCDCA) in ileal content followed a similar pattern as the pTreg distribution in the SI (Figure 7B, C). However, for CDCA ASF⁷ mice showed equal levels as ASF³ and for GCDCA Oligo-MM¹² mice displayed

equal amounts to ASF³ in the B-group (Figure 7D). The taurine-conjugate taurochenodeoxycholic acid (TCDCA) did not follow any pattern segregating with pTreg frequencies. The same was observed for cholic acid (CA). While CA and to a lesser extent glycocholic acid (GCA) were strongly correlated with pTreg frequencies (except for ASF⁷), taurocholic acid (TCA) did not correlate with pTreg frequencies in the SI (Figure 7D). α -muricholic acid (α -MCA) and β -muricholic acid (β -MCA) showed the pattern ASF³, ASF⁷<Oligo-MM¹²<SPF to a lesser extent, while there were no differences between groups visible for tauro- α -muricholic acid (T- α -MCA, Appendix Figure 18A). γ -muricholic acid/hyocholic acid (γ -MCA), glycohyocholic acid (GHCA), ω -muricholic acid (ω -MCA) and tauro- ω -muricholic acid (T- ω -MCA) concentrations were highest in SPF mice, however ASF³, ASF⁷ and Oligo-MM¹² mice had comparable levels or were equally not detectable (Appendix Figure 18A). This is intriguing since ω -MCA had been described as a pTreg inducer [47].

For the secondary BAs, SPF mice displayed the highest concentration of measured unconjugated secondary BAs (Figure 7E) except for 7-sulfo-cholic acid (7-SCA) that also did not correlate with pTreg frequencies in the SI and 12-ketolithocholic acid (12-KLCA) which was measured only in the SPF B group with a high concentration (Appendix Figure 18B). Regarding a concentration increase from ASF³ to Oligo-MM¹² which would suggest that the particular secondary BA would be a pTreg inducer, 7-dehydrocholic acid (7-DHCA), 7-ketolithocholic acid (7-KLCA), ursodeoxycholic acid (UDCA, in mice also a primary BA [125]), 3-dehydrocholic acid (3-DHCA) andursocholic acid (UCA) could be identified (Figure 7E). However, as for the primary BAs, ileum content samples from ASF⁷ mice displayed comparable concentrations to ASF³ mice. All other unconjugated secondary BAs that did not show differences between ASF³ and Oligo-MM¹² mice or were not detectable are displayed in the Appendix Figure 18B, including lithocholic acid (LCA) which derivatives were shown to be stimulatory for Th17 and Treg cells [46] and isodeoxycholic acid (IDCA) was described as a pTreg inducer [47]. Interestingly, the conjugated secondary BAs (to glycine or taurine) followed the patterns of most unconjugated secondary BAs. There were no differences visible comparing ASF³ and Oligo-MM¹² mice for the largest amount of secondary BAs (7,12 diketolithocholic acid (7,12-DKLCA), glycodeoxycholic acid (GDCA), glyoursodeoxycholic acid (GUDCA), taurohyodeoxycholic acid (THDCA), taurodeoxycholic acid (TDCA)) except for β -cholic acid-7 α -3one (Ca-7 α -3one), which was more abundant in the Oligo-MM¹² mice from the C group and tauroolithocholic acid (TLCA), which was more abundant in the Oligo-MM¹² mice from the B group (Appendix Figure 18C,D). Tauroursodeoxycholic acid (TUDCA) was unchanged in between all mouse groups (Appendix Figure 18D).

Regarding the SCFAs, SPF mice displayed the highest concentration of acetic acid, propionic acid, lactic acid and butyric acid compared to Oligo-MM¹² and ASF³ mouse groups of B and C indicating a

similar pattern as for the BAs (Figure 7F). Regarding a difference between ASF³ and Oligo-MM¹² only acetic acid showed a higher amount in Oligo-MM¹² mice and very slightly propionic acid. For butyric acid there were no differences visible comparing ASF³, ASF⁷ and Oligo-MM¹² mouse groups. Lactic acid was more abundant in ASF³ and ASF⁷ than in Oligo-MM¹² mice. Overall, the concentration of SCFAs was low. Only the ones that could be measured are shown in Figure 7F. isobutyric acid, 2-methylbutyric acid, valeric acid, 4-methylvaleric acid, hexanoic acid, desaminotyrosine, indol-3-acetic acid, indol-3-carboxyaldehyd were not detectable. Again, ASF⁷ mice did not show a higher abundance of any SCFA than ASF³ mice indicating none of these metabolites (measured BAs and SCFAs) was responsible for the higher pTreg frequency in the SI-LP in ASF⁷ mice compared to ASF³ mice.

All in all, a difference in microbial complexity and colonization resulted in changes in the ileal concentrations of primary and secondary BAs. Regarding conjugated primary BAs, glycine conjugates seemed to correlate more with microbial complexity than taurine-conjugates. Numerous primary and secondary BAs and the SCFA acetic acid that follow the pattern ASF³<Oligo-MM¹²<SPF could be implicated in pTreg induction, however they would not be responsible for induction in ASF⁷ animals compared to ASF³ animals. Furthermore, targeted measurement of BAs confirmed untargeted metabolomic analysis that indicated correlation of pTreg frequencies with the concentration of metabolites of the BA metabolism (e.g. cholic acid). Overall, the Oligo-MM¹² and SPF mouse groups that were either derived from B or C had similar concentrations of the measured metabolites indicating that mouse groups can be merged for analysis (as done in Figure 4).

III.1 Results

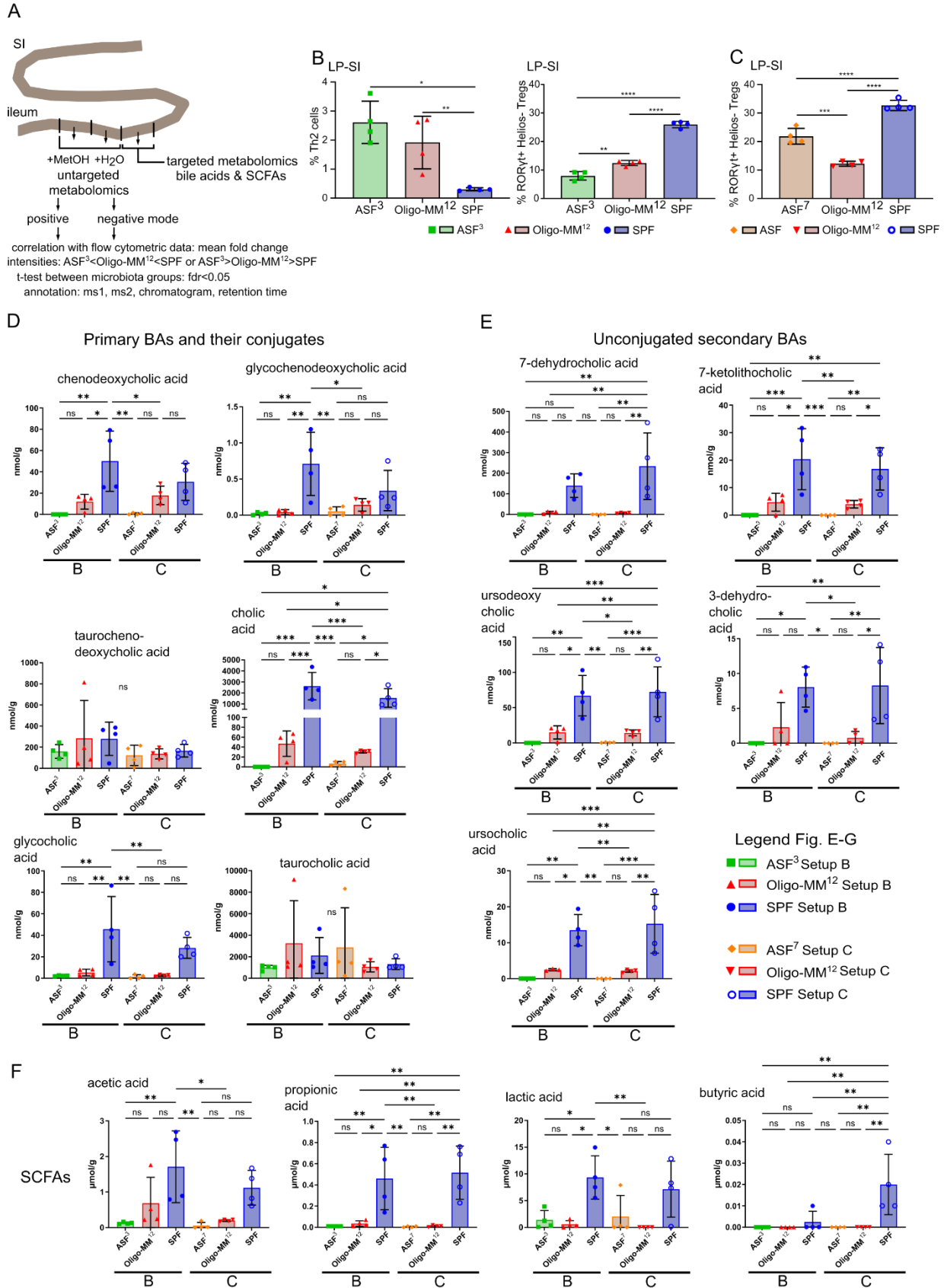


Figure 7: Untargeted and targeted metabolomic analysis of ileum content samples of gnotobiotic and SPF mouse groups

(A) Scheme of untargeted and targeted metabolomic analysis strategy of ileum content samples. For untargeted measurement the mouse groups from one experiment were the following: ASF³, Oligo-MM¹², SPF. For targeted analysis, samples from an additional experiment (ASF⁷, Oligo-MM¹², SPF) were included. **(B)** Frequencies of Th2 (GATA3⁺ of CD4⁺ T cells) and ROR γ t⁺ Helios⁻ Tregs (of Foxp3⁺ CD4⁺ T cells) of mice used for untargeted metabolomics. **(C)** % of ROR γ t⁺ Helios⁻ Tregs (of Foxp3⁺ CD4⁺ T cells) of mice used additionally to **(B)** for targeted metabolomics. **(D-F)** Targeted metabolomic analysis of BAs or SCFAs of mice analyzed for ROR γ t⁺ Helios⁻ Tregs and Th2 cell populations in the LP-SI in **(B)** and **(C)**. **(D)** Primary BAs and their conjugates (primary BAs conjugated to glycine or taurine). **(E)** Unconjugated secondary BAs. **(F)** Targeted measurement of SCFAs of ileum content samples. **(B-F)** Age of mice was 7-10 weeks and all were female. Statistics: one-way ANOVA with Tukey's multiple comparisons test between all samples and groups. Significance indicated as *p<0.05, **p<0.01, ***p<0.001, ****p<0.0001, ns: not significant. **(D-F)** Values below detection N/A and 0 were set as 0.

3.1.6 Reduced microbial complexity, reduced pTregs numbers and enhanced Th2 in steady state does not correlate with enhanced food allergy sensitization

The previous results in steady state showed that pTreg numbers were reduced in mouse groups with decreased microbial complexity (GF, ASF³<ASF⁷, Oligo-MM¹²<SPF), while Th2 cell frequencies were increased in the LP-SI (Figure 4A,B and Figure 6B,C). GF mice or mice treated with antibiotics have been reported to be more susceptible to sensitization with peanut food allergen [86]. In another study it was shown that GF or mice transferred with microbiota from cow's milk allergic children had significantly higher anaphylactic scores when challenged with the cow's milk allergen β -lactoglobulin (BLG) after sensitization than healthy microbiota-colonized mice [84].

A food allergy model was set up to test if these results could be repeated and if the mouse groups with a minimal number of bacterial strains (ASF⁷, Oligo-MM¹²) would be more susceptible to food allergen sensitization. Sensitized mice received cholera toxin (CT) in a combination with the common model allergen OVA orally (sens.). Mice of the different mouse groups GF, ASF⁷, Oligo-MM¹² and SPF were sensitized for five weeks. Control animals received CT only (ctrl). For anaphylaxis challenge OVA was given intravenously and the core body temperature was measured intrarectally. The maximum temperature difference compared to the body temperature before challenge was chosen as a parameter for anaphylaxis severity ($T\Delta_{\max}$ in °C). A schematic of the food allergy model and temperature readout is depicted in Figure 8A. The model was repeated twice in two independent experiments.

Comparing all sens. animals there were no significant differences in $T\Delta_{\max}$ between GF, ASF⁷, Oligo-MM¹² and SPF mice (Figure 8B). However, not all mice of all groups reacted with a core body temperature drop after allergen challenge. The number of animals that reacted was highest in GF

animals indicating a possible higher susceptibility to OVA sensitization. The mouse groups with lower bacterial complexity (ASF⁷, Oligo-MM¹²), however, were not more susceptible to sensitization than SPF mice and even displayed lower mean $T\Delta_{\max}$ (Figure 8B).

Murine MCPT-1 is a marker for mast cell degranulation which was also assessed in this model. Mouse groups did not differ significantly in mMCPT-1 levels in the serum (Figure 8C).

Regarding OVA-specific IgE in serum, concentrations were generally low. In Experiment 1 an increase in OVA-specific IgE from Day -1 (before sensitization) to Day 35 (after challenge) was observable to a higher extent in GF sens. mice compared to ASF⁷, Oligo-MM¹² and SPF mice (Figure 8D upper graph). In experiment 2, the highest levels of OVA-specific IgE in serum were reached by GF sens. mice, however, with great variability and the mean was similar to SPF sens. mice (Figure 8D lower graph). In both experiments, the sens. animals in the mouse groups with a lower bacterial variability (ASF⁷, Oligo-MM¹²) had either comparable OVA-specific IgE levels to SPF mice or were lower reflecting the $T\Delta_{\max}$ data (Figure 8D).

The pattern of an inverse correlation of ROR γ t⁺ Helios⁻ pTreg frequencies in the LP-SI with an increased microbial complexity that was observed in steady state, could also be recapitulated after sensitization with OVA. While GF animals (sens. and ctrl) had the lowest abundance of pTregs in the SI, ASF⁷ sens. and Oligo-MM¹² sens. showed medium frequency levels of pTregs, while the highest frequency was visible in SPF sens. mice (Figure 8E). Interestingly, sensitization with OVA induced pTreg frequencies independent of bacterial colonization: both GF sens. compared to GF ctrl and SPF sens. compared to SPF ctrl. showed higher pTreg frequencies (Figure 8E).

Regarding Th2 cell frequencies in the SI among the mouse groups, GF animals (sens. and ctrl) showed a significantly higher abundance of Th2 cells than ASF⁷ sens., Oligo-MM¹² sens. and SPF (sens. and ctrl) animals (Figure 8F). The higher frequency of Th2 cells in ASF⁷ and Oligo-MM¹² animals compared to SPF that was visible in Figure 4B though was not observable here since Th2 animals between all mouse groups except GF were comparable. Also, sensitization did not increase Th2 cell frequency in the LP-SI since both in the GF and SPF groups, the sens. animals did not display higher Th2 frequencies (Figure 8F).

All in all, GF animals showed a tendency of higher susceptibility to sensitization than ASF⁷, Oligo-MM¹² and SPF mice. A higher susceptibility to OVA sensitization of mice with a lower bacterial complexity than SPF mice (ASF⁷, Oligo-MM¹²) could not be observed even though changes in pTreg distribution pattern among the mouse groups that were observed in steady state were still visible after food allergy. It has to be noted however that during regular control check-ups contamination with *Paenibacillus sp* was found in cages of GF animals so it cannot be assumed that GF animals were completely germ-free (displayed as GF* in Figure 8).

III.1 Results

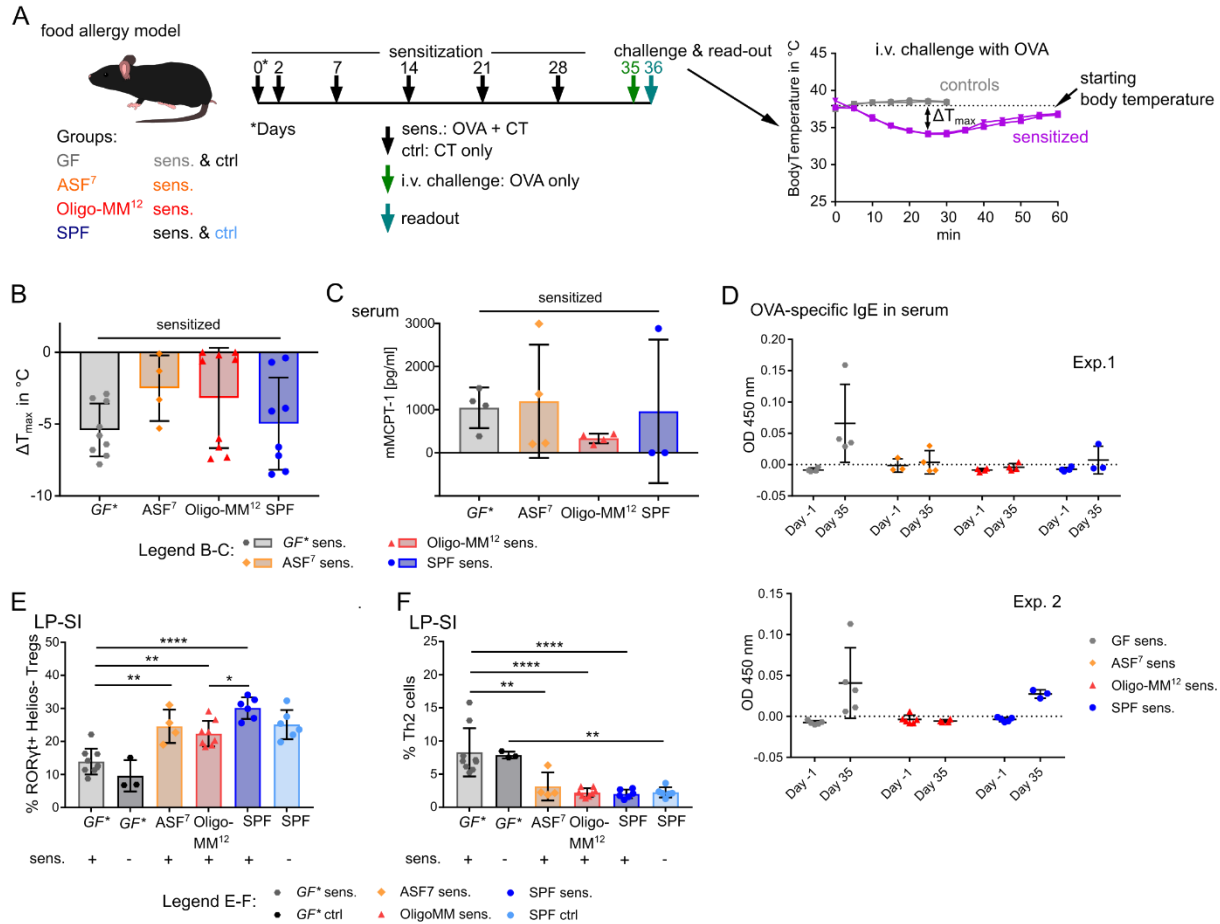


Figure 8: Oral sensitization of GF, ASF⁷, Oligo-MM¹² and SPF mice in a model of food allergy
(A) Scheme of the established food allergy model to determine oral sensitization to OVA in a combination with CT and i.v. challenge with OVA for allergic response (drop of core body temperature). Mouse groups: GF, ASF⁷, Oligo-MM¹² and SPF. For specifics regarding volumes and amount of reagents see Material and Methods. Sens. animals received OVA and CT, ctrl. received only CT in sensitization phase. Maximum temperature difference to starting body temperature ΔT_{max} was determined for each mouse. **(B)** ΔT_{max} of sens. animals of GF, ASF⁷, Oligo-MM¹² and SPF groups. **(C)** Serum MCP-1 measured after challenge (Day 35) in serum of sens. groups. **(D)** OVA-specific IgE ELISA in serum before sensitization start (Day -1) and after challenge (Day 35). **(E)** ROR γ t⁺ Helios⁺ Treg frequencies of Foxp3⁺ T cells (CD3⁺ CD4⁺) in LP-SI at day 36 (readout). **(F)** Percentage Th2 cells of Foxp3⁺ CD3⁺ CD4⁺ in LP-SI. **(E-F)** For gating see Appendix Figure 15. Statistics: one-way ANOVA with Tukey's multiple comparisons test, * $p < 0.05$, ** $p < 0.01$, *** $p < 0.001$, **** $p < 0.0001$. Significance is only shown for the comparisons within the sens. groups or sens. vs ctrl within a mouse group. All other comparisons are not significant. GF* means complete germ-free status cannot be assumed, as contamination of cages with *Paenibacillus sp* was found.

3.1.7 Summary

In short, mouse groups with different microbial complexity statuses in their intestine (GF, ASF³, Oligo-MM¹² and SPF) displayed frequency changes in ROR γ t⁺ Helios⁺ pTregs in SI, mLN and spleen correlating with microbial complexity. This correlation was slightly diminished when colonization

with bacteria happened at a later time point for ASF⁷ mice in contrast to mice born from mothers with the same microbial status. However, also ASF⁷ mice displayed significantly less pTregs in their SI than SPF animals. Th2 cells in the SI inversely correlated with pTregs and were enhanced in minimal microbiota mice. CDC2 frequencies were increased in mLNs and the SI in gnotobiotic animals further suggesting that minimal microbiota mice could be more prone to Th2 mediated diseases. However, in a food allergy model with OVA sensitization, ASF⁷ and Oligo-MM¹² did not show an enhanced susceptibility for sensitization in comparison to SPF mice. A higher microbial complexity aligns with increased abundance of various primary (specifically glycine-conjugated) and secondary BAs and SCFAs (acetic acid) which could play a role in pTreg induction.

3.2 Development of a novel monoclonal antibody specific for Galactose- α 1,3-Galactose questions alpha-Gal epitope expression by bacteria

3.2.1 Preamble

The induction of anti- α -Gal antibodies has been hypothesized to be mediated by the gut microbiota, since α -Gal-binding molecules bind to some intestinal bacteria, such as purified polyclonal human anti- α -Gal antibodies [104, 105] or Isolectin B4 from *Bandeiraea simplicifolia* (BSI-B₄) [106–108]. Furthermore, antibiotics have been shown to reduce pre-existing anti- α -Gal antibody titres of the IgG isotype [130] and oral introduction of *Escherichia coli* O86:B7 in *Ggta1* KO mice resulted in anti- α -Gal antibody (IgG, IgM) elevation [131]. However, BSI-B₄ and another α -Gal-binding lectin from the mushroom *Marasmius oreades* (MOA) [132] have reduced specificity to the α -Gal epitope, as they both also bind to the blood group B antigen. The currently most widely used α -Gal-specific monoclonal antibody is the clone M86, an IgM antibody which was developed by Galili *et al.* in *Ggta1* KO mice [133] and to some degree also chicken single-chain antibody variable-region fragments (scFv) developed by Cunningham *et al.* [134]. Neither of the two antibodies has been convincingly shown to stain bacteria to the author's knowledge. However, the monoclonal antibody M86 was indeed used to demonstrate α -Gal expression on parasites such as *Plasmodium* species [106]. As the M86 antibody is of the IgM isotype with limited affinity and purification properties, the aim of this thesis chapter was to develop a novel IgG antibody with high affinity for both the di- and trisaccharide α -Gal epitope (Gal- α 1,3-Gal and Gal- α 1,3-Gal- β 1,4-GlcNAc) with wide applicability. If specific, such an antibody would allow detection of the genuine α -Gal epitope on bacteria hypothesized to be inducers of human anti- α -Gal immunoglobulins. Results of this chapter have been published in [1] and are presented below.

3.2.2 Generation and screening of an α -Gal epitope-specific IgG antibody with wide applicability

3.2.2.1 The novel 27H8 monoclonal antibody specifically binds to Gal- α 1,3-Gal

In order to generate a monoclonal antibody specific for the α -Gal epitope determining structure Gal- α 1,3-Gal that is equally able to bind to the naturally occurring α -Gal epitope Gal- α 1,3-Gal- β 1,4-GlcNAc, α -galactosyltransferase knockout mice (*Ggta1* KO) [109] were immunized with Gal- α 1,3-Gal- β 1,4-GlcNAc coupled to OVA as carrier protein (α -Gal-OVA) according to the scheme depicted in Figure 9A. Splenic B cells were fused with the myeloma cell line P3X63-Ag8.653 and primary hybridoma supernatants were screened for IgG antibodies binding to Gal- α 1,3-Gal-BSA (α -Gal-DI-BSA) in a flow cytometric bead assay (Figure 9A). Screening for antibodies against Gal- α 1,3-Gal coupled to a

different carrier protein than used for immunization minimized the risk of pulling out antibody clones specific for the immunization molecule OVA. To further diversify immunization and screening molecule and avoid off-target (linker) specific antibodies, different linker lengths were selected with a 14-C-atom linker for the immunization molecule α -Gal-OVA and a 3-C-atom-linker for the screening molecule α -Gal-DI-BSA. Overall, 1536 supernatants from 4 immunized mice were screened and only two primary hybridoma supernatants (25G8 and 27H8) showed binding to α -Gal-DI-BSA. The determined isotype in the 25G8 primary hybridoma supernatant was IgG2b κ , that of 27H8 IgG1 κ . In a secondary screen, α -Gal-conjugated glycoproteins and respective control proteins without α -Gal were spotted on a membrane and incubated with either rat anti-mouse IgG1 (for 27H8) or rat anti-mouse IgG2b (for 25G8) and detected with anti-rat AP-labeled antibodies in a dot blot (Figure 9B). Both 25G8 and 27H8 primary hybridoma supernatants bound to α -Gal-conjugated MSA, α -Gal-OVA and the disaccharide and trisaccharide α -Gal epitopes conjugated to BSA (α -Gal-DI-BSA/ α -Gal-TRI-BSA). While 25G8 also strongly detected the carrier molecule OVA that was used for immunization, 27H8 showed only minimal binding to OVA (Figure 9B, upper two rows). Both primary hybridoma supernatants bound to glycolipids isolated from rabbit erythrocyte membranes rich in α -Gal [116]. Binding was prevented by cleaving the carbohydrate from the lipid through pre-incubation with EGCasel (Figure 9B), an enzyme hydrolysing the β -glycosidic covalent link between oligosaccharide and ceramide. In a second screening assay using a wet membrane and HRP-labeled secondary antibodies, binding of 25G8 to OVA was still visible while binding of 27H8 was not detectable at all (Figure 9C). Therefore, 27H8 hybridoma cells were chosen for subcloning by limiting dilution to generate a stable monoclonal hybridoma cell line. Antibodies were purified from monoclonal 27H8 supernatant with protein A and both, supernatant and purified 27H8 antibody were validated alongside in a secondary dot blot screening with direct detection using an AP-conjugated anti-mouse IgG antibody (Figure 9D). Both, the supernatant and purified 27H8 antibody showed a highly specific binding to all tested α -Gal carrying glycoproteins and -lipids but did not show any binding to OVA (Figure 9D). Thus, the initially observed weak binding of the primary 27H8 supernatant to OVA (Figure 9B) was most likely caused by a second hybridoma clone growing in the same well as 27H8, as in the first screening round monoclonality cannot be assumed. Next, the purified 27H8 antibody was conjugated to biotin. Successful biotinylation was validated in an ELISA by coating the biotinylated 27H8 as well as a biotinylated control antibody on plates followed by detection with streptavidin conjugated to HRP. The antibody 27H8 could be labeled with a similar efficiency as the control antibody (Figure 9E). The biotinylated 27H8 antibody in combination with Extravidin-AP showed a highly specific α -Gal detection without any detectable background staining to carrier molecules devoid of α -Gal (Figure 9F). In summary, the newly generated 27H8 monoclonal antibody

Figure 9: Generation, screening and biotinylation of a monoclonal IgG antibody recognizing galactose- α 1,3-galactose

(A) Schematic approach for the generation of a monoclonal anti- α -Gal antibody through immunization of *Ggta1* KO mice with Gal- α 1,3-Gal- β 1,4-GlcNAc-OVA (α -Gal-OVA) and screening of primary hybridoma supernatants (SNs) with Gal- α 1,3-Gal-BSA (α -Gal-DI-BSA). **(B)** Dot blot of 25G8 and 27H8 primary SNs on α -Gal-conjugated glycoproteins or -lipids, respective negative control proteins devoid of α -Gal and EGCase I-digested glycolipids (right). Detection with unlabeled rat anti-mouse (anti-m) isotype-specific secondary antibodies and anti-rat tertiary antibody labeled with AP. **(C)** Secondary screen on dot blots of 25G8 and 27H8 primary hybridoma SNs on α -Gal carrying glycoproteins and the respective negative control proteins. Detection with HRP-labeled secondary antibodies. See Appendix Figure 19A for uncropped blot. **(D)** 27H8 subcloned hybridoma SN and 27H8 purified antibody were screened as in **(B)**. **(E)** ELISA of 27H8 biotinylated antibody (27H8-biotin), IgG-biotin control, non-biotinylated 27H8 (27H8 w/o) and IgG1 Isotype control (IgG1 Isotype w/o) coated onto plates and detected by streptavidin-HRP. For details, see Material and Methods section. **(F)** 27H8-biotin antibody detected with Extravidin-AP was compared to 27H8 w/o detected by anti-IgG-AP. Further abbreviations (A-F): Dig., digested; w/o, without; ctrl, control; SA_v, streptavidin.

3.2.2.2 27H8 monoclonal antibody detects α -Gal epitopes of natural origin and offers a wide range of possible applications

To verify the specificity, the 27H8 monoclonal antibody was compared to the lectin BSI-B₄ and to the monoclonal IgM antibody M86, which are both widely used to detect the α -Gal epitope [93, 106, 133]. BSI-B₄ is specific for terminal α -galactose oligosaccharides [135] and therefore recognizes also the blood group B antigen, which differs from the α -Gal epitope only in the addition of one fucose residue and is thus structurally very similar [136, 137]. To assess whether 27H8 also binds to the blood group B, antigen lysates of whole blood from a type B donor were blotted on a membrane and the antibodies 27H8 and M86 or biotinylated BSI-B₄ applied for detection. While BSI-B₄ bound to the blood type B specimen as expected, neither 27H8 or M86 did (Figure 10A). Next, 27H8 was tested for its binding affinity to natural α -Gal epitopes. As pig kidney is naturally rich in α -Gal [138, 139] and reactions in α -Gal allergic patients are severe after ingestion [99], 27H8 antibody was tested for recognition of α -Gal in pig kidney lysates in a dot blot assay. 27H8 binding to wildtype (WT) pig kidney lysate was observed with strong staining intensity (Figure 10B left panel). Control staining with the secondary anti-mouse IgG-AP antibody gave a faint signal on WT pig kidney lysate as well as on *GGTA1* KO cells lysates without or after 27H8 staining. However, no cross-reactivity of the secondary antibody was observed in WT pig kidney tissue lysates digested with α -galactosidase, an enzyme that cleaves off terminal α -galactose [140], indicating a relevance of galactose glycosylation for background staining by the secondary antibody. To avoid this background staining, 27H8 antibody was tested on lysates from cultured pig kidney cells devoid of immunoglobulins. Here, background staining was not observed for anti-mouse IgG-AP on lysates from cultured cells and 27H8 bound exclusively to WT cultured pig kidney cells, but not to *GGTA1* KO cultured pig kidney cells (Figure 10B middle panel).

This result suggests that the secondary antibody used for detection still recognizes pig IgG antibodies present in whole kidney lysate despite anti-mouse-IgG-AP being highly cross-absorbed against immunoglobulins from various species. Additionally, 27H8 was tested on purified APN from HEK cells either expressing the α 1,3-galactosyltransferase or not. 27H8 only bound to α -Gal-APN and not to APN (Figure 10B right), further verifying its specificity to the α -Gal epitope. Importantly, 27H8 also recognized bovine thyroglobulin – a protein used for α -Gal specific IgE antibody detection assays for red meat allergy patients (ImmunoCAP, Thermo Fisher Scientific, also described in [141]) (Figure 10B right). Specific binding of 27H8 to WT but not to *GGTA1* KO pig kidney was also observed on tissue slides using a monoclonal secondary antibody in immunohistochemistry (Figure 10C). 27H8 bound to the same cellular structures as M86 (Figure 10C upper left), such as binding to cells of the nephron's tubular system but not to the glomerulus. Flow cytometry analysis of HEK cells expressing α -Gal-APN and APN confirmed specificity of 27H8 to natural α -Gal epitopes and highlights the broad range of applications of this antibody for detection of α -Gal epitopes in dot blot, histology and flow cytometry (Figure 10D). In conclusion, 27H8 monoclonal antibody is highly specific for the α -Gal epitope in natural settings, does not bind the blood type B antigen and offers a wide range of possibilities for application.

III.2 Results

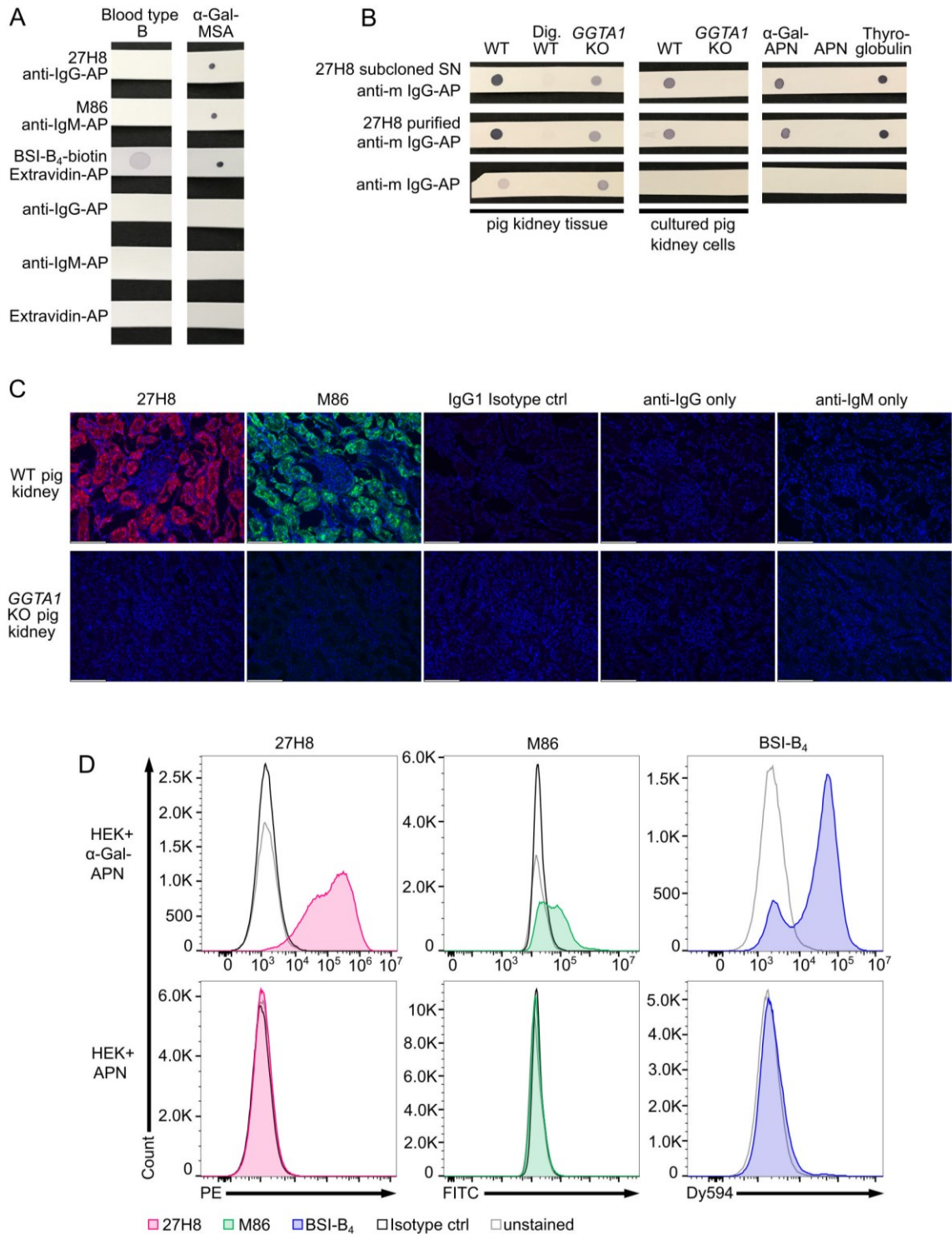


Figure 10: Specificity of 27H8 monoclonal antibody

(A) Dot blot stain of lysed whole blood from a type B blood donor and α -Gal-MSA by 27H8, M86 or BSI-B₄. **(B)** Screening of 27H8 subcloned hybridoma SN (upper row) and purified 27H8 antibody (middle row) on lysed kidney tissue or cultured kidney cells of WT and *GGTA1* KO pigs and on WT kidney tissue samples digested with α -Galactosidase (Dig. WT). Further screening molecules: APN glycosylated with α -Gal, APN only and (α -Gal-containing) bovine thyroglobulin. **(A-B)** Samples in a row were blotted on

one membrane. See Appendix Figure 19B,C for uncropped blots. **(C)** Immunofluorescence microscopy of pig kidney tissue specimens (WT and *GGTA1* KO) stained with 27H8 (red) and M86 (green) in the glomerulus region. IgG1 isotype ctrl and secondary antibody only stains (anti-IgG1/anti-IgM) served as controls for fluorescence signal. DNA stained with DAPI (blue). Scale bar (white, left corner): 124.4 μm . **(D)** Flow cytometry analysis of HEK cells expressing α -Gal- APN (upper panel) and APN only (lower panel) stained with 27H8 (red), M86 (green) and BSI-B₄ (blue). Controls: unstained (grey) and isotype controls (IgG1, IgM, in black). **(A-D)** If not otherwise indicated, 27H8 was applied in the purified version.

3.2.3 Monoclonal anti- α -Gal antibody 27H8 is superior to other α -Gal binding moieties binding with high affinity

After determining the specificity and applicability of 27H8 antibody, binding affinities of 27H8 for the di- and trisaccharide α -Gal epitopes were evaluated in a quantitative manner. Therefore, Surface Plasmon Resonance (SPR) analyses were performed with α -Gal-DI-BSA and α -Gal-TRI-BSA molecules (Figure 11A). Both analytes bound in a nanomolar concentration range to the coupled 27H8 antibody. The mean dissociation constant (K_D) was slightly higher for α -Gal-TRI-BSA (7.51 ± 1.9) than for α -Gal-DI-BSA (2.02 ± 1.0), indicating a higher affinity of 27H8 for the disaccharide than the trisaccharide epitope. However, this might be partly explained by 35 sugar residues being attached to one molecule BSA for the α -Gal-DI-BSA analyte, while α -Gal-TRI-BSA consisted of 33 sugar residues on average per protein. The Hill coefficients for the fitted binding curves of both analytes were smaller than one ($n < 1$), indicating negative cooperativity between the binding sites on 27H8 antibody (Figure 11A). Negative cooperativity suggests that the first binding analyte (α -Gal-DI-BSA or α -Gal-TRI-BSA) decreased the rate of subsequent analyte binding. As a full-length IgG antibody has two identical antigen-binding sites and due to the size of the BSA-conjugated analytes (66kDa + 33 or 35 sugar residues), it can be assumed that binding of one α -Gal-DI/TRI-BSA molecule to the first binding site on the 27H8 antibody may partially block the access of the second α -Gal-DI/TRI-BSA molecule to the second antigen-binding site as a result of steric hindrance. Next, the 27H8 antibody was compared to M86, the most widely used monoclonal antibody specific for the α -Gal epitope developed by Galili *et al.* [133]. This IgM antibody is commonly available as a hybridoma supernatant but for a direct affinity comparison both antibodies are ideally used in a purified format. While 27H8 antibody could be easily purified with protein A (Figure 9 D), M86 antibody was not purifiable in this study with commonly used purification reagents such as recombinant protein L (Cytiva Cpto™ L, Thermo Fisher Scientific, data not shown). Thus, the hybridoma supernatants of 27H8 and M86 were compared regarding their respective binding to α -Gal conjugated glycoproteins in an ELISA (Figure 11B). In order to titrate both antibodies to equal concentrations, the antibody amount in the supernatants was determined by interpolating OD 450 nm values to a standard curve of IgG1 and IgM isotype controls

by a standard immunoglobulin isotype ELISA. To analyze the values in the linear range of the standard curve and dynamic range of the assay, 27H8 supernatant and M86 supernatant had to be diluted to variable degrees, which decreases the accuracy of concentration measurements. Thus, the concentrations of immunoglobulins in 27H8 supernatant and M86 supernatant were estimated. Additionally, antibody concentration in the 27H8 supernatant stock was approximately 100 times higher than in the M86 supernatant (27H8 supernatant: $\sim 116.69 \mu\text{g/ml}$; M86 supernatant: $\sim 1.12 \mu\text{g/ml}$) (see Material and Methods). When comparing 27H8 supernatant and M86 supernatant titration curves on α -Gal-DI-BSA and α -Gal-TRI-BSA coated to ELISA-plates, it was observed that both antibodies bind the di- and trisaccharide epitopes of α -Gal with a similar avidity (Figure 11B upper panel). This similar binding property was also observed on α -Gal-OVA- (Figure 11B middle panel) and α -Gal-MSA-coated plates (Figure 11B lower panel). Supernatant of subcloned monoclonal 27H8 hybridoma did not bind respective proteins devoid of α -Gal, such as BSA, MSA and, importantly, it did not bind OVA (Figure 11B right), in contrast to the weak binding of the primary hybridoma supernatant to OVA (Figure 9B). To further confirm that 27H8 and M86 recognize the α -Gal epitope in a similar manner, blocking assays were performed in which the antibodies competed with each other for α -Gal binding (Figure 11C). α -Gal-MSA was coated onto ELISA-plates and incubated with increasing amounts of either 27H8 supernatant or M86 supernatant in a serial dilution to block the α -Gal epitope. The maximum concentration of M86 used for blocking was limited to $1 \mu\text{g/ml}$ due to the low stock concentration, while 27H8 supernatant was increased up to $100 \mu\text{g/ml}$. Afterwards, the respective competing antibody was added (27H8 to M86 block and M86 to 27H8 block) and detected with specific anti-IgG1 or anti-IgM antibodies, respectively. 27H8 supernatant binding was blocked by M86 at concentrations higher than $0.1 \mu\text{g/ml}$ while 27H8 supernatant blocked M86 binding gradually even at lower amounts (starting from $\sim 0.01 \mu\text{g/ml}$). This discrepancy might be explained by the different isotypes (IgG1 vs IgM) and steric inhibition by IgM pentamers, but also confirms the high affinity of 27H8 monoclonal IgG1 antibody to the α -Gal epitope. In brief, the novel 27H8 antibody binds the α -Gal epitope comparable to M86 in ELISA and displays high affinity for its epitope.

III.2 Results

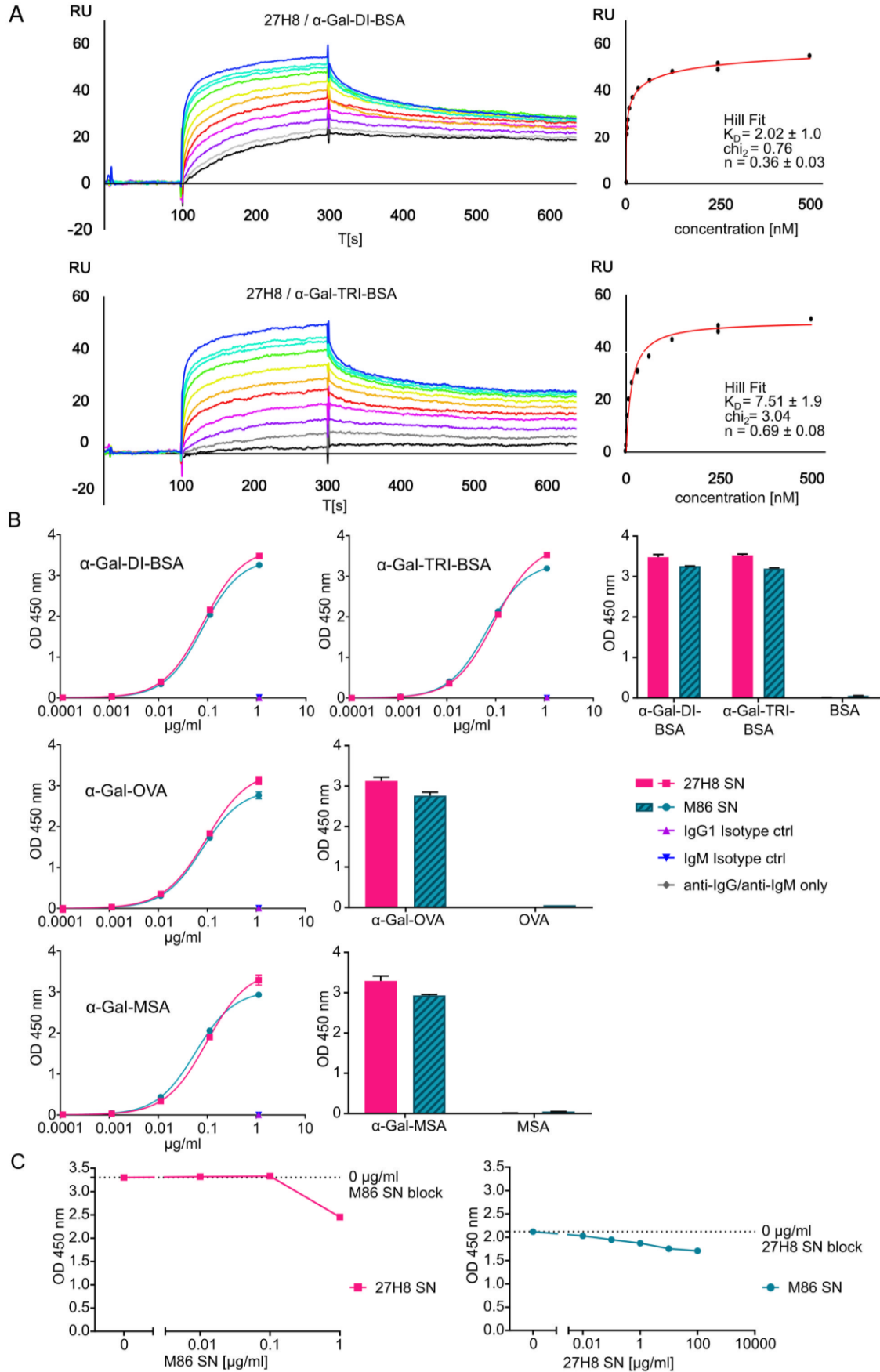


Figure 11: High affinity recognition of synthetic α -Gal epitopes

(A) Graphs show binding of synthetic α -Gal ligands to the coupled purified 27H8 antibody via surface plasmon resonance (SPR). Representative sensorgrams are displayed for 27H8/ α -Gal-DI-BSA (upper panel) and 27H8/ α -Gal-TRI-BSA (lower panel). For both pairs calculated equilibrium dissociation rate (K_D), error as standard deviation from three independent experiments, the χ^2 value for the curve fit and the Hill coefficient n are shown (right panel). Concentration series color code: black: 0.98 nM, gray: 1.95 nM, violet: 3.9 nM, magenta: 7.8 nM, red: 15.6 nM, orange: 31.2 nM, yellow: 62.5 nM, green: 125 nM, cyan: 250 nM, blue: 500 nM. RU: response units, T[s]: time in seconds. **(B)** Titration of 27H8 subcloned hybridoma SN and M86 hybridoma SN in ELISA on α -Gal conjugated glycoproteins (left) and direct comparison of glycoprotein and respective protein devoid of α -Gal at the highest concentration of 27H8 SN or M86 SN (1.12 μ g/ml) (right). **(C)** Epitope blocking of α -Gal-MSA coated to ELISA-plates: M86 SN block followed by 27H8 SN and anti-IgG1 detection (left panel) or 27H8 SN block by M86 SN and anti-IgM detection (right panel). **(B-C)** Concentration values (x-axis) are plotted in logarithmic scale, antibody binding is shown as OD 450 nm (y-axis).

3.2.4 Application of 27H8 antibody questions α -Gal expression by bacteria**3.2.4.1 *Staphylococcus aureus* does not express the α -Gal epitope**

Intestinal bacteria have been hypothesized to induce anti- α -Gal immunoglobulins (IgM, IgG) in humans [104]. Thus, this study investigated whether 27H8 antibody binds to bacteria reported to express α -1,3-galactosyltransferase-like genes (KEGG orthology number K03275 or K03278) as described by Montassier *et al.* [108], such as *H. pylori* [J99], *H. influenzae* (Hi375), *S. typhimurium* (ATCC 14028), *P. aeruginosa* (DSM 50071), *A. baumannii* (ATCC 17978) and *A. muciniphila* (ATCC BAA-835). Negative controls were selected according to literature, such as *E. coli* K12 [106]. *E. coli* DH5 α and strains from the gram positive bacterium *S. aureus* were further included, though it was reported that most α -Gal expressing bacteria were supposed to be gram-negative [108]. Surprisingly, none of the tested bacterial lysates could be stained with the 27H8 antibody in a dot blot experiment, except *S. aureus* Mu50 and as positive control α -Gal-TRI-BSA (Figure 12A). The binding of 27H8 to *S. aureus* was not only observed in a dot blot but also by bacterial flow cytometry (Figure 12B). The fluorescence intensity increased in the secondary antibody only sample (anti-IgG1-PE) relative to the unstained control indicating a substantial background stain (Figure 12B, left panel). However, the first IgG1 isotype control that was applied (Southern Biotech) did not give the same fluorescence signal as 27H8 antibody when applying the same concentration (data not shown). It was further observed that 27H8 binding to *S. aureus* is a shared pattern for multiple strains but when applying a polyclonal IgG isotype control, the same staining intensity was observed as for 27H8 (Figure 12C). This result suggested that the binding of 27H8 to *S. aureus* strains was likely a common feature of IgG antibodies regardless of specificity and was not due to a specific binding to the α -Gal epitope present on this bacterium. To further demonstrate that *S. aureus* does indeed not express α -Gal, the α -Gal epitope was cleaved and removed by various approaches and 27H8 binding was examined thereafter.

First, the α -Gal carrying oligosaccharide was removed in the *S. aureus* sample by EGCase I digestion, but in contrast to control digestion of glycolipids, no signal was lost for *S. aureus* (Figure 12D). Furthermore, when comparing pig kidney tissue lysate and *S. aureus* lysate digested with α -Galactosidase, there was a significant signal reduction for the mammalian sample observable, but not for the bacterial sample (Figure 12E). Finally, when the membrane of blotted samples of pig kidney tissue lysate, α -Gal-MSA and *S. aureus* lysate was pre-incubated with periodic acid, a treatment that destroys all carbohydrate determinants [142], the staining intensity of 27H8 was lost or substantially reduced for pig kidney and α -Gal MSA, but not for the *S. aureus* sample (Figure 12F). Thus, the 27H8 antibody binds to a structure in *S. aureus* that is not part of an oligosaccharide connected to a sphingolipid, does not contain α -galactose residues and is not even a carbohydrate. Most probably, 27H8 binds to protein A, as already implied for human polyclonal anti- α -Gal antibodies binding to *S. aureus* human isolates [105]. In line with this result, there was no staining of *S. aureus* samples with M86 in a dot blot detectable as IgM antibodies are typically not bound by protein A (data not shown). Furthermore, and in contrast to meat allergic patients, enhanced IgG or IgE titers against bovine thyroglobulin (a molecule routinely used to detect anti- α -Gal antibodies in patient serum samples, [141]) was not observable in our selection of atopic dermatitis patients (Figure 12G). This patient group was selected as atopic dermatitis patients are usually strongly colonized by *S. aureus* [143]. Serum IgM titers against thyroglobulin were unchanged between the groups. Altogether, these data strongly indicate that *S. aureus* binds via protein A to the constant part of the 27H8 antibody and does not express α -Gal itself.

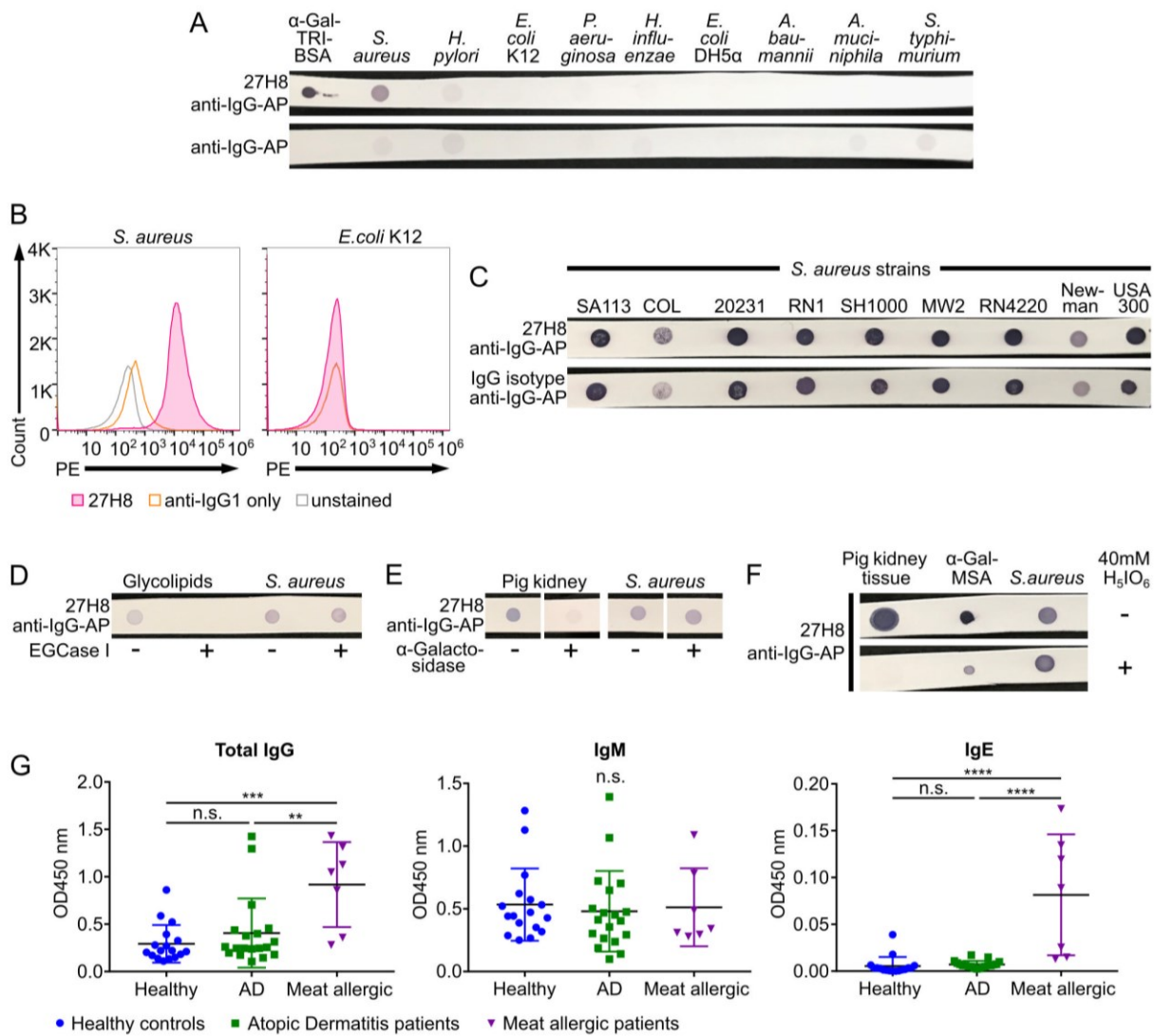


Figure 12: *Staphylococcus aureus* strains bind 27H8 independent of α -Gal expression

(A) Dot blots of the positive control α -Gal-TRI-BSA and lysed bacterial species *S. aureus* (strain Mu50), *H. pylori*, *E. coli* strains K12 and DH5 α , *P. aeruginosa*, *H. influenzae*, *A. baumannii*, *A. muciniphila* and *S. typhimurium*. (B) Histograms of flow cytometric analysis of *S. aureus* strain 20231 and *E. coli* K12 stained with 27H8 and anti-IgG1-PE. (C) Multiple *S. aureus* strains stained with 27H8 and IgG isotype in dot blot. (D) Dot blot of glycolipids and *S. aureus* strain SH1000 digested or not with EGCase I as indicated. (E) Dot blot of pig kidney lysate and *S. aureus* strain SH1000 digested or not with α -Galactosidase as indicated. Uncropped blots depicted in Appendix Figure 19D. (F) Pig kidney lysate, α -Gal-MSA and *S. aureus* strain 20231 blotted on membrane and either incubated with periodic acid (H5IO6) or not. (A, D-F) Detection with 27H8 and anti-IgG-AP. (A-F) 27H8 was applied in the purified version. (G) ELISA of human IgG, IgM and IgE binding to thyroglobulin in serum samples from healthy controls, Atopic Dermatitis (AD) or red meat allergic patients. Each symbol represents an individual subject. Statistics: one-way ANOVA with Tukey's multiple comparisons test, **p<0.01, ***p<0.001, ****p<0.0001, n.s.: not significant.

3.2.4.2 27H8 and M86 antibodies do not bind to *E. coli* O86:B7 nor to other members of the intestinal microbiota

As there was no binding of 27H8 antibody observed when tested on lysates of cultivated bacteria in a dot blot (Figure 12A), binding of 27H8 to *E. coli* O86:B7 was investigated. This strain was reported to express α -Gal detected by BSI-B₄ in multiple studies [106, 107, 144], and is frequently used as a positive control as it has also been shown to induce anti- α -Gal antibodies in *Ggta1* KO mice after oral inoculation [131]. Surprisingly, neither 27H8 nor M86 antibody bound to *E. coli* O86:B7 while BSI-B₄ strongly stained this bacterial strain (Figure 13A). This was specific for *E. coli* O86:B7 because the negative control *E. coli* BL21, described in [145], was not stained by the lectin. Further bacteria were selected, such as an *E. coli* strain isolated from human feces (*E. coli* HS) and *Lactobacillus rhamnosus* which showed minimal α -Gal positive staining by BSI-B₄ in [107]. No specific binding of 27H8 or M86 was observed for these two strains (Figure 13A). BSI-B₄ did not bind to *E. coli* HS and showed a slight signal shift compared to the unstained control for *L. rhamnosus*. Technical errors of 27H8 applied in flow cytometry could be ruled out since α -Gal expressing HEK cells were indeed stained by this antibody using the same technique (Figure 10D). The binding of BSI-B₄ to *E. coli* O86:B7 in contrast to 27H8 and M86 could also be observed in a dot blot using lysates of this strain (Figure 13B). As it had been suggested that the induction of anti- α -Gal antibodies and also immunological tolerance towards this epitope might be driven by the intestinal microbiota [104], 27H8 binding to intestinal bacteria was questioned. Therefore, bacteria from the intestinal compartments of *Ggta1* KO mice were incubated with 27H8 for antibody binding and bacterial flow cytometry was performed. To avoid anti-mouse secondary antibody attaching to murine immunoglobulins contained in the samples, the biotinylated version of 27H8 and BSI-B₄ as control were applied. While BSI-B₄-biotin bound to a large amount of intestinal bacteria from the SI, cecum and colon, this was not visible for the biotinylated 27H8 antibody, as there was no signal shift observable exceeding the streptavidin-PE only control or the biotinylated IgG1 control (Figure 13C). To confirm that also the biotinylated version of 27H8 binds to α -Gal in flow cytometry, the same technical setup as for the intestinal bacteria was applied to splenocytes from *Ggta1* KO and WT mice. While biotinylated 27H8 bound to splenocytes from WT mice, no binding to splenocytes from *Ggta1* KO mice was detectable (Figure 13D). Altogether, it can be concluded that neither of the two α -Gal binding monoclonal antibodies 27H8 or M86 bind to structures on the bacterial surface or in lysates, while the lectin BSI-B₄ indeed binds to bacterial epitopes most likely in a non- α -Gal epitope specific manner.

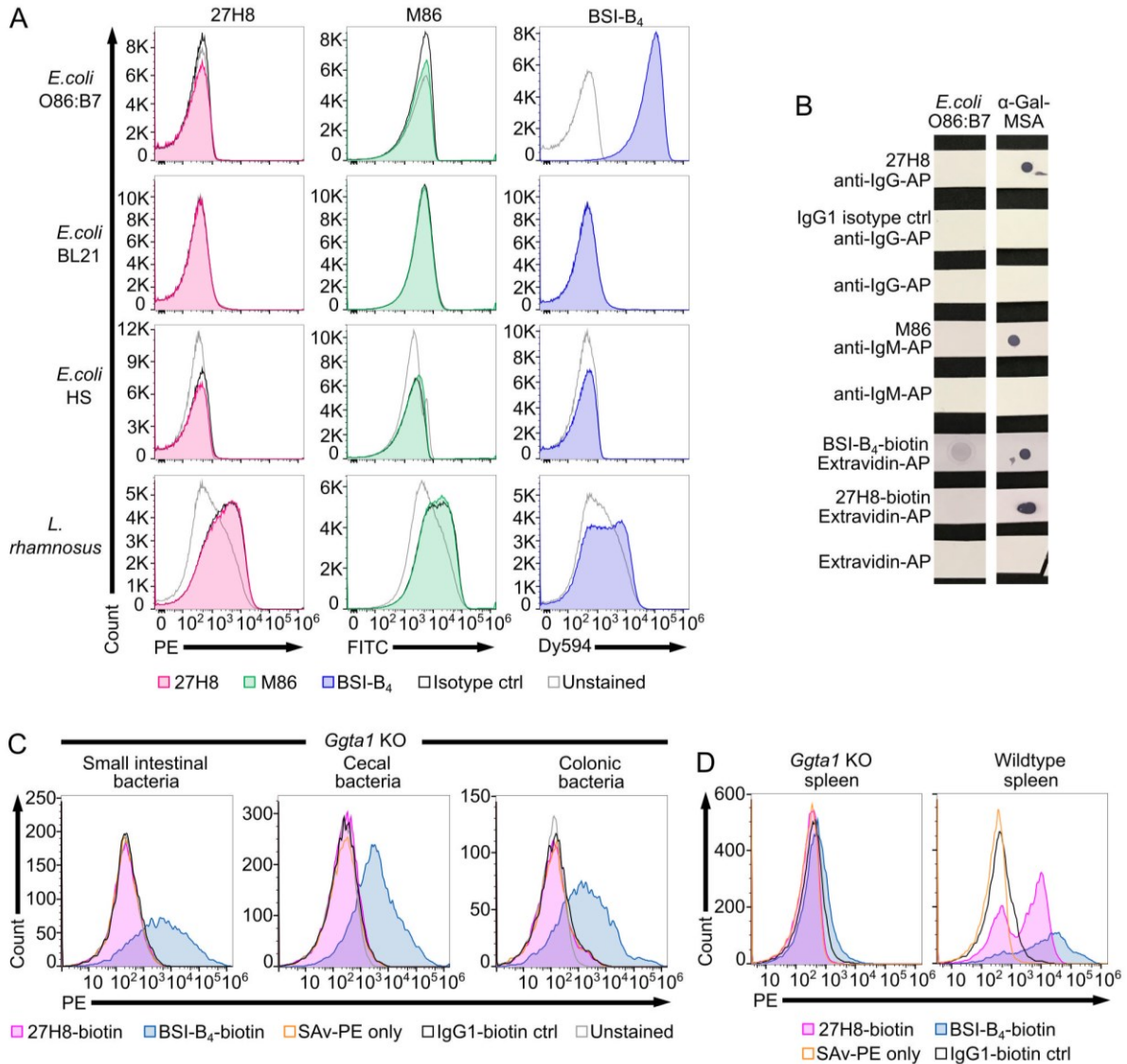


Figure 13: No binding of 27H8 and M86 to intestinal bacteria in contrast to BSI-B4

(A) Histograms of flow cytometric analysis of cultured bacterial strains stained with 27H8, M86 and BSI-B₄ and respective isotype controls (IgG1 and IgM). Strains: *E. coli* O86:B7, *E. coli* BL21, *E. coli* Human Species (HS) and *L. rhamnosus*. **(B)** Dot blot stain of lysed *E. coli* O86:B7 and α-Gal-MSA as positive control. Uncropped blot depicted in Appendix Figure 19E. **(C)** Representative histogram blots of flow cytometric analysis of intestinal content (derived from SI, cecum and colon) from *Ggta1* KO mice (n=3) stained with 27H8-biotin and BSI-B₄, pre-gated for SYBR green positive bacteria (Appendix Figure 20A). **(D)** Live splenocytes of *Ggta1* KO and WT mouse (Appendix Figure 20B) stained with 27H8-biotin and BSI-B₄. **(C, D)** Control staining with IgG1-biotin isotype and SAV-PE only.

3.2.5 Summary

In conclusion, the development of a novel IgG1 antibody called 27H8 is described that showed highly specific binding to both synthetic and naturally occurring a-Gal epitopes. The 27H8 monoclonal

antibody showed high affinity to the a-Gal epitope and could be widely applied for a-Gal epitope detection in ELISA, dot blots, immunohistochemistry and flow cytometry. 27H8 antibody did not bind specifically to bacteria originating from the intestinal tract while cross-specific BSI-B4 stained cultured or intestinal bacteria. Therefore, the monoclonal antibody 27H8 can be used as a novel tool for a-Gal detection with high sensitivity and specificity. Lastly, the results of this study question the role of the intestinal microbiota as a major source of the a-Gal epitope for sensitization.

4 DISCUSSION

The aim of this thesis was to investigate the impact of the intestinal microbiome on immune tolerance and the susceptibility to food allergies. This work was conducted in two subprojects. First, gnotobiotic mouse models (GF, ASF³, ASF⁷, Oligo-MM¹² in comparison to SPF) were used to reveal an impact of microbial complexity on immune tolerance regulation. Secondly, a novel IgG antibody against the α -Gal epitope was established to test if intestinal bacteria could be actual inducers of abundant anti- α -Gal immunoglobulins in humans possibly relevant in red meat allergy.

4.1 Use of gnotobiotic animals to reveal an impact of the intestinal microbiome on immune tolerance

4.1.1 Immune cell changes correlating with microbial complexity

GF mice and antibiotics treated mice have been reported to display reduced levels of ROR γ t⁺ Helios-Tregs in the colon [33, 34]. By mono-colonizing mice with individual bacterial strains of different phyla Sefik *et al.* were able to show that different strains are able to induce colonic ROR γ t⁺ Helios-Tregs to a varying extent and that this capacity is independent of their phylum [34]. This redundant ROR γ t⁺ Helios-Treg inducing capacity was also confirmed by Geva-Zatorsky *et al.* as one-quarter of diverse bacterial species in their mono-colonization experiments were found to induce this cell type [85]. The results of this thesis show that ROR γ t⁺ Helios-Tregs (pTregs) are also reduced in animals with a lower microbial complexity than SPF animals in the SI – the intestinal segment with a possible high relevance for food allergy. Animals colonized with 3 ASF strains (ASF³) displayed the lowest frequency of ROR γ t⁺ Helios-Tregs, animals colonized with 12 different strains (Oligo-MM¹²) a higher pTreg frequency than ASF³ but a lower than SPF animals, which displayed the highest frequency of pTregs in the SI. These results align with ROR γ t⁺ Helios-Tregs frequencies in the SI of gnotobiotic animals reported by Wyss *et al.* [146]. Oligo-MM¹² animals in that study displayed more ROR γ t⁺ Helios-Tregs than GF and less than SPF animals in the spleen, mLNs, and colon. In contrast, in the SI, pTreg frequencies in SPF mice did not exceed Oligo-MM¹² animals which were observable in the results of this thesis. The difference in the results for the SI can be explained by a likely difference in microbiome composition between SPF animals used by Wyss *et al.* and the SPF animals used in this thesis exhibiting more pTreg inducing bacteria in their intestines. ROR γ t⁺ Helios-Tregs correlated with microbial complexity also in the mLNs and spleen (ASF³<Oligo-MM¹²<SPF) indicating that microbiome - immune system interactions that take place in the intestine also have relevance for the immune training of other organs highlighting the relevance of the intestine for systemic Treg cell

biology. Since ASF⁷ strains displayed a higher frequency than Oligo-MM¹² mice, the number of bacterial strains alone cannot be the sole deciding factor for pTreg levels. This aligns also with experiments conducted by mono-colonizing mice [34]. Different bacterial strains are able to induce pTregs to a various extend despite close evolutionary relationships [34]. The additional strains in the ASF⁷ consortium compared to ASF³ could be stronger pTreg inducers than strains present in the Oligo-MM¹² mice. Another possibility is that since ASF⁷ mice in these experiments were colonized only later in life, the changes in pTregs actually reflect only this later colonization by bacteria compared to the more physiologic colonization right after birth. This would explain also the drastic increase in overall Tregs, relatively high abundance of Th17, GATA3+ Helios+ Tregs and ILC3s observed in this mouse group compared to ASF³ and Oligo-MM¹² animals. The so-called 'weaning reaction', an immunological response to the changed microbiota due to the introduction of solid foods, is required during a specific time window that otherwise leads to a susceptibility to inflammatory pathologies in the adult [147]. Another factor that impacts ROR γ t+ Treg frequencies (at least in the colon) is the so-called 'homeostatic setpoint' [148] determined by the mother's humoral response. This maximum quantitative capacity to generate ROR γ t+ Tregs is mediated by maternally transferred IgA and determined postnatally early in life [148]. Experiments that included the ASF⁷ mouse group should therefore be repeated with ASF⁷ animals colonized right after birth (born from ASF⁷ mothers) in order to exclude effects of a later time point in colonization on immune cell frequency changes.

Interestingly, Th2 cells were inversely correlated with pTreg frequencies in the intestine. This fits to data that microbiota-devoid animals exhibit an increased amount of total IgE [79] and an increased susceptibility to food allergies [86] and shows that minimal microbiota mice might also display a Th2-dominated immune bias possibly leading to increased allergic susceptibility.

ILC2s and ILC3 ratios, based on the relative amount of all lineage negative cells, did not correlate with microbial complexity. These results were gained from either processing the SI as a whole or when investigating the spatial distributions among duodenum, jejunum and ileum between mice of differential complexity. For the lamina propria of the whole SI, there was a slight increase in frequency in ILC3s visible in ASF³, but Oligo-MM¹² and SPF mice showed equal frequencies among lineage negative cells. ASF⁷ mice interestingly had the lowest frequencies in ILC2s and the highest in ILC3s, which indicates that the time of colonization might influence ILC frequencies. In food allergy-prone mice with a gain-of-function mutation in the IL-4 receptor α -chain (*IL4raF709*), ILC2s were increased and IL-4 secretion of ILC2 contributed to the allergic response by reducing allergen-specific Treg cells [149]. An ILC2 correlation with simultaneously enhanced Th2 cell frequencies was not observable in the SI in this study. Furthermore, a correlation between relative amounts of pTregs and ILC3s that could be reasoned from their positive correlation in the human intestine [38] could also not be

confirmed here. In previous studies microbial colonization also did not result in changed overall ILC3 frequencies [85]. It is noteworthy, that the gating strategy applied here using lineage negative cells as a pre-gate for ILCs might lack specificity and should include more surface and transcription factor markers for each individual ILC population. Here, ILC identification was included in a panel focused on Treg / Th2 cell identification which did not allow further markers to be included due to flow cytometric acquisition limits.

Results from the investigation of cDC populations revealed ratio changes in cDC subpopulations (cDC1s vs cDC2s) between the ASF³, Oligo-MM¹² and SPF animals that correlated with microbial complexity and pTreg frequencies and thus with Th2 cell frequencies in the SI. The cDC subpopulations that correlated with pTreg frequencies included CD8 α +, CD11b+ CD103- or CD103+ CD11b- cDCs in the SI. CD103+ CD11b- belong to cDC1s in non-lymphoid tissues [19]. The frequency of CD11b+ CD103- subpopulations of SIRP α + cDC2s increased with microbial complexity. In mLNs, CD103+ CD11b- migratory cDC frequencies correlated with pTreg frequencies and to a minor extent also with CD8 α + resident cDC1 frequencies. SIRP α + cDC2 frequencies correlated in the SI and in both migratory and resident mLNs cell fractions with Th2 cell frequencies as they were enhanced in the SI of animals with the lowest microbial complexities (ASF³ and Oligo-MM¹²). These results suggest that in particular either the CD11b+ CD103- cDC2 or the CD103+ CD11b- cDC1 frequencies are correlated with the capacity of the microbiota to induce pTreg induction. Studies hint towards the involvement of the latter: CD103+cDCs of the intestinal lamina propria or mLNs have been found to produce a substantial amount of retinoic acid (RA) and TGF- β both favoring efficient pTreg induction [37]. These cells displayed the highest expression of genes producing RA (*Aldh1a2*) and TGF β 2 (*Tgfb*) in overall mLNs via single cell sequencing, while CD11b+ DCs had the lowest expression of these genes of a pTreg signature [37]. Furthermore, this study showed that mLNs of GF animals showed a selective expansion of CD103+ CD11b+ populations [37], which aligns with the increased relative abundance observed in ASF³ and Oligo-MM¹² here. One explanation why pTregs are lower in the animals with lower microbial complexity could indeed be that CD103+ cDCs are reduced, but this can only be attributed to the CD11b- fraction (cDC1s). A reduced relative abundance would lead to a higher ratio of other cDC subpopulations. The reduction of cDC1s could then lead to an increased frequency of cDC2s (in particular double positive CD103+ CD11b+) that could then drive the Th2 cell increase. Surprisingly though is the decreased frequency of CD11b single positive cDCs in mice with a lower microbial complexity, which has not been reported before. Whether this population is associated with decreased pTreg induction or merely a bystander effect is still an open question. This is particularly relevant because CD11b+ DCs in mLNs have been found to rather have genes expressed associated with pathogen sensing and the initiation of inflammatory responses than a pTreg induction profile

[37], however these results stem from mLNs and not the lamina propria. Another study shows that in particular CD11b⁺ CD103⁺ DCs induce anti-parasitic Th2 responses in the SI, whereas CD11b⁺ CD103⁻ perform this function in the colon [150]. This observation fits with the data presented here: DP CD11b⁺ CD103⁺ in the LP-SI and of migratory DCs in the mLNs are inversely correlated with microbial complexity and correlate with Th2 frequencies in the LP-SI possibly driving the increased number of Th2 cells. While cDC ratio changes are clearly visible in the results here, others have shown that DCs play a minor role in pTreg induction while ROR γ t⁺ expressing APCs, ILC3s or Thetis cells play the major role [38–40].

Lastly, the objective here was to investigate the impact of microbial complexity on immune cell frequencies by using gnotobiotic mice of different microbial complexities (ASF^{3/7}, Oligo-MM¹², SPF). It was thereby assumed that the total number of bacteria (independent of strains) in each consortium would roughly be the same and only the complexity (number of different strains) would differ. This was not tested here and should be obtained in future studies to differentiate between the impact of reduced bacterial numbers and bacterial strain complexity. Quantitative PCR analysis or 16S rRNA analysis of SI-content would allow such a distinction.

4.1.2 Untargeted and targeted metabolomics reveal increased primary and secondary bile acids in SPF compared to gnotobiotic animals

In order to identify metabolites that could be implicated in pTreg induction or Th2 cell frequency enhancement in the LP-SI an untargeted metabolomics approach was applied. The overall metabolites of the ileal contents of ASF³, Oligo-MM¹² and SPF animals revealed differences in the BA metabolism by correlating feature intensities with microbial complexities. Therefore, a targeted metabolomics measurement of BAs was applied including the quantitative measurement of SCFAs which have been reported as pTreg inducers [43] to test if differences in BAs/SCFAs would explain the pTreg/Th2 phenotype between the differentially colonized mice. Targeted metabolomics of BAs revealed that in particular glycine-conjugated primary BAs were increased in SPF animals and Oligo-MM¹² animals compared to ASF³ and ASF⁷, while taurine-conjugated primary BAs did not correlate with microbial complexity. Several primary BAs aligned with microbial complexity (CDCA, GCDCA, CA, GCA) as well as secondary BAs (7-KLCA, UDCA, 3-DHCA, UCA), but ASF³ and ASF⁷ animals generally showed comparable BA concentrations. This alignment of microbial complexity with both primary and secondary BAs is interesting as bacteria have been more in focus for their role in secondary BA production as they possess a whole variety of species-dependent enzymes for modifying primary BAs [151]. Other groups also reported that GF animals show less primary BAs compared to SPF animals and regulate BA synthesis in the liver *via* farnesoid X receptor (FXR) dependent mechanisms [152].

The results confirm that the intestinal microbiota indeed also regulates the production of primary BAs possibly *via* direct receptor binding. Sinha *et al.* found that the presence of the secondary BAs LCA and deoxycholic acid (DCA) are reduced in ileal pouches from ulcerative colitis patients compared to familial adenomatous polyposis patients and a supplementation of these secondary BAs has anti-inflammatory effects as it was associated with a reduction of the chemokines and cytokines CCL5, CXCL10, IL-17A and TNF α [153]. LCA was not detectable in this study. DCA was not detectable in both Oligo-MM¹² and ASF³/ASF⁷, but detectable in SPF mice, reflecting the importance of microbial status for the production of this BA. A direct correlation of pTregs with these secondary BAs for possible anti-inflammatory effects cannot be seen as ASF^{3/7} and Oligo-MM¹² mice showed equal levels. Screening studies to identify pTreg inducing BAs have found that isoDCA and ω -MCA increased Foxp3 induction *via* DCs *in vitro* and isoDCA producing bacteria were able to increase colonic ROR γ ^t+ Tregs *in vivo* [47]. IsoDCA and LCA were both below detection limit for all tested groups, ω -MCA was not detectable in both Oligo-MM¹² and ASF³/ASF⁷, but detectable in SPF mice. Thus, ω -MCA could be involved in pTreg induction in SPF mice, but it seems unlikely that this BA is causative for the enhanced frequency of pTregs in the LP-SI in Oligo-MM¹² mice compared to ASF³ mice. Campbell *et al.* further showed that the FXR in DCs could be implicated in isoDCA signaling for Treg generation [47]. Signaling of known BA receptors such as FXR, pregnane X receptor, vitamin D receptor or TGR5 [154] on immune cells could be an interesting further step to investigate mechanisms by which the identified primary and secondary BAs (CDCA, GCDCA, CA, GCA, 7-KLCA, UDCA, 3-DHCA, UCA) could mitigate pTreg induction. Song *et al.* reported that both diet and microbial composition has a profound impact on BA concentrations [45]. When feeding SPF mice with a minimal diet supplemented with one or more primary or secondary BAs, they found a further induction of pTregs (they are defined as ROR γ ^t+ Helios⁻ Tregs as in this study) to a variable extend: in particular a mix of the murine primary BAs CA/UDCA/CDCA (or either two of this mix) or of the secondary BAs DCA/LCA/oxidized BAs. A correlation of pTreg numbers and the particular primary BAs can be confirmed in this study: CA, UDCA (a secondary BA in humans, but also a primary BA in mice [125] listed as a secondary BA here) and CDCA all follow the pattern ASF³<Oligo-MM¹²<SPF. However, this cannot be confirmed for the secondary BAs. As mentioned above, LCA was not detectable and DCA only in SPF mice. Oxidized BAs were not measured due to (non)availability of standards. A further study found that the secondary BAs and LCA derivatives 3-oxo-LCA and isoalloLCA both induced Treg differentiation [46]. IsoalloLCA is greatly reduced in patients with inflammatory bowel diseases [155]. Both 3-oxo-LCA and isoalloLCA were not measured in this study again due to (non)availability of standards. Altogether this highlights that a number of primary (in particular glycine-conjugates) and secondary BAs could be implicated in pTreg induction with possible redundant roles. It should

be further investigated whether the identified BAs are directly acting on pTreg induction via *in vitro* assays or are a mere bystander effect of the generally changed metabolite composition between SPF and gnotobiotic animals (ASF^{3/7}, Oligo-MM¹²). Furthermore, due to possible redundant roles of different BAs in pTreg induction it is possible that the metabolites inducing pTregs in the different mouse groups might not overlap but are rather a representation of the variety of metabolites that are able to induce pTregs.

SCFAs are generated by fermentation of dietary fibers by commensal bacteria and have been further implicated in pTreg induction in the intestine, i.e. butyric acid induces the differentiation of (p)Treg cells in mice [42, 43, 156]. A targeted metabolomics measurement in this study revealed that SPF mice display the highest amount of the measured SCFAs in comparison to ASF^{3/7} and Oligo-MM¹² mice. Only acetic acid and slightly propionic acid showed a slightly higher amount in Oligo-MM¹² reflecting pTreg frequency distributions in the different mouse groups. These results do not completely replicate the results gained from *in vitro* studies in which Foxp3+ induction from naïve CD4+ T cells was measured [43]. Arpaia *et al.* showed that butyrate, isovalerate, propionate and isobutyrate display the highest capacity for Treg induction in contrast to acetate. This might reflect the difference of *in vivo* and *in vitro* measurements, but indicates that further cells could be implicated in pTreg induction that are induced by SCFAs and are not present in the *in vitro* system. Also, SCFAs were measured in the ileum as the focus lay on pTreg frequencies in the LP-SI and not the colon. Furusawa *et al.* reported that feeding SPF mice with butyrate increased Tregs (Neutropilin-1-, Foxp3+) in the colon to the highest extent, propionate to medium amounts, while acetate was comparable to the control group [156]. These results indicate that SCFAs presumably play a subordinate role in pTreg frequency differences correlating with microbial complexity in this study. The high amount of SCFAs in SPF mice relative to the gnotobiotic groups could thus be a bystander effect. Acetic acid should be taken into focus if there is indeed a pTreg inducing effect observed in this study that has not been identified by others.

Regarding other molecules that were identified in the untargeted metabolomics measurements could be correlated to pTreg or Th2 frequencies in the LP-SI of ASF³, Oligo-MM¹² and SPF mice, further targeted measurements with the according molecules as standards should be performed. This is necessary as the feature annotations in untargeted measurements are the most probable but may not be accurate. A current bottleneck in untargeted metabolomics interpretation is the annotation accuracy, which has to be continuously improved i.e. through the standardization of the queried public databases for annotations [157]. The most accurate measurement can be achieved by running internal standards on the same machine in parallel. Due to the high variety of measured metabolites a standard for every feature may though be difficult to achieve.

In vitro cellular assays incubating CD4+ naïve T cells with the identified molecules and investigating

their differentiation to Foxp3 expressing Tregs could be a further step. It should be taken into account that both the intestinal environment or further immune cells (DCs, ILC3s or Thetis cells) need to be included in these *in vitro* systems as microbial metabolites could act on these cells for pTreg induction rather than directly on naïve T cells. Butyrate has also been found to act on DCs by histone deacetylase inhibition for Treg induction [43].

A further limitation of the study is that most metabolites that were increased in SPF mice did not show differences between ASF^{3/7} and Oligo-MM¹² animals and were disregarded for a possible pTreg inducing effect. In fact, they were below the limit of detection for all gnotobiotic mice, so an actual difference between ASF^{3/7} and Oligo-MM¹² could not be evaluated.

4.1.3 Food allergy model

As pTreg frequencies in the SI, mLNs and spleen decreased with microbial complexity and Th2 cell frequencies in the SI were increased in ASF³, ASF⁷ and Oligo-MM¹² mice, a food allergy model was conducted to investigate if these changes in the immune cell populations would also lead to an exacerbated phenotype in food allergy. The food allergy model was set up sensitizing orally with OVA antigen and challenging i.v. to induce an anaphylactic shock, one of the major risks for food allergic patients. The data showed that even though GF* animals consistently reacted during the challenge, ASF⁷, Oligo-MM¹² and SPF displayed a great variability (some showed a decline in core body temperature, others did not). Furthermore, gnotobiotic groups with a minimal microbiota (ASF⁷, Oligo-MM¹²) did not show greater anaphylaxis (ΔT_{\max}) and allergic parameters than SPF mice (MPCT-1 levels in serum, OVA-specific IgE). This data indicates that even though pTregs are decreased, the susceptibility to and severity of symptoms in food allergy did not increase. A relationship between pTregs numbers and an enhanced allergy susceptibility can therefore not be stated. The low-diversity microbiota groups used in this study, have also been shown to display increased IgE levels as reported for ASF in [81] and for Oligo-MM¹² in [146], which would suggest enhanced allergy susceptibility. However, pTreg induction of minimal microbiota mice compared to GF mice did also not correlate with the inhibition of hyper IgE formation [146].

Furthermore, there is also the possibility that due to the choice of model the correlation between a minimal microbiota and an increased susceptibility for food allergy could not be visible. Next to CT other groups have relied on staphylococcal enterotoxin B (SEB) which seems to correlate more with typical food allergic parameters such as eosinophilia [83, 158]. Others have relied in such studies on *Il4raF709* mice that are genetically prone to food allergy which additionally display dysbiotic flora promoting food allergy [89]. Using non-food allergy prone mice as in this study allowed for testing the impact of the microbiome in a more physiological setting and successful sensitization could be

demonstrated as a majority of mice did react with a drop in core body temperature reflecting anaphylaxis.

Since the mean ΔT_{\max} was lower in ASF⁷ and Oligo-MM¹² mice than SPF mice, it could be possible that the immune system of the minimal microbiota mice might be underdeveloped by not having the capacity to elicit a full blown allergic response observable under dysbiotic conditions. It has also been reported that GF mice are more protected in a food allergy model with systemic sensitization and oral challenge as the critical step of mast cell homing was prevented in these mice [159]. In the results of this study, GF* mice did indeed react with a consistent anaphylaxis compared to all other tested groups (ASF⁷, Oligo-MM¹², SPF) and therefore rather showed a higher susceptibility for food allergy than SPF / conventional mice.

Other groups have also shown that colonization with commensal bacteria protects against sensitization with peanut allergen [86]. In their food allergy model (using peanut allergen and CT sensitization), GF mice showed increased peanut-specific serum IgE compared to SPF mice and the mean ΔT_{\max} was greater in GF than in SPF mice without reaching significance, and the variability between mice of one group was also high. Mono-colonisation with *Clostridium* species prevented anaphylaxis in this study [86]. This highlights that certain species might indeed be preventive for allergen sensitization and not an increased complexity per se. Both ASF⁷ and Oligo-MM¹² mice contained *Clostridium* species which could explain why their mean ΔT_{\max} was lower than GF* mice and fewer mice reacted with a temperature drop than GF* mice. It would be further interesting to screen for the abundance and distribution of different bacterial species in the ASF⁷, Oligo-MM¹² and SPF mice and assess if individual bacterial strains and their possible alteration during the sensitization phase could be correlated with the degree of ΔT_{\max} .

Feehley *et al.* used a similar food allergy model but sensitizing with BLG and oral challenge [84]. They observed a significant drop in body temperature of GF mice compared to mice transferred with healthy infant microbiota. The ΔT_{\max} in that study was $\sim 1^{\circ}\text{C}$ while the ΔT_{\max} observed here was $\sim 5^{\circ}\text{C}$. This means that based on the choice of allergen and setup food allergy models can differ quite distinctly, but all readouts display a great variability between single mice.

It would further be interesting to include the ASF³ mouse group in the food allergy setting as their Th2 increase was more pronounced than in Oligo-MM¹² mice and see if it reflects the GF status. Also, the contamination of GF* mice with *Paenibacillus sp* should be taken into account as it might have shifted the results.

It is noteworthy that pTreg frequencies in the LP-SI were increased upon OVA administration in GF* and SPF mice. This indicates that allergen administration independent of microbial colonization can enhance the frequency of pTregs. Oral administration of OVA-antigen has been shown to induce *de*

novo Treg induction in mLNs rather than the expansion of a pre-existing population [160]. Whether these induced pTregs are OVA-specific needs to be further elucidated. The impact of inflammation, a possible disrupted barrier and enhanced contact to foreign antigens as a consequence of CT administration should also be taken into account. As both sens. and ctrl animals received CT treatment the addition of OVA-antigen must be crucial in pTreg induction.

4.1.4 Future directions of microbiota and host relationship

While correlations between microbial colonization and pTreg / Th2 frequencies in the intestine could be demonstrated, causal relationships of the cellular and bacterial players still need to be elucidated. The way to identify these relationships here was to analyze microbial metabolites in gnotobiotic (colonized with strains from the ASF and Oligo-MM¹² consortia) and SPF animals that could impact pTregs by correlating intestinal cellular frequencies with untargeted and targeted metabolomics of ileum content samples. Next to the metabolomic profile, metagenomics, metatranscriptomics and metaproteomics could be viable tools to identify bacterial genes and pathways that could impact host immune tolerance. This requires knowledge of bacterial genes, proteins and functions of the intestinal microbiome. Using such meta-omics approaches would allow to functionally characterize the intestinal microbiome. Developing these fields and techniques is ongoing and is critical to advance the knowledge for host-microbiota relationships [161].

While a more complex and physiological system of several bacterial strains in one community was used here, mono-colonization and identifying the immunostimulatory capacities of single bacterial strains could also be an important and viable tool. Mono-colonization experiments combining immunophenotyping and transcriptomics provided insights into the redundancy and diversity of the effect of different bacterial species altering immune pathways [162].

A summary of the presented investigation of the intestinal microbiome effects on immune cell tolerance is displayed in Figure 14.

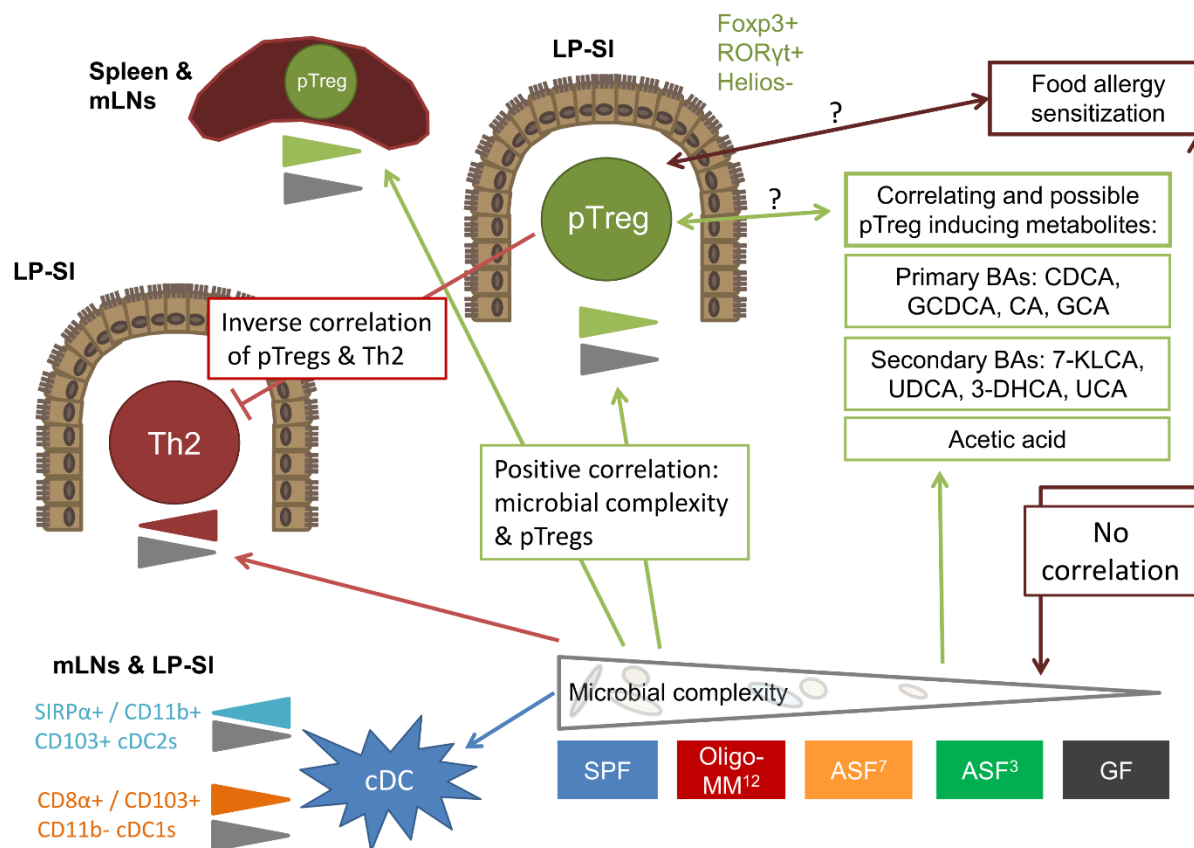


Figure 14: Graphical summary of results presented in chapter 3.1

In a comparative analysis of gnotobiotic mice and SPF mice, microbial complexity was directly correlated with pTreg frequencies in LP-SI, spleen, mLNs; inversely with Th2 frequency in LP-SI, linked to cDC subpopulations frequency changes in mLNs and LP-SI (inversely correlated with SIRP α / CD11b $^+$ CD103 $^+$ cDC2s and positively correlated with CD8 α $^+$ / CD103 $^+$ CD11b $^-$ cDC1s) and positively correlated with depicted primary and secondary BAs. An enhanced sensitization susceptibility of low complexity mice (ASF 7 and Oligo-MM 12 compared to SPF) in a model of food allergy (OVA) was not observed. The direct interaction of cell types and metabolites remains to be investigated. Gradients (\triangleleft / \triangleright) indicate relative abundance (colour) or microbial complexity (grey).

4.2 A novel IgG antibody for Gal- α 1,3-Gal detection questioning α -Gal epitope expression by bacteria

Humans naturally display antibodies reactive to Gal- α 1,3-Gal, the determining structure of the α -Gal epitope, which exhibit a broad range of pathogen reactivity and can also bind to non- α -Gal epitopes such as human blood group B, A and O [105]. Different approaches have been used to purify such polyclonal and potentially cross-reactive anti- α -Gal antibodies [104, 163], yet they may also bind to non-Gal- α 1,3-Gal expressing organisms [105]. Previously, it has been hypothesized that anti- α -Gal

antibodies are induced by members of the intestinal microbiota, as *Escherichia coli*, *Klebsiella* and *Salmonella* strains can bind to polyclonal anti- α -Gal antibodies purified with Gal- α 1,3-Gal- β 1,4-Glc [104]. For instance, oral inoculation of *Ggta1* KO mice with the *E. coli* strain O86:B7 has been shown to elicit enhanced anti- α -Gal titers [131]. However, only the expression of α -Gal-like structures has been demonstrated for *E. coli* O86:B7 to date as an additional fucose residue is attached to Gal- α 1,3-Gal [164]. To determine if bacteria express the α -Gal epitope defined as Gal- α 1,3-Gal or Gal- α 1,3-Gal- β 1,4-GlcNAc without further residues attached to the second last galactose, the use of polyclonal, cross-reactive human anti- α -Gal antibodies might therefore lead to false positive results. Similarly, the lectins BSI-B₄ and MOA, binding also to α -Gal-like structures such as the blood group B antigen, do not exclusively recognize the α -Gal epitope. However, both polyclonal human anti- α -Gal antibodies and lectins have been used to demonstrate α -Gal epitope expression by bacteria and the microbiota in the past [106, 108].

4.2.1 Development of an α -Gal specific IgG antibody

Monoclonal antibodies allow a more precise epitope recognition after excluding cross-specificity as presented in this study. This thesis describes the development of a novel monoclonal IgG1 antibody called 27H8 which binds to both the di- and trisaccharide α -Gal epitope with high affinity but does not display cross-reactivity to the blood group B antigen. The results demonstrate that the 27H8 monoclonal antibody recognizes the same α -Gal containing structures as the most commonly used monoclonal IgM antibody called M86. The M86 antibody also bound to both the di- and trisaccharide α -Gal epitope (Gal- α 1,3-Gal or Gal- α 1,3-Gal- β 1,4-GlcNAc). The specificity to the disaccharide is confirmed in a study by Langley *et al.* who show the crystal structure of the M86-Gal- α 1,3-Gal complex and demonstrate that the tryptophan residue at Kabat position 33 (W33) is crucial for M86 binding [165]. This IgM antibody has been developed by Galili *et al.* in a similar approach by immunizing *Ggta1* KO mice but with α -Gal rich rabbit red blood cells [133] in contrast to synthetic α -Gal-OVA used in this study. Since SPR-affinity studies indicate that the K_Ds of the variable regions of the pentamer IgM antibody M86 genetically engineered to scFv-IgE antibodies [166] are higher than 27H8, the assumption can be drawn that 27H8 variable regions bind to α -Gal at a higher affinity than M86. A broad screening approach was used in this thesis by utilizing cell lysates and purified α -Gal-rich proteins and lipids, and specificity of 27H8 to α -Gal was demonstrated via enzymatic digestion, the use of *Ggta1* KO mice and pigs and the transgenic expression of α 1,3-galactosyltransferase in HEK cells. The 27H8 antibody recognizes α -Gal-conjugated proteins or natural α -Gal-rich compounds and glycolipids and is applicable in dot blot, immunohistochemistry, ELISA and flow cytometry, demonstrating robustness in its α -Gal epitope recognition. As the 27H8 antibody does not bind to the

blood group B antigen, it can be concluded that further residues on the core galactose would limit antibody binding to α -Gal. This characteristic is shared with the M86 antibody which also did not recognize the blood group B antigen. Even though the sequence of 27H8 antibody is not displayed in this thesis, it can be said that it differs in the amino acid sequence in both variable regions from M86 [167], but shares the W33 residue in the CDRH1 – a common feature of human anti- α -Gal binders [165]. Despite the similarity in α -Gal-epitope specificity, the 27H8 antibody displays unique features and advantages when compared to M86. Next to the increased affinity, 27H8 is easily purifiable and can thus be directly labeled with fluorophores or enzymes for example to design improved ELISA systems.

4.2.2 Do bacteria express the α -Gal epitope?

The 27H8 antibody was then used to test the hypothesis if intestinal bacteria are a major source of α -Gal possibly involved in the sensitization of the human immune system against this epitope. Therefore, 27H8 antibody was applied to lysates of bacteria hypothesized to be α -Gal expressing organisms via their expression of α 1,3-galactosyltransferase-like genes [108]. Strikingly, binding of 27H8 to *H. pylori*, *H. influenzae*, *S. typhimurium*, *P. aeruginosa*, *A. baumannii* and *A. muciniphila* could not be detected. This lack of binding could also be demonstrated for *E. coli* O86:B7, another human *E. coli* isolate, *L. rhamnosus* and more generally for the majority of murine intestinal bacteria isolated from *Ggta1* KO mice. As this is a negative result, it cannot be excluded that the 27H8 antibody binds to bacteria not tested in this setup or under different experimental conditions. However, as 27H8 also failed to stain murine intestinal bacteria derived from a host devoid of α -Gal, it can be proposed that intestinal bacteria are generally devoid of the native α -Gal epitope. Similarly, the use of M86 for bacterial α -Gal epitope detection has not shown convincingly the presence of the genuine α -Gal epitope, and many studies relied on the use of lectins for this purpose [106–108]. In this setting, binding of M86 to bacteria could equally not be observed when applied in flow cytometry or to lysates of cultured bacteria. It can therefore be concluded that either Gal- α 1,3-Gal is not present on the tested bacteria of the intestinal microbiome, or it must be part of a more complex structure that shields antibody recognition by high-affine 27H8 and also M86 antibodies. Consequently, the defining α -Gal epitope structure Gal- α 1,3-Gal without further residues attached may not be expressed by bacteria at all. Another possibility might be that the α -Gal epitope is only revealed after processing the bacterial oligosaccharide structures by the host. Therefore, it should be carefully differentiated between the expression of the actual α -Gal epitope, namely Gal- α 1,3-Gal, and the expression of α -Gal-like glycans, e.g. α -Galactose residues connected via 1,3 linkage to other saccharides or further residues connected to the core galactose to avoid incorrect assumptions. In contrast to non-primate mammals and certain

parasites, intestinal bacteria have been shown to express only α -Gal-like oligosaccharide structures [168] that may elicit initially low affine anti- α -Gal IgM antibodies. According to this scenario, a second yet to be discovered genuine α -Gal epitope source could then trigger affinity maturation and IgG antibody production from this pool of B cells. The induction of human anti- α -Gal IgM (or potentially even IgG) might then be due to antigens similar to the α -Gal epitope expressed on bacterial surfaces that result in cross-reactive immunoglobulins that also recognize the α -Gal epitope. These antibodies however would be functional enough to induce immediate hyperacute xenograft rejection described as one of the major causes inhibiting the feasibility of xenotransplantation of pig organs into human hosts [6].

4.2.3 Future prospects of 27H8 antibody and implications of the α -Gal epitope

Additional methods to elucidate glycan structures on microbes may be nucleic magnetic resonance spectroscopy or reversed immunoglycomics as shown for *Leishmania major* [169]. Moreover, control experiments related to the destruction of the α -Gal epitope by using enzymatic digestion or periodate should be applied when investigating a possible α -Gal expression by microorganisms or other sources, as also described for anti- α -Gal IgE antibodies [139]. Such control experiments are necessary to document the specificity of the tools for anti- α -Gal epitope recognition. For example, with these methods the binding of 27H8 antibody to *S. aureus* strains was found to be independent from the α -Gal epitope, an observation that was also made for human anti- α -Gal antibodies in another study. Also in that study, these antibodies might have bound to protein A and not to the genuine α -Gal epitope [105].

In future studies, it will be interesting to apply 27H8 antibody to parasites suggested to express the actual α -Gal epitope, such as *Trypanosoma brucei* [170], *Ascaris lumbricoides* [171] and also *Plasmodium* species [106, 172] in order to investigate whether recognition of the α -Gal epitope is generally used by the immune system to recognize parasites. Additionally, 27H8 can be used to gain mechanistic insight into the 'red meat allergy' phenomenon mediated via tick bites [173], as compartmentalized α -Gal expression in tick species has been shown by an overlay staining of MOA and M86 [174]. Also, xenotransplantation approaches of mammalian and in particular pig organs transplanted into human recipients heavily rely on the complete absence of the α -Gal epitope or the need to eradicate transplant reactive anti- α -Gal antibodies in the recipient prior to transplantation. The 27H8 antibody may be used to develop diagnostic tests and tools for α -Gal expression in diets and prior to organ transplantation and develop more sensitive sandwich ELISA tests to determine anti- α -Gal isotype levels in patients.

Other aspects of the immune response against the α -Gal epitope will be furthermore important to

elucidate and crucial research questions remain to be answered. Does α -Gal-containing food play a role in the induction of human anti- α -Gal antibodies? Are these human anti- α -Gal antibodies implicated in the development of the α -Gal syndrome regarding the conversion of high-specific anti- α -Gal IgG molecules to the IgE isotype? A recent study has shown that food antigens indeed elicit systemic IgG responses in up to 50% of individuals from an Israeli population correlating with dietary intake [175]. Which factors decide this possible isotype switch to IgE? To investigate this, the establishment of a mouse model of α -Gal allergy will be necessary to allow studying the α -Gal syndrome in an experimental setting.

Furthermore, it would be interesting to better understand if human antibodies against blood groups and antibodies against the α -Gal epitope are promoted in a similar way. There are in fact studies showing that people with blood group B display less anti- α -Gal antibodies in their serum [176].

4.3 Concluding remarks

Altogether, this thesis describes a rigorously characterized and novel monoclonal IgG1 antibody that reliably recognizes the α -Gal epitope with high affinity and specificity. Using this novel tool, it can be proposed to carefully re-evaluate bacterial α -Gal expression as a major epitope source and advocated for essential control stainings using several isotypes and enzymatic cleavage of the epitope to prove genuine α -Gal epitope expression in a given sample. This study further shows that intestinal bacteria and their metabolites have a broad impact on the immune response by influencing Treg, Th cell and DC populations. If focusing on specific antigens inducing immunoglobulins it should be carefully evaluated if the bacteria actually expresses these epitopes or that next to the microbiota also other factors such as diet should be taken into consideration as antigen source. Further organisms such as viruses and fungi could also play a role in epitope presentation.

5 APPENDIX

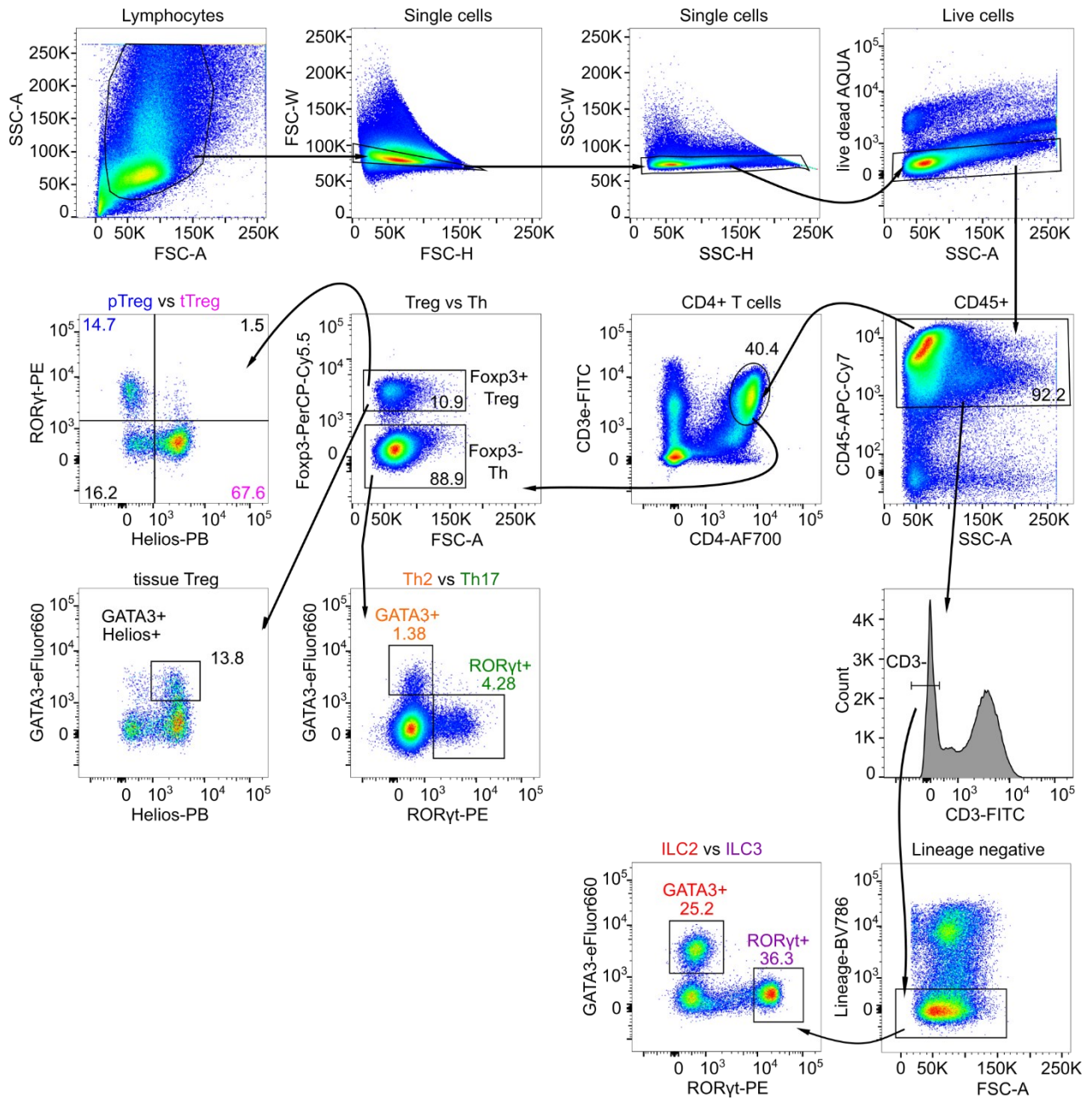


Figure 15: Gating strategy for T cell and ILC panel

Gating strategy for T helper (Th) and regulatory T cell (Treg) and innate lymphoid cell (ILC) subsets in flow cytometry.

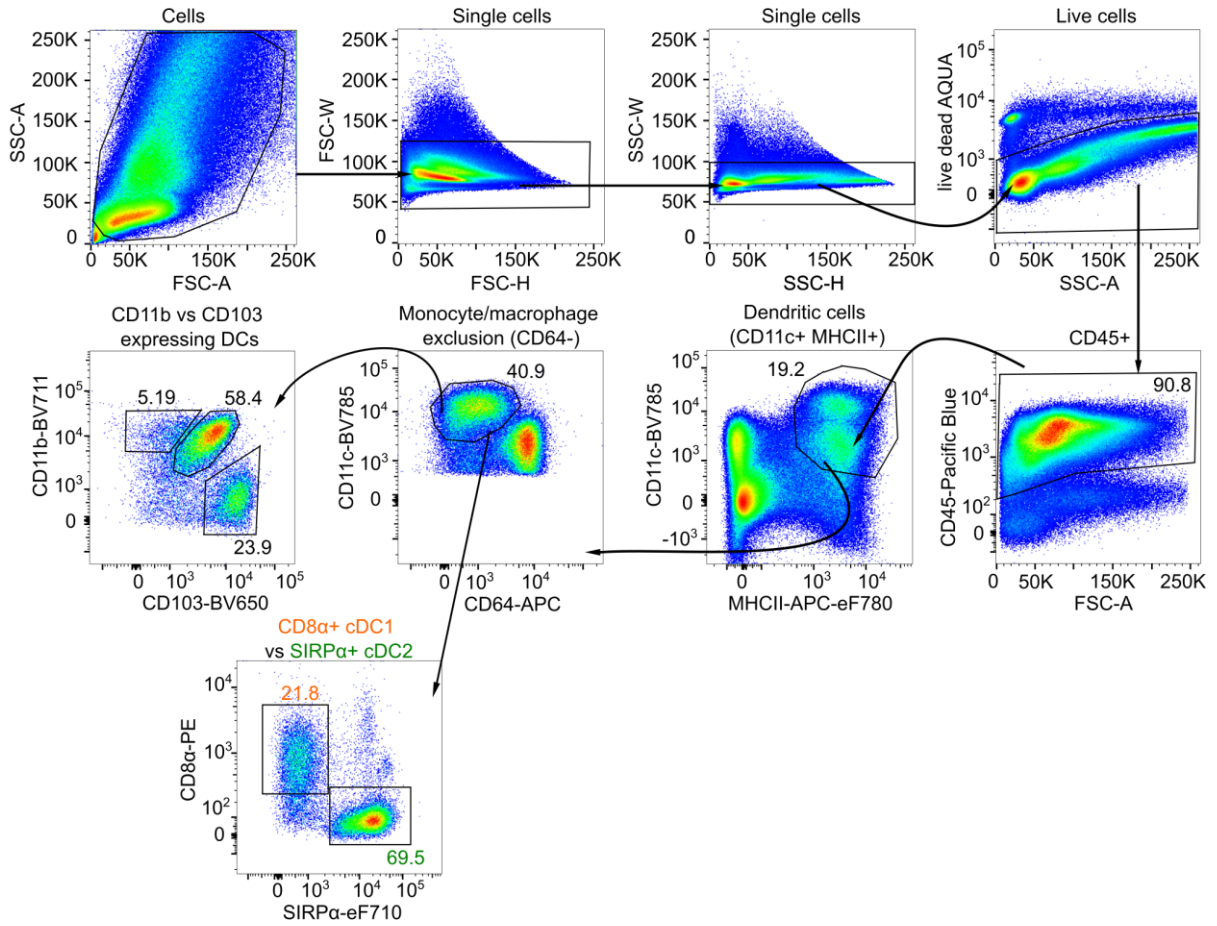


Figure 16: Gating strategy for DC subpopulations in SI and colon

Gating of dendritic cell (DC) subpopulations in small intestine and colon. Depicted is the SI from an ASF³ mouse.

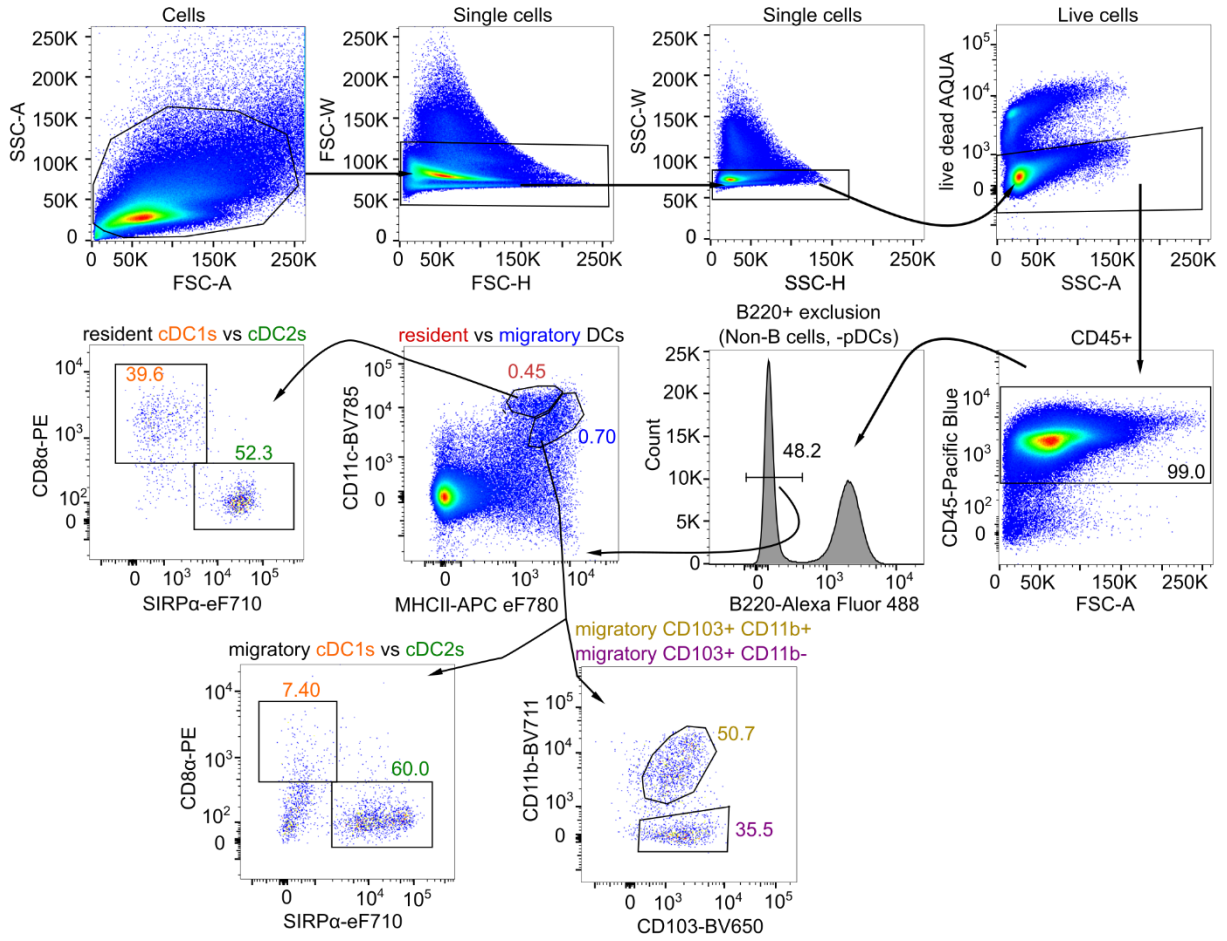


Figure 17: Gating strategy for DC subpopulations in mLNs
 Depicted are the mLNs from an ASF³ mouse.

Table 7: Feature table untargeted metabolomics in ddH₂O negative mode correlating with RORyt+ Helios- Treg percentages

Ileum content samples of ASF³, Oligo-MM¹², SPF mice (4 per group) dissolved in ddH₂O and measured in negative ionization mode via untargeted metabolomics. Features were selected according to availability of ms1 annotation, ms2 fragmentation pattern availability and similarity to annotation, and chromatogram quality. Intensities of features in the table follow mean ASF³<Oligo-MM¹² and Oligo-MM¹²<SPF pattern (negative mean difference (diff.)). Table is sorted according to mean diff. ASF³ vs Oligo-MM¹² maximum to minimum. The three most likely annotations are shown with the most likely in bold. Significant fdr values (<0.05) are bold and marked with *. Abbr.: fdr, false discovery rate; ID, identifier; vs, versus; STD, standard.

<i>Feature ID</i>	<i>Mass annotation (ms1)</i>	<i>ASF³ vs Oligo-MM¹²: fdr</i>	<i>ASF³ vs Oligo-MM¹²: mean diff.</i>	<i>Oligo-MM¹² vs SPF: fdr</i>	<i>Oligo-MM¹² vs SPF: mean diff.</i>
FT0739	Cholic acid; STD_beta-Muricholic acid; STD_g-Muricholic acid/Hyochoolic acid	0.32	-1.53	0.10	-0.85
FT0735	STD_7-Dehydrocholic acid;STD_3-Dehydrocholic acid; 3,7-Dihydroxy-12-oxocholanoic acid	0.62	-0.80	0.05*	-0.85
FT0493	N-Acetylneuraminic acid	0.57	-0.47	0.01*	-0.73
FT0976	STD_Cholic acid-7-sulphate; Jamaicamide B; Repaglinide	0.73	-0.33	0.08	-0.84
FT0906	STD_Glycohychoolic acid; STD_Glycocholic acid; GLYCOCHOLATE	0.72	-0.30	0.12	-0.83
FT0038	STD_Taurin	0.73	-0.22	0.16	-1.15
FT0130	Uric acid	0.73	-0.21	0.46	-0.30
FT0121	STD_L-Fucose; 2-DEOXY-D-GLUCOSE; 2-DEOXY-D-GLUCOSE	0.72	-0.19	0.12	-0.46
FT0161	STD_D-Mannitol; STD_D-Sorbitol;STD_Dulcitol	0.73	-0.17	0.44	-0.22
FT0883	MMV595321; Valechlorin; NCGC00380518-01_C22H30O8_(5S,10Z,11aR)-5-Acetoxy-6,10-bis(hydroxymethyl)-3-methylene-2-oxo-2,3,3a,4,5,8,9,11a-octahydrocyclodeca[b]furan-4-yl 2-methylbutanoate	0.43	-0.16	0.97	-0.01
FT0160	STD_D-Mannitol; STD_D-Sorbitol; STD_Dulcitol	0.73	-0.11	0.29	-0.22
FT0131	Uric acid; 4(3H)-quinazolinone; Ureidopropionic acid	0.81	-0.10	0.28	-0.38
FT0079	STD_L-Glutamic Acid; N-Acetylserine;N-Methyl-D-aspartic acid	0.73	-0.09	0.25	-0.38
FT0579	STD_Maltitol; Lactitol;Lactitol	0.92	-0.05	0.23	-0.36
FT0805	NCGC00380476-01! 5,7-dihydroxy-2-(4-hydroxyphenyl)-6-[3,4,5-trihydroxy-6-(hydroxymethyl)oxan-2-yl]-2,3-dihydrochromen-4-one	0.91	-0.03	0.06	-0.27
FT0181	STD_D-Galacturonic acid; STD_D-Glucuronic acid;2-Ketogluconic	0.98	-0.01	0.63	-0.12

V. Appendix

FT0201	Cysteine-S-sulfate	0.99	-0.01	0.78	-0.10
FT0072	2-Hydroxyquinoline ;4-Hydroxyquinoline; 1H-Indole-3-carboxaldehyde	1.00	0.00	0.75	-0.09

Table 8: Feature table untargeted metabolomics in ddH₂O positive mode correlating with RORyt+ Helios- Treg percentages

For description see Table 7 except that ileum samples were measured in positive mode.

<i>Feature ID</i>	<i>Mass annotation (ms1)</i>	<i>ASF³ vs Oligo-MM¹²: fdr</i>	<i>ASF³ vs Oligo-MM¹²: mean diff.</i>	<i>Oligo-MM¹² vs SPF: fdr</i>	<i>Oligo-MM¹² vs SPF: mean diff.</i>
FT1298	STD_Ursocholic acid ;STD_Cholic acid;STD_Allocholic acid	0.66	-0.80	0.03*	-1.78
FT0090	STD_Taurin	0.66	-0.52	0.03*	-1.21
FT1154	STD_5β-Cholic acid-3α-ol-7-one (7-KLCA) ;STD_5β-Cholic acid-3	0.66	-0.41	0.10	-0.72
FT1219	STD_3-Dehydrocholic acid ;3,7-Dihydroxy-12-oxocholanoic acid;	0.66	-0.34	0.14	-0.55
FT0162	STD_Guanine ; D-Malic acid;Velcorin	0.74	-0.29	0.60	-0.27
FT0778	Glutamyltyrosine	0.66	-0.27	0.97	-0.01
FT0073	L-Proline ;Proline;2-Furanmethanol	0.66	-0.26	0.58	-0.09
FT0091	STD_Taurin	0.66	-0.20	0.05*	-1.31
FT0094	STD_Thymine ;2,3-Diaminopropionic acid;L-2,3-DIAMINOPROPIONIC	0.71	-0.18	0.63	-0.15
FT0463	Glu-Thr ;N2-Succinyl-L-glutamic acid 5-semialdehyde;Glutamylt	0.66	-0.15	0.33	-0.15
FT0404	Valylvaline ;Valyl-Valine;Hypusine	0.70	-0.15	0.16	-0.31
FT0153	STD_L-Glutamic Acid	0.66	-0.14	0.93	-0.02
FT0232	STD_D-Mannitol ;STD_Dulcitol ;STD_D-Sorbitol	0.70	-0.14	0.30	-0.37
FT1014	STD_D-Lactose*H2O ; STD_Melibiose; STD_D-Trehalose	0.66	-0.13	0.10	-0.51
FT0558	8-Oxo-2-deoxyadenosine ; 2'-Deoxyguanosine;STD_Adenosine	0.74	-0.12	0.31	-0.35
FT0305	STD_D-Sorbitol ; STD_Dulcitol ;STD_D-Mannitol	0.70	-0.12	0.29	-0.31
FT0304	STD_O-Acetyl-L-carnitine ;1H-Indole, 3-methyl-1- (trimethylsi	0.80	-0.10	0.31	-0.49
FT0306	STD_Dulcitol ;STD_D-Sorbitol;STD_D-Mannitol	0.73	-0.10	0.05*	-0.45
FT0233	STD_D-Mannitol ; STD_Dulcitol; STD_D-Sorbitol	0.70	-0.08	0.25	-0.33
FT1706	Isoflavone base + 2O, O-MalonylHex	0.70	-0.08	0.12	-0.77
FT1133	NCGC00385306-01_C21H23NO5 ; 7-Hydroxydehydroglaucine	0.70	-0.08	0.16	-0.53
FT0186	STD_D, L-Carnitine ; STD_L-Carnitine	0.75	-0.07	0.46	-0.21

Table 9: Feature table untargeted metabolomics in methanol (MetOH) negative mode correlating with RORyt+ Helios- Treg percentages

For description see Table 7 except that ileum samples were dissolved in methanol.

<i>Feature ID</i>	<i>Mass annotation (ms1)</i>	<i>ASF³ vs Oligo-MM¹²: fdr</i>	<i>ASF³ vs Oligo-MM¹²: mean diff.</i>	<i>Oligo-MM¹² vs SPF: fdr</i>	<i>Oligo-MM¹² vs SPF: mean diff.</i>
FT0835	STD_Isoodeoxycholic acid; STD_Ursodeoxycholic acid; STD_Deoxycholic acid	0.51	-0.89	0.05*	-0.95
FT0874	STD_7-Dehydrocholic acid; STD_3-Dehydrocholic acid; 3,7-Dihydroxy-12-oxocholanoic acid	0.51	-0.88	0.03*	-1.04
FT0834	STD_Isoodeoxycholic acid; STD_Ursodeoxycholic acid; STD_Hyodeoxycholic acid	0.78	-0.51	0.43	-0.64
FT0119	STD_L-Fucose; 2-DEOXY-D-GLUCOSE	0.78	-0.35	0.10	-0.58
FT0574	N-Acetylneuraminic acid	0.71	-0.32	0.004*	-0.72
FT1082	STD_Glycohyocholic acid; STD_Glycocholic acid; GLYCOCHOLATE	0.14	-0.32	0.005*	-1.00
FT0182	N-Acetylglutamic acid	0.78	-0.25	0.03*	-0.77
FT0828	STD_5β-Cholic acid-3α-ol-7-one (7-KLCA); STD_5β-Cholic acid-7α-ol-3-one; STD_5β-Cholic acid-3α-ol-6-one (A)	0.78	-0.24	0.03*	-0.74
FT0993	STD_beta-Muricholic acid; NCGC00380550-01_C24H40O5_4-[[5-(6-Hydroxy-5,5,8a-trimethyl-2-methylenedecahydro-1-naphthalenyl)-3-methylpentyl]oxy]-4-oxobutanoic acid	0.78	-0.22	0.01*	-0.95
FT0071	N-Acetylserine; STD_L-Glutamic Acid	0.78	-0.20	0.02	-0.77
FT0356	Pseudouridine; Chalcone; 1-Methoxyphenanthrene	0.78	-0.20	0.27	-0.37
FT0163	STD_D-Mannitol; STD_D-Sorbitol; STD_Dulcitol	0.78	-0.19	0.09	-0.39
FT0192	STD_D-Galacturonic acid; STD_D-Glucuronic acid; Glucuronic acid	0.51	-0.15	0.10	-0.23
FT0633	4-Dodecylbenzenesulfonic Acid; 2-Dodecylbenzenesulfonic acid;	0.78	-0.12	0.36	-0.23
FT0034	STD_Taurin	0.94	-0.11	0.01*	-1.17
FT0795	STD_Maltitol; MMV676449; Lactitol	0.78	-0.09	0.04*	-0.44
FT0166	4-Pyridoxic acid; 3,5-Dihydroxyphenylglycine;Aminoadipic acid	0.78	-0.09	0.47	-0.03
FT0072	STD_L-Glutamic Acid; N-Acetylserine	0.78	-0.08	0.004*	-0.84
FT0691	STD_Maltitol; Lactitol;Lactitol	0.98	-0.03	0.10	-0.44
FT1367	STD_Raffinose; Raffinose; Maltotriose	0.99	0.004	0.45	-0.06

Table 10: Feature table untargeted metabolomics in MetOH positive mode correlating with RORyt+ Helios- Treg percentages

For description see Table 7 except that ileum samples were dissolved in methanol and measured in positive mode.

<i>Feature ID</i>	<i>Mass annotation (ms1)</i>	<i>ASF³ vs Oligo-MM¹²: fdr</i>	<i>ASF³ vs Oligo-MM¹²: mean diff.</i>	<i>Oligo-MM¹² vs SPF: fdr</i>	<i>Oligo-MM¹² vs SPF: mean diff.</i>
FT1545	STD_5β-Cholic acid-3α-ol-7-one (7-KLCA) ; STD_5 β -Cholic acid-3 α -ol-12-one (12-KLCA), STD_5 β -Cholic acid-3 α -ol-6-one (6-KLCA)	0.82	-1.05	0.34	-0.44
FT1781	STD_Ursocholic acid ; STD_Cholic acid; 3a,7a,12b-Trihydroxy-5b-cholanoic acid	0.56	-1.05	0.01*	-1.61
FT1643	STD_3-Dehydrocholic acid ; STD_7-Dehydrocholic acid; 3,7-Dihydroxy-12-oxocholanoic acid	0.82	-0.99	0.12	-0.81
FT1783	STD_Ursocholic acid ; STD_Cholic acid; STD_Allocholic acid	0.82	-0.96	0.02*	-1.47
FT1782	STD_Cholic acid ; STD_Ursocholic acid; STD_beta-Muricholic acid	0.82	-0.87	0.01*	-1.69
FT1846	STD_alpha-Muricholic acid ; STD_g-Muricholic acid/Hyocholic acid	0.82	-0.39	0.16	-0.52
FT0278	beta-D-Glucosamine ; Glucosamine; Galactosamine	0.82	-0.34	0.18	-0.16
FT0382	STD_Dulcitol ;STD_D-Sorbitol;STD_D-Mannitol	0.82	-0.25	0.05*	-0.55
FT1826	PF-1052_130138 ; PF-1052_130138; Boviquinone 4	0.82	-0.24	0.004*	-0.98
FT0681	Prolylphenylalanine ; N-Phenylacetyl pyroglutamic acid; NCGC001	0.82	-0.23	0.53	-0.14
FT1759	STD_3-Dehydrocholic acid ; 3-hydroxypentadecanoyl carnitine; 3,7-Dihydroxy-12-oxocholanoic acid	0.82	-0.22	0.005*	-1.26
FT2547	STD_Raffinose ; Caffeoylferuloylspermidine; Maltotriose	0.82	-0.19	0.93	0.01
FT0287	STD_D-Mannitol ; STD_Dulcitol ;STD_D-Sorbitol	0.82	-0.17	0.02*	-0.55
FT0100	STD_Taurin	0.95	-0.17	0.02*	-1.37
FT0265	STD_Citruline ; Citrulline; 1-(Hydroxymethyl)-5,5-dimethyl-2,4-imidazolidinedione	0.82	-0.15	0.001*	-0.95
FT1627	STD_5β-Cholic acid-3α-ol-6,7-dione (6,7-DKLCA) ; STD_5 β -Cholic acid-3 α -ol-7,12-dione (7,12-DKLCA); Urapidil	0.82	-0.11	0.01*	-0.79
FT0507	teasperin ; Sinapyl alcohol	0.99	-0.10	0.53	-0.33
FT0416	Prolylproline ; Metyrosine; Tyrosine methylester	0.82	-0.09	0.12	-0.48
FT0941	Oxamniquine ; Glutamylhistidine	0.82	-0.09	0.04*	-0.58

V. Appendix

FT0223	5-Aminovaleric acid betaine ; 4-aminovaleric acid betaine; Pregabalin	0.92	-0.08	0.31	-0.46
FT2401	STD_Taurodeoxycholic acid ; STD_Taurochenodeoxycholic acid; STD_Tauroursodeoxycholic	0.95	-0.08	0.49	-0.26
FT1906	Dicoumaroyl Spermidine ; N1,N10-Dicoumaroylspermidine; Lunarine	0.83	-0.08	0.73	-0.07
FT0669	gamma-Glutamylleucine ; Isoleucylglutamate; gamma-Glutamylisoleucine	0.82	-0.08	0.32	-0.07
FT0128	STD_D-Pyroglutamic acid ; STD_L-Pyroglutamic acid	0.82	-0.08	0.004*	-0.86
FT1679	Fesoterodine fumarate (Toviaz) ; LysoPA(P-16:0e/0:0); N-Arachidonoyl GABA	0.82	-0.08	0.002*	-1.34
FT1845	STD_beta-Muricholic acid ; cholic acid; STD_alpha-Muricholic ac	0.82	-0.08	0.002*	-1.38
FT2680	STD_Raffinose ; Rugulosin; Yuccaol C	0.82	-0.08	0.81	-0.05
FT0772	gamma-Glutamylglutamine ; Glu-Gln; Ribothymidine	0.93	-0.07	0.67	-0.06
FT1361	STD_Turanose ; STD_Lactulose ; STD_Sucrose	0.95	-0.05	0.002*	-1.47
FT1948	NCGC00380493-01_C17H24O12_4H-Pyran-4-one, 2-methyl-3-[[6-O-[(2R,3R,4R)-tetrahydro-3,4-dihydroxy-4-(hydroxymethyl)-2-furanyl]-beta-D-glucopyranosyl]oxy]-	0.94	-0.04	0.47	-0.13
FT0082	L-PROLINE ; 2-Furanmethanol	0.93	-0.04	0.18	-0.26
FT2575	STD_Raffinose ; Maltotriose	0.93	-0.02	0.13	-0.22
FT0290	STD_D-Mannitol ; STD_Dulcitol; STD_D-Sorbitol	0.99	-0.02	0.05*	-0.57
FT1048	NCGC00381425-0118-hydroxy-8-(3-octyloxiran-2-yl)octanoic acid	0.99	-0.02	0.18	-0.52
FT0389	NALPHA-ACETYL-L-LYSINE ; N6-Acetyl-L-lysine;	0.95	-0.02	0.27	-0.12
FT0961	Fenpropimorph	0.99	-0.02	0.55	-0.14
FT2545	STD_Raffinose ; Maltotriose;	0.99	-0.01	0.92	0.01
FT0066	STD_L-Serine ; Serine; Malonic semialdehyde	0.99	-0.01	0.97	0.01
FT0604	Glu-Thr ; N2-Succinyl-L-glutamic acid 5-semialdehyde; Glutamylthreonine	1.00	-0.01	0.37	-0.23

Table 11: Feature table untargeted metabolomics in MetOH positive mode correlating with Th2 percentages

Ileum content samples of ASF³, Oligo-MM¹², SPF mice (4 per group) dissolved in MetOH and measured in positive ionization mode via untargeted metabolomics. Features were selected according to availability of ms1 annotation, ms2 fragmentation pattern availability and similarity to annotation, and chromatogram quality. Intensities of features in the table follow mean SPF<Oligo-MM¹² and Oligo-MM¹²<ASF³ pattern (positive mean difference (diff.) for both cases). Table is sorted according to mean diff. ASF³ vs Oligo-MM¹² maximum to minimum. The three most likely annotations are shown with the most likely in bold. Significant fdr values (<0.05) are bold and marked with *. Abbr.: fdr, false discovery rate; ID, identifier; vs, versus; STD, standard.

Feature ID	Mass annotation (ms1)	ASF ³ vs Oligo-MM ¹² : fdr	ASF ³ vs Oligo-MM ¹² : mean diff.	Oligo-MM ¹² vs SPF: fdr	Oligo-MM ¹² vs SPF: mean diff.
FT0464	NCGC00380942-01_C13H20O2_1H-Indene-3-carboxylic acid, 3a,4,5,6,7,7a-hexahydro-3a,7,7-trimethyl-	0.82	0.41	0.95	0.03
FT1542	(S,E)-2-(4,8-dimethylnona-3,7-dien-1-yl)-5-hydroxy-2-methyl-2H-chromene-7,8-dicarbaldehyde ; Prostaglandin E2; (13E)-11a-Hydroxy-9,15-dioxoprost-13-enoic acid	0.82	0.31	0.47	0.08
FT1097	Linoleoyl ethanolamide ; 8,11,14-Eicosatrienoic acid; 5,8,11-Eicosatrienoic acid	0.66	0.30	0.02*	0.41
FT0825	Questin_120240 ; Wogonin; 6-dihydroxy-7-methoxy-2-phenyl-4H-chromen-4-one	0.82	0.28	0.95	0.02
FT1360	STD_Lactulose ; STD_Turanose; STD_Maltose	0.82	0.26	0.21	0.33
FT1335	STD_D-Trehalose ; STD_D-Lactose*H2O; STD_Melibiose	0.82	0.25	0.16	0.30
FT2189	NCGC00384848-01_C21H36O10_2-[3,8-Dihydroxy-8-(hydroxymethyl)-3-methyl-2-oxodecahydro-5-azulenyl]-2-propanyl hexopyranoside	0.82	0.23	0.005*	0.74
FT2549	STD_18:1 Lyso PC (1-(9Z-Octadecenoyl)-sn-glycero-3-phosphocholine)	0.82	0.20	0.32	0.33
FT2576	STD_Raffinose; Maltotriose	0.88	0.19	0.73	0.13
FT0095	Niacinamide ; 2-Acetylpyrazine; N-Nitroso-pyrrolidine	0.88	0.19	0.04*	0.59
FT2698	STD_18:1 Lyso PC (1-(9Z-Octadecenoyl)-sn-glycero-3-phosphocholine) , LPC 18:1	0.83	0.16	0.47	0.15
FT2536	LPC 18:2 ; LysoPC(18:2(9Z,12Z)); 2-linoleoyl-sn-glycero-3-phosphocholine	0.82	0.16	0.18	0.25
FT2629	STD-Tauro-alpha-Muricholic acid ; STD-Taurocholic acid; STD-Tauro-omega-Muricholic acid	0.82	0.14	0.10	0.32
FT1224	STD_D-Lactose*H2O ; STD_Melibiose; STD_D-Trehalose	0.86	0.13	0.15	0.39

V. Appendix

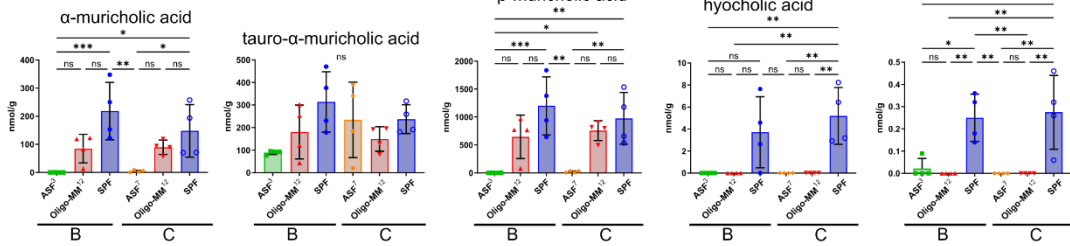
FT0677	Asp-Glu ; L-beta-aspartyl-L-glutamic acid; Aspartyl-Glutamate	0.82	0.13	0.002*	0.78
FT1449	STD_Riboflavin	0.83	0.12	0.15	0.36
FT2548	STD_18:1 Lyso PC (1-(9Z-Octadecenoyl)-sn-glycero-3-phosphocholine)	0.90	0.12	0.74	0.08
FT2506	STD-Tauro-omega-Muricholic acid ; STD-Taurocholic acid, STD-Tauro-alpha-Muricholic acid	0.82	0.11	0.47	0.16
FT0783	STD_Palmitoleic acid ; Hypogeic acid; Trans-Hexa-dec-2-enoic acid	0.94	0.10	0.47	0.19
FT0162	Methyl nicotinate ; m-Aminobenzoic acid; 3-Pyridylacetic acid	0.83	0.10	0.10	0.43
FT2110	NCGC00169680-02!(2S,3S,4S,5R,6S)-3,4,5-trihydroxy-6-(5-hydroxy-6-methoxy-4-oxo-2-phenylchromen-7-yl)oxyoxane-2-carboxylic acid	0.82	0.09	0.17	0.36
FT1008	Asterina; Glutamyltyrosine ; gamma-Glutamyltyrosine	0.86	0.07	0.01	0.44
FT2535	LPC 18:2 ; LysoPC(18:2(9Z,12Z)); 2-linoleoyl-sn-glycero-3-phosp	0.91	0.07	0.30	0.19
FT1415	STD_Myristoyl-L-carnitine ; MG(0:0/18:2(9Z,12Z)/0:0); MG(18:2(9Z,12Z)/0:0/0:0)	0.82	0.07	0.47	0.18
FT1768	MMV675997; Licoricidin; Kanzonol H	0.82	0.07	0.001*	0.90
FT0263	Arginine	0.90	0.06	0.27	0.26
FT0123	N-Methylproline ; L-PIPECOLIC ACID; Pipelic acid	0.92	0.06	0.79	0.05
FT1190	Erucamide	0.93	0.05	0.47	0.17
FT0189	STD_Lysine ; N-Methylproline; L-PIPECOLIC ACID	0.91	0.05	0.72	0.06
FT2215	alpha-Tocopherol acetate ; Soyasapogenol D; (+)-alpha-Tocopherol Acetateacid ester	0.95	0.05	0.005*	1.01
FT1235	Rhodotulic acid	0.82	0.04	0.01*	0.45
FT2336	alpha-Tocopherol acetate ; Soyasapogenol D; (+)-alpha-Tocopherol Acetateacid ester	0.98	0.03	0.002*	1.03
FT4134	DP7 ; 3-Oxotetracosanoyl-CoA; Maltoheptaose	0.97	0.03	0.09*	0.26
FT0279	D-(+)-Glucosamine ; Galactosamine; D-Mannosamine	0.99	0.03	0.01	0.38
FT1893	MMV031011 ; Tri(butoxyethyl) phosphate; 7-Hydroxymitragynine	0.92	0.02	0.01	0.77
FT3913	Soyasapogenol A base + O-HexA-Hex-Hex ; Madecassoside; Asiaticoside B	0.99	0.02	0.10	0.40
FT0180	4-Guanidinobutanoic acid ; Dihydrothymine; Squamolone	0.99	0.02	0.01*	0.36
FT0314	NEPSILON,NEPSILON,NEPSILON-TRIMETHYLLYSINE , Gabapentin	0.99	0.01	0.39	0.12
FT2040	Fluocinolone Acetonide	0.98	0.01	0.002*	0.44

V. Appendix

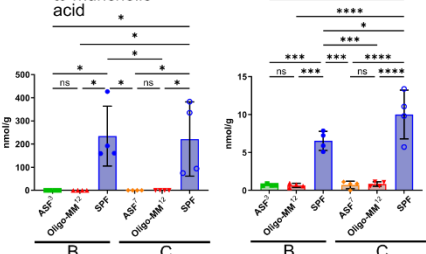
FT0313	N-alpha-Acetyl-L-lysine ; N-epsilon-Acetyllysine	0.98	0.01	0.05*	0.21
FT1933	22-Hydroxy-2-hopen-1-one ; Oleanane - 4H, + 2O; 4,4-Dimethyl-14a-formyl-5a-cholesta-8,24-dien-3b-ol	0.99	0.01	0.01*	0.26
FT0797	Asp-Phe ; Aspartylphenylalanine; L-beta-aspartyl-L-phenylalanin	0.99	0.01	0.001*	1.17
FT0211	STD_Histidine	0.99	0.01	0.77	0.04
FT0592	Octopine ; Asparaginyl-Proline	1.00	0.001	0.001*	0.48

A

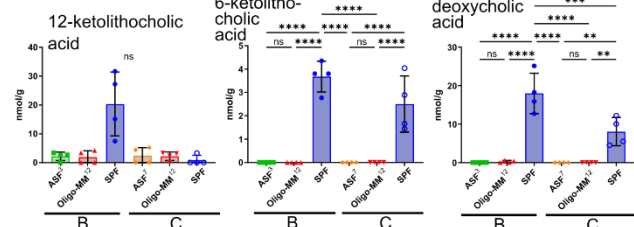
Primary BAs and their conjugates



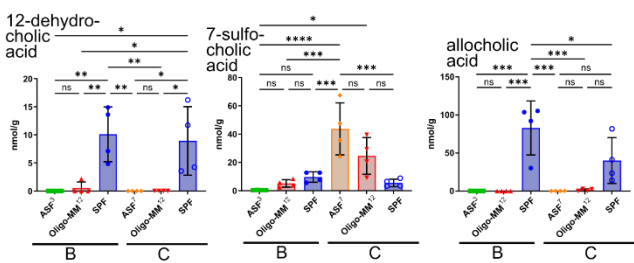
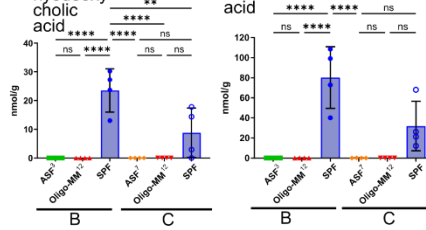
A



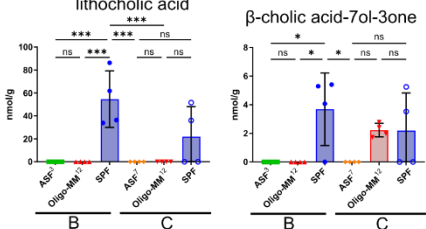
B Unconjugated secondary BAs



B



B

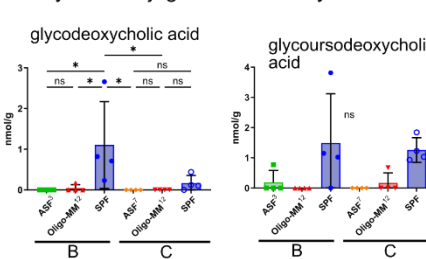


Non-detectable unconjugated secondary BAs:
 lithocholic acid
 alloithocholic acid
 isolithocholic acid
 isodeoxycholic acid
 lithocholenic acid
 obeticholic acid
 dehydrolithocholic acid
 6,7-diketolithocholic acid
 apocholic acid

Legend

- ASF³ Setup B
- ▲ Oligo-MM¹² Setup B
- SPF Setup B
- ◆ ASF⁷ Setup C
- ▼ Oligo-MM¹² Setup C
- SPF Setup Setup C

C



Non-detectable glycine conjugated secondary BAs:
 glycohyodeoxycholic acid
 glycolithocholic acid

D

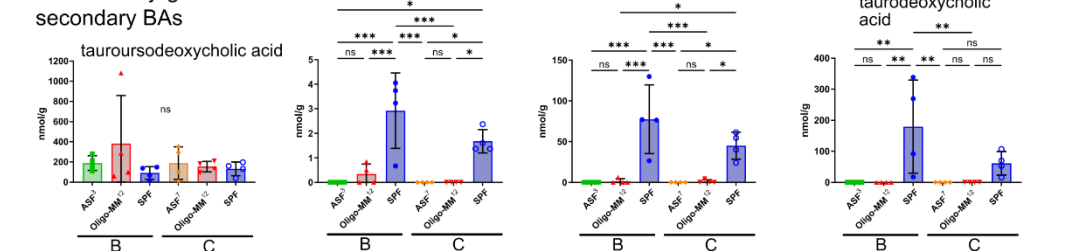


Figure 18: Targeted metabolomics measurement of ileum content

Targeted measurement of primary BAs and their conjugates to taurine and glycine (A), unconjugated secondary BAs (B), glycine-conjugated secondary BAs (C) and taurine-conjugated secondary BAs (D) not presented in Figure 7. Statistics: one-way ANOVA with Tukey's multiple comparisons test, **p<0.01, ***p<0.001, ****p<0.0001, n.s.: not significant.

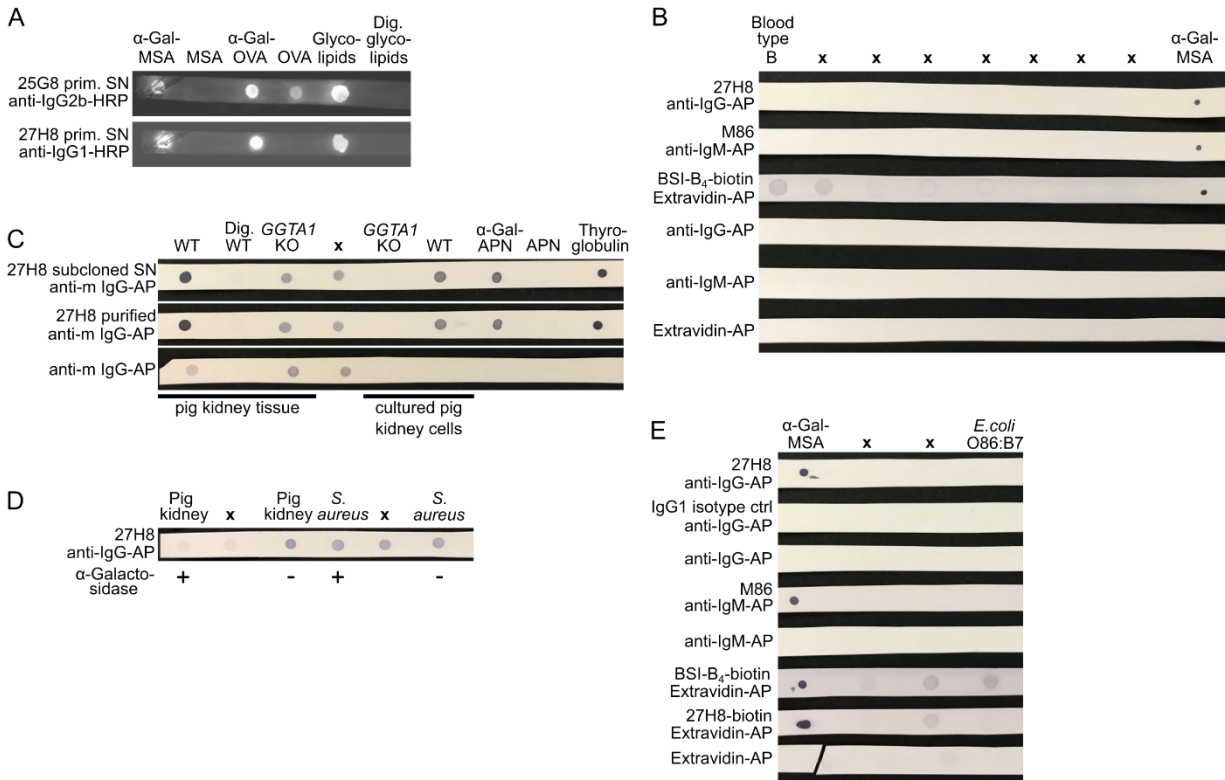


Figure 19. Uncropped blots appearing in results chapter 3.2

(A) Uncropped dot blot of Figure 9C, (B) of Figure 10A, (C) of Figure 10B, (D) of Figure 12E, (E) of Figure 13B. Samples not mentioned in the manuscript due to irrelevance and which have been used only to test conditions are labeled with x.

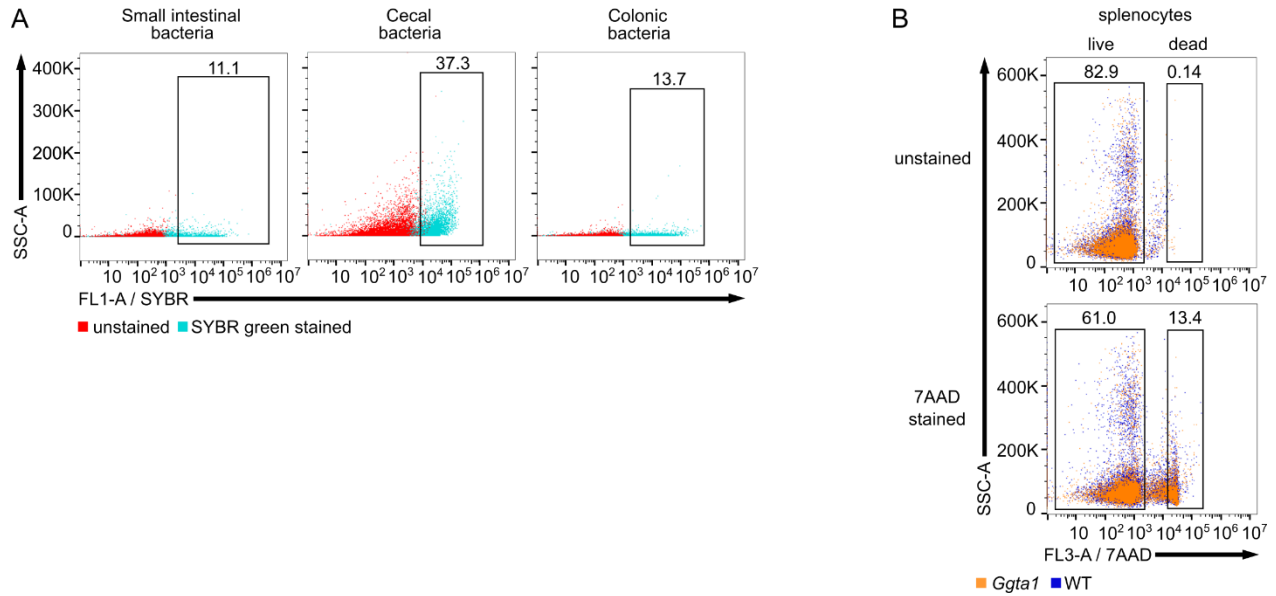


Figure 20: Representative gating for live cells and bacteria

Representative flow cytometry plots displaying pre-gating for bacterial and live cell identification for plots shown in Figure 13C-D. **(A)** Identification of bacteria via SYBR green positive staining of intestinal contents of small intestine, cecum and colon **(B)** Identification of live murine splenocytes via staining with 7AAD.

6 REFERENCES

- [1] Kreft L, Schepers A, Hils M, Swiontek K, Flatley A, Janowski R, Mirzaei MK, Dittmar M, Chakrapani N, Desai MS, et al. A novel monoclonal IgG1 antibody specific for Galactose-alpha-1,3-galactose questions alpha-Gal epitope expression by bacteria. *Frontiers in Immunology*. 2022;**13**:958952. doi:10.3389/fimmu.2022.958952
- [2] Kreft L, Hoffmann C, Ohnmacht C. Therapeutic Potential of the Intestinal Microbiota for Immunomodulation of Food Allergies. *Frontiers in Immunology*. 2020;**11**:1853. doi:10.3389/fimmu.2020.01853
- [3] Kawai T, Akira S. The role of pattern-recognition receptors in innate immunity: update on Toll-like receptors. *Nature Immunology*. 2010;**11**(5):373–384. doi:10.1038/ni.1863
- [4] Wu J, Chen ZJ. Innate Immune Sensing and Signaling of Cytosolic Nucleic Acids. *Annual Review of Immunology*. 2014;**32**(1):461–488. doi:10.1146/annurev-immunol-032713-120156
- [5] Rathinam VAK, Vanaja SK, Fitzgerald KA. Regulation of inflammasome signaling. *Nature Immunology*. 2012;**13**(4):333–342. doi:10.1038/ni.2237
- [6] Boksa M, Zeyland J, Słomski R, Lipiński D. Immune Modulation in Xenotransplantation. *Archivum Immunologiae et Therapiae Experimentalis*. 2015;**63**(3):181–192. doi:10.1007/s00005-014-0317-7
- [7] Phelps CJ, Koike C, Vaught TD, Boone J, Wells KD, Chen S-H, Ball S, Specht SM, Polejaeva IA, Monahan JA, et al. Production of α 1,3-Galactosyltransferase-Deficient Pigs. *Science*. 2003;**299**(5605):411–414. doi:10.1126/science.1078942
- [8] Montgomery RA, Stern JM, Lonze BE, Tatapudi VS, Mangiola M, Wu M, Weldon E, Lawson N, Deterville C, Dieter RA, et al. Results of Two Cases of Pig-to-Human Kidney Xenotransplantation. *New England Journal of Medicine*. 2022;**386**(20):1889–1898. doi:10.1056/NEJMoa2120238
- [9] Griffith BP, Goerlich CE, Singh AK, Rothblatt M, Lau CL, Shah A, Lorber M, Grazioli A, Saharia KK, Hong SN, et al. Genetically Modified Porcine-to-Human Cardiac Xenotransplantation. *New England Journal of Medicine*. 2022;**387**(1):35–44. doi:10.1056/NEJMoa2201422
- [10] Sun PD. Structure and Function of Natural-Killer-Cell Receptors. *Immunologic Research*. 2003;**27**(2–3):539–548. doi:10.1385/IR:27:2-3:539
- [11] Swanson JA, Hoppe AD. The coordination of signaling during Fc receptor-mediated phagocytosis. *Journal of Leukocyte Biology*. 2004;**76**(6):1093–1103. doi:10.1189/jlb.0804439
- [12] Smith KGC, Clatworthy MR. Fc γ RIIB in autoimmunity and infection: evolutionary and therapeutic implications. *Nature Reviews Immunology*. 2010;**10**(5):328–343. doi:10.1038/nri2762
- [13] Geissmann F, Manz MG, Jung S, Sieweke MH, Merad M, Ley K. Development of Monocytes, Macrophages, and Dendritic Cells. *Science*. 2010;**327**(5966):656–661. doi:10.1126/science.1178331

VI. References

- [14] Murray PJ, Wynn TA. Protective and pathogenic functions of macrophage subsets. *Nature Reviews Immunology*. 2011;**11**(11):723–737. doi:10.1038/nri3073
- [15] Zhu J, Yamane H, Paul WE. Differentiation of Effector CD4 T Cell Populations. *Annual Review of Immunology*. 2010;**28**(1):445–489. doi:10.1146/annurev-immunol-030409-101212
- [16] Jiang Q, Yang G, Xiao F, Xie J, Wang S, Lu L, Cui D. Role of Th22 Cells in the Pathogenesis of Autoimmune Diseases. *Frontiers in Immunology*. 2021;**12**:688066. doi:10.3389/fimmu.2021.688066
- [17] Paul WE, Zhu J. How are TH2-type immune responses initiated and amplified? *Nature Reviews Immunology*. 2010;**10**(4):225–235. doi:10.1038/nri2735
- [18] Zhu J, Min B, Hu-Li J, Watson CJ, Grinberg A, Wang Q, Killeen N, Urban JF, Guo L, Paul WE. Conditional deletion of Gata3 shows its essential function in TH1-TH2 responses. *Nature Immunology*. 2004;**5**(11):1157–1165. doi:10.1038/ni1128
- [19] Sun T, Nguyen A, Gommerman JL. Dendritic Cell Subsets in Intestinal Immunity and Inflammation. *The Journal of Immunology*. 2020;**204**(5):1075–1083. doi:10.4049/jimmunol.1900710
- [20] Luciani C, Hager FT, Cerovic V, Lelouard H. Dendritic cell functions in the inductive and effector sites of intestinal immunity. *Mucosal Immunology*. 2022;**15**(1):40–50. doi:10.1038/s41385-021-00448-w
- [21] Iwasaki A, Medzhitov R. Control of adaptive immunity by the innate immune system. *Nature Immunology*. 2015;**16**(4):343–353. doi:10.1038/ni.3123
- [22] Artis D, Spits H. The biology of innate lymphoid cells. *Nature*. 2015;**517**(7534):293–301. doi:10.1038/nature14189
- [23] Spits H, Artis D, Colonna M, Diefenbach A, Di Santo JP, Eberl G, Koyasu S, Locksley RM, McKenzie ANJ, Mebius RE, et al. Innate lymphoid cells — a proposal for uniform nomenclature. *Nature Reviews Immunology*. 2013;**13**(2):145–149. doi:10.1038/nri3365
- [24] Josefowicz SZ, Lu L-F, Rudensky AY. Regulatory T Cells: Mechanisms of Differentiation and Function. *Annual Review of Immunology*. 2012;**30**(1):531–564. doi:10.1146/annurev.immunol.25.022106.141623
- [25] Fontenot JD, Rasmussen JP, Williams LM, Dooley JL, Farr AG, Rudensky AY. Regulatory T cell lineage specification by the forkhead transcription factor Foxp3. *Immunity*. 2005;**22**(3):329–341. doi:10.1016/j.immuni.2005.01.016
- [26] Roncarolo MG, Gregori S, Bacchetta R, Battaglia M, Gagliani N. The Biology of T Regulatory Type 1 Cells and Their Therapeutic Application in Immune-Mediated Diseases. *Immunity*. 2018;**49**(6):1004–1019. doi:10.1016/j.immuni.2018.12.001
- [27] Delacher M, Imbusch CD, Weichenhan D, Breiling A, Hotz-Wagenblatt A, Träger U, Hofer AC, Kägebein D, Wang Q, Frauhammer F, et al. Genome-wide DNA-methylation landscape defines specialization of regulatory T cells in tissues. *Nature Immunology*. 2017;**18**(10):1160–1172. doi:10.1038/ni.3799

VI. References

- [28] Curotto de Lafaille MA, Lafaille JJ. Natural and Adaptive Foxp3+ Regulatory T Cells: More of the Same or a Division of Labor? *Immunity*. 2009;**30**(5):626–635. doi:10.1016/j.immuni.2009.05.002
- [29] Geuking MB, Cahenzli J, Lawson MAE, Ng DCK, Slack E, Hapfelmeier S, McCoy KD, Macpherson AJ. Intestinal Bacterial Colonization Induces Mutualistic Regulatory T Cell Responses. *Immunity*. 2011;**34**(5):794–806. doi:10.1016/j.immuni.2011.03.021
- [30] Josefowicz SZ, Niec RE, Kim HY, Treuting P, Chinen T, Zheng Y, Umetsu DT, Rudensky AY. Extrathymically generated regulatory T cells control mucosal TH2 inflammation. *Nature*. 2012;**482**(7385):395–399. doi:10.1038/nature10772
- [31] Kim KS, Hong SW, Han D, Yi J, Jung J, Yang BG, Lee JY, Lee M, Surh CD. Dietary antigens limit mucosal immunity by inducing regulatory T cells in the small intestine. *Science*. 2016;**351**(6275):858–863. doi:10.1126/science.aac5560
- [32] Tanoue T, Atarashi K, Honda K. Development and maintenance of intestinal regulatory T cells. *Nature Reviews Immunology*. 2016;**16**(5):295–309. doi:10.1038/nri.2016.36
- [33] Ohnmacht C, Park JH, Cording S, Wing JB, Atarashi K, Obata Y, Gaboriau-Routhiau V, Marques R, Dulauroy S, Fedoseeva M, et al. The microbiota regulates type 2 immunity through ROR γ t+ T cells. *Science*. 2015;**349**(6251):989–993. doi:10.1126/science.aac4263
- [34] Sefik E, Geva-Zatorsky N, Oh S, Konnikova L, Zemmour D, McGuire AM, Burzyn D, Ortiz-Lopez A, Lobera M, Yang J, et al. Individual intestinal symbionts induce a distinct population of ROR γ + regulatory T cells. *Science*. 2015;**349**(6251):993–997. doi:10.1126/science.aaa9420
- [35] Bhaumik S, Mickael ME, Moran M, Spell M, Basu R. ROR γ t Promotes Foxp3 Expression by Antagonizing the Effector Program in Colonic Regulatory T Cells. *The Journal of Immunology*. 2021;**207**(8):2027–2038. doi:10.4049/jimmunol.2100175
- [36] Thornton AM, Korty PE, Tran DQ, Wohlfert EA, Murray PE, Belkaid Y, Shevach EM. Expression of Helios, an Ikaros Transcription Factor Family Member, Differentiates Thymic-Derived from Peripherally Induced Foxp3 + T Regulatory Cells. *The Journal of Immunology*. 2010;**184**(7):3433–3441. doi:10.4049/jimmunol.0904028
- [37] Esterházy D, Loschko J, London M, Jove V, Oliveira TY, Mucida D. Classical dendritic cells are required for dietary antigen- mediated peripheral regulatory T cell and tolerance induction. *Nature Immunology*. 2016;**17**(5):545–555. doi:10.1002/aur.1474.Replication
- [38] Lyu M, Suzuki H, Kang L, Gaspal F, Zhou W, Goc J, Zhou L, Zhou J, Zhang W, Artis D, et al. ILC3s select microbiota-specific regulatory T cells to establish tolerance in the gut. *Nature*. 2022;**610**(7933):744–751. doi:10.1038/s41586-022-05141-x
- [39] Kedmi R, Najjar TA, Mesa KR, Grayson A, Kroehling L, Hao Y, Hao S, Pokrovskii M, Xu M, Talbot J, et al. A ROR γ t+ cell instructs gut microbiota-specific Treg cell differentiation. *Nature*. 2022;**610**(7933):737–743. doi:10.1038/s41586-022-05089-y
- [40] Akagbosu B, Tayyebi Z, Shibu G, Paucar Iza YA, Deep D, Parisotto YF, Fisher L, Pasolli HA, Thevin V, Elmentaite R, et al. Novel antigen-presenting cell imparts Treg-dependent tolerance to gut microbiota. *Nature*. 2022;**610**(7933):752–760. doi:10.1038/s41586-022-05309-5

VI. References

- [41] Dethlefsen L, McFall-Ngai M, Relman DA. An ecological and evolutionary perspective on human–microbe mutualism and disease. *Nature*. 2007;**449**(7164):811–818. doi:10.1038/nature06245
- [42] Smith PM, Howitt MR, Panikov N, Michaud M, Gallini CA, Bohlooly-Y M, Glickman JN, Garrett WS. The Microbial Metabolites, Short-Chain Fatty Acids, Regulate Colonic T reg Cell Homeostasis. *Science*. 2013;**341**(6145):569–573. doi:10.1126/science.1241165
- [43] Arpaia N, Campbell C, Fan X, Dikiy S, van der Veecken J, DeRoos P, Liu H, Cross JR, Pfeffer K, Coffey PJ, et al. Metabolites produced by commensal bacteria promote peripheral regulatory T-cell generation. *Nature*. 2013;**504**(7480):451–455. doi:10.1038/nature12726
- [44] Verma R, Lee C, Jeun E-J, Yi J, Kim KS, Ghosh A, Byun S, Lee C-G, Kang H-J, Kim G-C, et al. Cell surface polysaccharides of *Bifidobacterium bifidum* induce the generation of Foxp3 + regulatory T cells. *Science Immunology*. 2018;**3**(28):eaat6975. doi:10.1126/sciimmunol.aat6975
- [45] Song X, Sun X, Oh SF, Wu M, Zhang Y, Zheng W, Geva-Zatorsky N, Jupp R, Mathis D, Benoist C, et al. Microbial bile acid metabolites modulate gut RORγ+ regulatory T cell homeostasis. *Nature*. 2020;**577**(7790):410–415. doi:10.1038/s41586-019-1865-0
- [46] Hang S, Paik D, Yao L, Kim E, Trinath J, Lu J, Ha S, Nelson BN, Kelly SP, Wu L, et al. Bile acid metabolites control TH17 and Treg cell differentiation. *Nature*. 2019;**576**(7785):143–148. doi:10.1038/s41586-019-1785-z
- [47] Campbell C, McKenney PT, Konstantinovskiy D, Isaeva OI, Schizas M, Verter J, Mai C, Jin W-B, Guo C-J, Violante S, et al. Bacterial metabolism of bile acids promotes generation of peripheral regulatory T cells. *Nature*. 2020;**581**(7809):475–479. doi:10.1038/s41586-020-2193-0
- [48] Edwards-Salmon SE, Padmanabhan SL, Kuruvilla M, Levy JM. Increasing Prevalence of Allergic Disease and Its Impact on Current Practice. *Current Otorhinolaryngology Reports*. 2022;**10**(3):278–284. doi:10.1007/s40136-022-00406-5
- [49] D’Amato G, Vitale C, De Martino A, Viegi G, Lanza M, Molino A, Sanduzzi A, Vatrella A, Annesi-Maesano I, D’Amato M. Effects on asthma and respiratory allergy of Climate change and air pollution. *Multidisciplinary Respiratory Medicine*. 2015;**10**(1):39. doi:10.1186/s40248-015-0036-x
- [50] Feehley T, Stefka AT, Cao S, Nagler CR. Microbial regulation of allergic responses to food. *Seminars in Immunopathology*. 2012;**34**(5):671–688. doi:10.1007/s00281-012-0337-5
- [51] Akdis CA. Does the epithelial barrier hypothesis explain the increase in allergy, autoimmunity and other chronic conditions? *Nature Reviews Immunology*. 2021;**21**(11):739–751. doi:10.1038/s41577-021-00538-7
- [52] Dispenza MC. Classification of hypersensitivity reactions. *Allergy and Asthma Proceedings*. 2019;**40**(6):470–473. doi:10.2500/aap.2019.40.4274
- [53] Novak N, Kraft S, Bieber T. IgE receptors. *Current Opinion in Immunology*. 2001;**13**(6):721–726. doi:10.1016/S0952-7915(01)00285-0
- [54] Gowthaman U, Chen JS, Zhang B, Flynn WF, Lu Y, Song W, Joseph J, Gertie JA, Xu L, Collet MA, et al. Identification of a T follicular helper cell subset that drives anaphylactic IgE. *Science*. 2019;**365**:eaaw6433. doi:10.1126/science.aaw6433

VI. References

- [55] Wynn TA. Type 2 cytokines: mechanisms and therapeutic strategies. *Nature Reviews Immunology*. 2015;**15**(5):271–282. doi:10.1038/nri3831
- [56] Knipper JA, Willenborg S, Brinckmann J, Bloch W, Maaß T, Wagener R, Krieg T, Sutherland T, Munitz A, Rothenberg ME, et al. Interleukin-4 Receptor α Signaling in Myeloid Cells Controls Collagen Fibril Assembly in Skin Repair. *Immunity*. 2015;**43**(4):803–816. doi:10.1016/j.immuni.2015.09.005
- [57] Conner ER, Saini SS. The Immunoglobulin E Receptor: Expression and Regulation. *Current Allergy and Asthma Reports*. 2005;**5**:191–196.
- [58] Hils M, Wölbing F, Hilger C, Fischer J, Hoffard N, Biedermann T. The History of Carbohydrates in Type I Allergy. *Frontiers in Immunology*. 2020;**11**:586924. doi:10.3389/fimmu.2020.586924
- [59] Aalberse R, Kohste V, Clemens J. Immunoglobulin E antibodies that crossreact with vegetable foods, pollen, and Hymenoptera venom. *Journal of Allergy and Clinical Immunology*. 1981;**68**(5):356–364. doi:10.1016/0091-6749(81)90133-0
- [60] Altmann F. The Role of Protein Glycosylation in Allergy. *International Archives of Allergy and Immunology*. 2007;**142**(2):99–115. doi:10.1159/000096114
- [61] Iweala OI, Nagler CR. The Microbiome and Food Allergy. *Annual Review of Immunology*. 2019;**37**(1):377–403. doi:10.1146/annurev-immunol-042718-041621
- [62] Kattan J. The Prevalence and Natural History of Food Allergy. *Current Allergy and Asthma Reports*. 2016;**16**(7):47. doi:10.1007/s11882-016-0627-4
- [63] Venter C, Patil V, Grundy J, Glasbey G, Twiselton R, Arshad SH, Dean T. Prevalence and cumulative incidence of food hyper-sensitivity in the first 10 years of life. *Pediatric Allergy and Immunology*. 2016;**27**(5):452–458. doi:10.1111/pai.12564
- [64] McGowan EC, Keet CA. Prevalence of self-reported food allergy in the National Health and Nutrition Examination Survey (NHANES) 2007-2010. *Journal of Allergy and Clinical Immunology*. 2013;**132**(5). doi:10.1016/j.jaci.2013.07.018
- [65] Branum AM, Lukacs SL. Food Allergy Among Children in the United States. *Pediatrics*. 2009;**124**(6):1549–1555. doi:10.1542/peds.2009-1210
- [66] Leung ASY, Wong GWK, Tang MLK. Food allergy in the developing world. *Journal of Allergy and Clinical Immunology*. 2018;**141**(1):76–78.e1. doi:10.1016/j.jaci.2017.11.008
- [67] Strachan DP. Hay fever, hygiene, and household size. *British Medical Journal*. 1989;**299**(6710):1259–1260. doi:10.1136/bmj.299.6710.1259
- [68] Prioult G, Nagler-Anderson C. Mucosal immunity and allergic responses: lack of regulation and/or lack of microbial stimulation? *Immunological Reviews*. 2005;**206**(1):204–218. doi:10.1111/j.0105-2896.2005.00277.x
- [69] Noverr MC, Huffnagle GB. The “microflora hypothesis” of allergic diseases. *Clinical & Experimental Allergy*. 2005;**35**(12):1511–1520. doi:10.1111/j.1365-2222.2005.02379.x
- [70] Hanski I, von Hertzen L, Fyhrquist N, Koskinen K, Torppa K, Laatikainen T, Karisola P, Auvinen P, Paulin L, Mäkelä MJ, et al. Environmental biodiversity, human microbiota, and

VI. References

- allergy are interrelated. *Proceedings of the National Academy of Sciences*. 2012;**109**(21):8334–8339. doi:10.1073/pnas.1205624109
- [71] Lack G. Epidemiologic risks for food allergy. *Journal of Allergy and Clinical Immunology*. 2008;**121**(6):1331–1336. doi:10.1016/J.JACI.2008.04.032
- [72] Wesemann DR, Nagler CR. The Microbiome, Timing, and Barrier Function in the Context of Allergic Disease. *Immunity*. 2016;**44**(4):728–738. doi:10.1016/j.immuni.2016.02.002
- [73] Parrish A, Boudaud M, Kuehn A, Ollert M, Desai MS. Intestinal mucus barrier: a missing piece of the puzzle in food allergy. *Trends in Molecular Medicine*. 2022;**28**(1):36–50. doi:10.1016/j.molmed.2021.10.004
- [74] Braun-Fahrländer C, Riedler J, Herz U, Eder W, Waser M, Grize L, Maisch S, Carr D, Gerlach F, Bufe A, et al. Environmental Exposure to Endotoxin and Its Relation to Asthma in School-Age Children. *New England Journal of Medicine*. 2002;**347**(12):869–877. doi:10.1056/NEJMoa020057
- [75] Stein MM, Hrusch CL, Gozdz J, Igartua C, Pivniouk V, Murray SE, Ledford JG, Dos Santos MM, Anderson RL, Metwali N, et al. Innate immunity and asthma risk in amish and hutterite farm children. *New England Journal of Medicine*. 2016;**375**(5):411–421. doi:10.1056/NEJMoa1508749
- [76] Ege MJ, Frei R, Bieli C, Schram-Bijkerk D, Waser M, Benz MR, Weiss G, Nyberg F, van Hage M, Pershagen G, et al. Not all farming environments protect against the development of asthma and wheeze in children. *Journal of Allergy and Clinical Immunology*. 2007;**119**(5):1140–1147. doi:10.1016/j.jaci.2007.01.037
- [77] Ege MJ, Strachan DP, Cookson WOCM, Moffatt MF, Gut I, Lathrop M, Kabesch M, Genuneit J, Büchele G, Sozanska B, et al. Gene-environment interaction for childhood asthma and exposure to farming in Central Europe. *Journal of Allergy and Clinical Immunology*. 2011;**127**(1). doi:10.1016/j.jaci.2010.09.041
- [78] Hill DA, Siracusa MC, Abt MC, Kim BS, Kobuley D, Kubo M, Kambayashi T, Larosa DF, Renner ED, Orange JS, et al. Commensal bacteria-derived signals regulate basophil hematopoiesis and allergic inflammation. *Nature Medicine*. 2012;**18**(4):538–546. doi:10.1038/nm.2657
- [79] McCoy KD, Harris NL, Diener P, Hatak S, Odermatt B, Hangartner L, Senn BM, Marsland BJ, Geuking MB, Hengartner H, et al. Natural IgE production in the absence of MHC class II cognate help. *Immunity*. 2006;**24**(3):329–339. doi:10.1016/j.immuni.2006.01.013
- [80] Herbst T, Sichelstiel A, Schär C, Yadava K, Bürki K, Cahenzli J, McCoy K, Marsland BJ, Harris NL. Dysregulation of allergic airway inflammation in the absence of microbial colonization. *American Journal of Respiratory and Critical Care Medicine*. 2011;**184**(2):198–205. doi:10.1164/rccm.201010-1574OC
- [81] Cahenzli J, Köller Y, Wyss M, Geuking MB, McCoy KD. Intestinal microbial diversity during early-life colonization shapes long-term IgE levels. *Cell Host and Microbe*. 2013;**14**(5):559–570. doi:10.1016/j.chom.2013.10.004
- [82] Hong S-W, O E, Lee JY, Lee M, Han D, Ko H-J, Sprent J, Surh CD, Kim KS. Food antigens drive spontaneous IgE elevation in the absence of commensal microbiota. *Science Advances*. 2019;**5**:eaaw1507. doi:10.1126/sciadv.aaw1507

VI. References

- [83] Abdel-Gadir A, Stephen-Victor E, Gerber GK, Noval Rivas M, Wang S, Harb H, Wang L, Li N, Crestani E, Spielman S, et al. Microbiota therapy acts via a regulatory T cell MyD88/ROR γ t pathway to suppress food allergy. *Nature Medicine*. 2019;**25**(7):1164–1174. doi:10.1038/s41591-019-0461-z
- [84] Feehley T, Plunkett CH, Bao R, Choi Hong SM, Culleen E, Belda-Ferre P, Campbell E, Aitoro R, Nocerino R, Paparo L, et al. Healthy infants harbor intestinal bacteria that protect against food allergy. *Nature Medicine*. 2019;**25**(3):448–453. doi:10.1038/s41591-018-0324-z
- [85] Geva-Zatorsky N, Sefik E, Kua L, Pasman L, Tan TG, Ortiz-Lopez A, Yanortsang TB, Yang L, Jupp R, Mathis D, et al. Mining the Human Gut Microbiota for Immunomodulatory Organisms. *Cell*. 2017;**168**(5):928–943. doi:10.1016/j.cell.2017.01.022
- [86] Stefka AT, Feehley T, Tripathi P, Qiu J, McCoy K, Mazmanian SK, Tjota MY, Seo G-Y, Cao S, Theriault BR, et al. Commensal bacteria protect against food allergen sensitization. *Proceedings of the National Academy of Sciences*. 2014;**111**(36):13145–13150. doi:10.1073/pnas.1412008111
- [87] Ohnmacht C. Tolerance to the Intestinal Microbiota Mediated by ROR(γ t) + Cells. *Trends in Immunology*. 2016;**37**(7):477–486. doi:10.1016/j.it.2016.05.002
- [88] Mathias CB, Hobson SA, Garcia-Lloret M, Lawson G, Poddighe D, Freyschmidt EJ, Xing W, Gurish MF, Chatila TA, Oettgen HC. IgE-mediated systemic anaphylaxis and impaired tolerance to food antigens in mice with enhanced IL-4 receptor signaling. *Journal of Allergy and Clinical Immunology*. 2011;**127**(3):795-805.e6. doi:10.1016/j.jaci.2010.11.009
- [89] Noval Rivas M, Burton OT, Wise P, Zhang Y, Hobson SA, Garcia Lloret M, Chehoud C, Kuczynski J, DeSantis T, Warrington J, et al. A microbiota signature associated with experimental food allergy promotes allergic sensitization and anaphylaxis. *Journal of Allergy and Clinical Immunology*. 2013;**131**(1):201–212. doi:10.1016/j.jaci.2012.10.026
- [90] Noval Rivas M, Burton OT, Wise P, Charbonnier LM, Georgiev P, Oettgen HC, Rachid R, Chatila TA. Regulatory T cell reprogramming toward a Th2-Cell-like lineage impairs oral tolerance and promotes food allergy. *Immunity*. 2015;**42**(3):512–523. doi:10.1016/j.immuni.2015.02.004
- [91] Wohlfert EA, Grainger JR, Bouladoux N, Konkel JE, Oldenhove G, Ribeiro CH, Hall JA, Yagi R, Naik S, Bhairavabhotla R, et al. GATA3 controls Foxp3 + regulatory T cell fate during inflammation in mice. *Journal of Clinical Investigation*. 2011;**121**(11):4503–4515. doi:10.1172/JCI57456
- [92] Platts-Mills TA, Hilger C, Jappe U, van Hage M, Gadermaier G, Spillner E, Lidholm J, Keshavarz B, Aalberse RC, van Ree R, et al. Carbohydrate epitopes currently recognized as targets for IgE antibodies. *Allergy*. 2021;**76**(8):2383–2394. doi:10.1111/all.14802
- [93] Galili U, Shohet SB, Kobrin E, Stults CL, Macher BA. Man, apes, and Old World monkeys differ from other mammals in the expression of alpha-galactosyl epitopes on nucleated cells. *The Journal of biological chemistry*. 1988;**263**(33):17755–17762. doi:10.1016/s0021-9258(19)77900-9

VI. References

- [94] Commins SP, James HR, Kelly LA, Pochan SL, Workman LJ, Perzanowski MS, Kocan KM, Fahy J V., Nganga LW, Ronmark E, et al. The relevance of tick bites to the production of IgE antibodies to the mammalian oligosaccharide galactose- α -1,3-galactose. *Journal of Allergy and Clinical Immunology*. 2011;**127**(5):1286–1293. doi:10.1016/j.jaci.2011.02.019
- [95] Fischer J, Eberlein B, Hilger C, Eyer F, Eyerich S, Ollert M, Biedermann T. Alpha-gal is a possible target of IgE-mediated reactivity to antivenom. *Allergy*. 2017;**72**(5):764–771. doi:10.1111/all.13073
- [96] Commins SP, Platts-Mills TAE. Anaphylaxis syndromes related to a new mammalian cross-reactive carbohydrate determinant. *Journal of Allergy and Clinical Immunology*. 2009;**124**(4):652–657. doi:https://doi.org/10.1016/j.jaci.2009.08.026
- [97] Mullins RJ, James H, Platts-Mills TAE, Commins S. Relationship between red meat allergy and sensitization to gelatin and galactose- α -1,3-galactose. *Journal of Allergy and Clinical Immunology*. 2012;**129**(5):1334-1342.e1. doi:10.1016/j.jaci.2012.02.038
- [98] Caponetto P, Fischer J, Biedermann T. Gelatin-containing sweets can elicit anaphylaxis in a patient with sensitization to galactose- α -1,3-galactose. *The Journal of Allergy and Clinical Immunology: In Practice*. 2013;**1**(3):302–303. doi:10.1016/j.jaip.2013.01.007
- [99] Fischer J, Hebsaker J, Caponetto P, Platts-Mills TAE, Biedermann T. Galactose-alpha-1,3-galactose sensitization is a prerequisite for pork-kidney allergy and cofactor-related mammalian meat anaphylaxis. *Journal of Allergy and Clinical Immunology*. 2014;**134**(3):755–759. doi:10.1016/j.jaci.2014.05.051
- [100] Hilger C, Fischer J, Wölbing F, Biedermann T. Role and Mechanism of Galactose-Alpha-1,3-Galactose in the Elicitation of Delayed Anaphylactic Reactions to Red Meat. *Current Allergy and Asthma Reports*. 2019;**19**(1):1–11. doi:10.1007/s11882-019-0835-9
- [101] Chung CH, Mirakhur B, Chan E, Le Q-T, Berlin J, Morse M, Murphy BA, Satinover SM, Hosen J, Mauro D, et al. Cetuximab-Induced Anaphylaxis and IgE Specific for Galactose- α -1,3-Galactose. *New England Journal of Medicine*. 2008;**358**(11):1109–1117. doi:10.1056/NEJMoa074943
- [102] Galili U, Rachmilewitz EA, Peleg A, Flechner I. A unique natural human IgG antibody with anti-alpha-galactosyl specificity. *Journal of Experimental Medicine*. 1984;**160**(5):1519–1531. doi:10.1084/jem.160.5.1519
- [103] Bernth-Jensen JM, Møller BK, Jensenius JC, Thiel S. Biological variation of anti- α Gal-antibodies studied by a novel Time-Resolved ImmunoFluorometric Assay. *Journal of Immunological Methods*. 2011;**373**(1–2):26–35. doi:10.1016/j.jim.2011.07.017
- [104] Galili U, Mandrell RE, Hamadeh RM, Shohet SB, Griffiss JM. Interaction between human natural anti-alpha-galactosyl immunoglobulin G and bacteria of the human flora. *Infection and Immunity*. 1988;**56**(7):1730–1737. doi:10.1128/iai.56.7.1730-1737.1988
- [105] Bernth Jensen JM, Petersen MS, Ellerman-Eriksen S, Møller BK, Jensenius JC, Sørensen UBS, Thiel S. Abundant human anti-Gal α 3Gal antibodies display broad pathogen reactivity. *Scientific Reports*. 2020;**10**(1):4611. doi:10.1038/s41598-020-61632-9
- [106] Yilmaz B, Portugal S, Tran TM, Gozzelino R, Ramos S, Gomes J, Regalado A, Cowan PJ, D'Apice AJF, Chong AS, et al. Gut microbiota elicits a protective immune response against malaria

VI. References

- transmission. *Cell*. 2014;**159**(6):1277–1289. doi:10.1016/j.cell.2014.10.053
- [107] Singh S, Bastos-Amador P, Thompson JA, Truglio M, Yilmaz B, Cardoso S, Sobral D, Soares MP. Glycan-based shaping of the microbiota during primate evolution. *eLife*. 2021;**10**:e67450. doi:10.7554/eLife.67450
- [108] Montassier E, Al-Ghalith GA, Mathé C, Le Bastard Q, Douillard V, Garnier A, Guimon R, Raimondeau B, Touchefeu Y, Duchalais E, et al. Distribution of Bacterial α 1,3-Galactosyltransferase Genes in the Human Gut Microbiome. *Frontiers in Immunology*. 2020;**10**:3000. doi:10.3389/fimmu.2019.03000
- [109] Thall AD, Malý P, Lowe JB. Oocyte Gal α 1,3Gal Epitopes Implicated in Sperm Adhesion to the Zona Pellucida Glycoprotein ZP3 Are Not Required for Fertilization in the Mouse. *Journal of Biological Chemistry*. 1995;**270**(37):21437–21440. doi:10.1074/jbc.270.37.21437
- [110] Orcutt RP, Gianni FJ, Judge RJ. Development of an “altered Schaedler flora” for NCI gnotobiotic rodents. *Microecology and Therapy*. 1987;**17**:59.
- [111] Brugiroux S, Beutler M, Pfann C, Garzetti D, Ruscheweyh H-J, Ring D, Diehl M, Herp S, Lötscher Y, Hussain S, et al. Genome-guided design of a defined mouse microbiota that confers colonization resistance against *Salmonella enterica* serovar Typhimurium. *Nature Microbiology*. 2017;**2**:16215. doi:10.1038/nmicrobiol.2016.215
- [112] Garzetti D, Brugiroux S, Bunk B, Pukall R, McCoy KD, Macpherson AJ, Stecher B. High-quality whole-genome sequences of the Oligo-Mouse-Microbiota bacterial community. *Genome Announcements*. 2017;**5**(42):9–10. doi:10.1128/genomeA.00758-17
- [113] Fischer K, Kraner-Scheiber S, Petersen B, Rieblinger B, Buermann A, Flisikowska T, Flisikowski K, Christan S, Edlinger M, Baars W, et al. Efficient production of multi-modified pigs for xenotransplantation by ‘combineering’, gene stacking and gene editing. *Scientific Reports*. 2016;**6**:29081. doi:10.1038/srep29081
- [114] Chakrapani N, Fischer J, Swiontek K, Codreanu-Morel F, Hannachi F, Morisset M, Mugemana C, Bulaev D, Blank S, Bindslev-Jensen C, et al. α -Gal present on both glycolipids and glycoproteins contributes to immune response in meat-allergic patients. *Journal of Allergy and Clinical Immunology*. 2022;**150**(2):396-405.e11. doi:10.1016/j.jaci.2022.02.030
- [115] Galili U, Wigglesworth K, Abdel-Motal UM. Intratumoral Injection of α -gal Glycolipids Induces Xenograft-Like Destruction and Conversion of Lesions into Endogenous Vaccines. *The Journal of Immunology*. 2007;**178**(7):4676–4687. doi:10.4049/jimmunol.178.7.4676
- [116] Abdel-Motal UM, Wigglesworth K, Galili U. Intratumoral injection of α -gal glycolipids induces a protective anti-tumor T cell response which overcomes Treg activity. *Cancer Immunology, Immunotherapy*. 2009;**58**(10):1545–1556. doi:10.1007/s00262-009-0662-2
- [117] Mehlich J, Fischer J, Hilger C, Swiontek K, Morisset M, Codreanu-Morel F, Schiener M, Blank S, Ollert M, Darsow U, et al. The basophil activation test differentiates between patients with alpha-gal syndrome and asymptomatic alpha-gal sensitization. *Journal of Allergy and Clinical Immunology*. 2019;**143**(1):182–189. doi:10.1016/j.jaci.2018.06.049

VI. References

- [118] Desai MS, Seekatz AM, Koropatkin NM, Kamada N, Hickey CA, Wolter M, Pudlo NA, Kitamoto S, Terrapon N, Muller A, et al. A Dietary Fiber-Deprived Gut Microbiota Degrades the Colonic Mucus Barrier and Enhances Pathogen Susceptibility. *Cell*. 2016;**167**(5):1339-1353.e21. doi:10.1016/j.cell.2016.10.043
- [119] Köhler G, Milstein C. Continuous cultures of fused cells secreting antibody of predefined specificity. *Nature*. 1975;**256**(5517):495-497. doi:10.1038/256495a0
- [120] Jackson MA, Pearson C, Ilott NE, Huus KE, Hegazy AN, Webber J, Finlay BB, Macpherson AJ, Powrie F, Lam LH. Accurate identification and quantification of commensal microbiota bound by host immunoglobulins. *Microbiome*. 2021;**9**:33. doi:10.1186/s40168-020-00992-w
- [121] Chambers MC, Maclean B, Burke R, Amodei D, Ruderman DL, Neumann S, Gatto L, Fischer B, Pratt B, Egertson J, et al. A cross-platform toolkit for mass spectrometry and proteomics. *Nature Biotechnology*. 2012;**30**(10):918-920. doi:10.1038/nbt.2377
- [122] Benton HP, Want EJ, Ebbels TMD. Correction of mass calibration gaps in liquid chromatography-mass spectrometry metabolomics data. *Bioinformatics*. 2010;**26**(19):2488-2489. doi:10.1093/bioinformatics/btq441
- [123] Smith CA, Want EJ, O'Maille G, Abagyan R, Siuzdak G. XCMS: Processing Mass Spectrometry Data for Metabolite Profiling Using Nonlinear Peak Alignment, Matching, and Identification. *Analytical Chemistry*. 2006;**78**(3):779-787. doi:10.1021/ac051437y
- [124] Tautenhahn R, Böttcher C, Neumann S. Highly sensitive feature detection for high resolution LC/MS. *BMC Bioinformatics*. 2008;**9**:504. doi:10.1186/1471-2105-9-504
- [125] Wahlström A, Sayin SI, Marschall HU, Bäckhed F. Intestinal Crosstalk between Bile Acids and Microbiota and Its Impact on Host Metabolism. *Cell Metabolism*. 2016;**24**(1):41-50. doi:10.1016/j.cmet.2016.05.005
- [126] Basic M, Bleich A. Gnotobiotics: Past, present and future. *Laboratory Animals*. 2019;**53**(3):232-243. doi:10.1177/0023677219836715
- [127] Ivanov II, Atarashi K, Manel N, Brodie EL, Shima T, Karaoz U, Wei D, Goldfarb KC, Santee CA, Lynch S V., et al. Induction of Intestinal Th17 Cells by Segmented Filamentous Bacteria. *Cell*. 2009;**139**(3):485-498. doi:10.1016/j.cell.2009.09.033
- [128] Panduro M, Benoist C, Mathis D. Tissue Tregs. *Annual Review of Immunology*. 2016;**34**(1):609-633. doi:10.1146/annurev-immunol-032712-095948
- [129] De Aguiar Vallim TQ, Tarling EJ, Edwards PA. Pleiotropic roles of bile acids in metabolism. *Cell Metabolism*. 2013;**17**(5):657-669. doi:10.1016/j.cmet.2013.03.013
- [130] Mañez R, Blanco FJ, Díaz I, Centeno A, Lopez-Pelaez E, Hermida M, Davies HFS, Katopodis A. Removal of bowel aerobic gram-negative bacteria is more effective than immunosuppression with cyclophosphamide and steroids to decrease natural α -Galactosyl IgG antibodies. *Xenotransplantation*. 2001;**8**(1):15-23. doi:10.1034/j.1399-3089.2001.00082.x
- [131] Posekany KJ, Pittman HK, Bradfield JF, Haisch CE, Verbanac KM. Induction of cytolytic anti-Gal antibodies in α -1,3-galactosyltransferase gene knockout mice by oral inoculation with *Escherichia coli* O86:B7 bacteria. *Infection and Immunity*. 2002;**70**(11):6215-6222. doi:10.1128/IAI.70.11.6215-6222.2002

VI. References

- [132] Winter HC, Mostafapour K, Goldstein IJ. The mushroom *Marasmius oreades* lectin is a blood group type B agglutinin that recognizes the Gal α 1,3Gal and Gal α 1,3Gal, β 1,4GlcNAc porcine xenotransplantation epitopes with high affinity. *Journal of Biological Chemistry*. 2002;**277**(17):14996–15001. doi:10.1074/jbc.M200161200
- [133] Galili U, LaTemple DC, Radic MZ. A sensitive assay for measuring alpha-Gal epitope expression on cells by a monoclonal anti-Gal antibody. *Transplantation*. 1998;**65**(8):1129–1132. doi:10.1097/00007890-199804270-00020
- [134] Cunningham S, Starr E, Shaw I, Glavin J, Kane M, Joshi L. Development of a convenient competitive ELISA for the detection of the free and protein-bound nonhuman galactosyl- α -(1,3)-galactose epitope based on highly specific chicken single-chain antibody variable-region fragments. *Analytical Chemistry*. 2013;**85**(2):949–955. doi:10.1021/ac302587q
- [135] Cooper DKC, Koren E, Oriol R. Oligosaccharides and Discordant Xenotransplantation. *Immunological Reviews*. 1994;**141**(1):31–58. doi:10.1111/j.1600-065X.1994.tb00871.x
- [136] Landsteiner K, Miller CP. Serological Studies on the Blood of the Primates: III. Distribution of Serological Factors Related to Human Isoagglutinogens in the Blood of Lower Monkeys. *Journal of Experimental Medicine*. 1925;**42**(6):863–872. doi:10.1084/jem.42.6.863
- [137] Rispens T, Derksen NIL, Commins SP, Platts-Mills TA, Aalberse RC. IgE Production to α -Gal Is Accompanied by Elevated Levels of Specific IgG1 Antibodies and Low Amounts of IgE to Blood Group B Poh LNF, editor. *PLoS ONE*. 2013;**8**(2):e55566. doi:10.1371/journal.pone.0055566
- [138] Morisset M, Richard C, Astier C, Jacquenet S, Croizier A, Beaudouin E, Cordebar V, Morel-Codreanu F, Petit N, Moneret-Vautrin DA, et al. Anaphylaxis to pork kidney is related to IgE antibodies specific for galactose- α -1,3-galactose. *Allergy*. 2012;**67**(5):699–704. doi:10.1111/j.1398-9995.2012.02799.x
- [139] Hilger C, Fischer J, Swiontek K, Hentges F, Lehnert C, Eberlein B, Morisset M, Biedermann T, Ollert M. Two galactose- α -1,3-galactose carrying peptidases from pork kidney mediate anaphylactogenic responses in delayed meat allergy. *Allergy*. 2016;**71**(5):711–719. doi:10.1111/all.12835
- [140] Luo Y, Wen J, Luo C, Cummings RD, Cooper DKC. Pig xenogeneic antigen modification with green coffee bean α -galactosidase. *Xenotransplantation*. 1999;**6**(4):238–248. doi:10.1034/j.1399-3089.1999.00035.x
- [141] Gonzalez-Quintela A, Dam Laursen AS, Vidal C, Skaaby T, Gude F, Linneberg A. IgE antibodies to alpha-gal in the general adult population: relationship with tick bites, atopy, and cat ownership. *Clinical & Experimental Allergy*. 2014;**44**(8):1061–1068. doi:10.1111/cea.12326
- [142] Woodward MP, Young WW, Bloodgood RA. Detection of monoclonal antibodies specific for carbohydrate epitopes using periodate oxidation. *Journal of Immunological Methods*. 1985;**78**(1):143–153. doi:10.1016/0022-1759(85)90337-0
- [143] Leyeden JJ, Marples RR, Kligman AM. Staphylococcus aureus in the lesions of atopic dermatitis. *British Journal of Dermatology*. 1974;**90**(5):525–525. doi:10.1111/j.1365-2133.1974.tb06447.x

VI. References

- [144] Singh S, Thompson JA, Yilmaz B, Li H, Weis S, Sobral D, Truglio M, Aires da Silva F, Aguiar S, Carlos AR, et al. Loss of α -gal during primate evolution enhanced antibody-effector function and resistance to bacterial sepsis. *Cell Host and Microbe*. 2021;**29**(3):347-361.e12. doi:10.1016/j.chom.2020.12.017
- [145] Cabezas-Cruz A, Mateos-Hernández L, Alberdi P, Villar M, Riveau G, Hermann E, Schacht A-M, Khalife J, Correia-Neves M, Gortazar C, et al. Effect of blood type on anti- α -Gal immunity and the incidence of infectious diseases. *Experimental & Molecular Medicine*. 2017;**49**(3):e301. doi:10.1038/emm.2016.164
- [146] Wyss M, Brown K, Thomson CA, Koegler M, Terra F, Fan V, Ronchi F, Bihan D, Lewis I, Geuking MB, et al. Using Precisely Defined in vivo Microbiotas to Understand Microbial Regulation of IgE. *Frontiers in Immunology*. 2020;**10**:3107. doi:10.3389/fimmu.2019.03107
- [147] Al Nabhani Z, Dulauroy S, Marques R, Cousu C, Al Bounny S, Déjardin F, Sparwasser T, Bérard M, Cerf-Bensussan N, Eberl G. A Weaning Reaction to Microbiota Is Required for Resistance to Immunopathologies in the Adult. *Immunity*. 2019;**50**(5):1276-1288.e5. doi:10.1016/j.immuni.2019.02.014
- [148] Ramanan D, Sefik E, Galván-Peña S, Wu M, Yang L, Yang Z, Kostic A, Golovkina T V., Kasper DL, Mathis D, et al. An Immunologic Mode of Multigenerational Transmission Governs a Gut Treg Setpoint. *Cell*. 2020;**181**(6):1–15. doi:10.1016/j.cell.2020.04.030
- [149] Noval Rivas M, Burton OT, Oettgen HC, Chatila T. IL-4 production by group 2 innate lymphoid cells promotes food allergy by blocking regulatory T-cell function. *Journal of Allergy and Clinical Immunology*. 2016;**138**(3):801-811.e9. doi:10.1016/j.jaci.2016.02.030
- [150] Mayer JU, Demiri M, Agace WW, MacDonald AS, Svensson-Frej M, Milling SW. Different populations of CD11b+ dendritic cells drive Th2 responses in the small intestine and colon. *Nature communications*. 2017;**8**(1):15820. doi:10.1038/ncomms15820
- [151] Ridlon JM, Kang D-J, Hylemon PB. Bile salt biotransformations by human intestinal bacteria. *Journal of Lipid Research*. 2006;**47**(2):241–259. doi:10.1194/jlr.R500013-JLR200
- [152] Sayin SI, Wahlström A, Felin J, Jäntti S, Marschall HU, Bamberg K, Angelin B, Hyötyläinen T, Orešič M, Bäckhed F. Gut microbiota regulates bile acid metabolism by reducing the levels of tauro-beta-muricholic acid, a naturally occurring FXR antagonist. *Cell Metabolism*. 2013;**17**(2):225–235. doi:10.1016/j.cmet.2013.01.003
- [153] Sinha SR, Haileselassie Y, Nguyen LP, Tropini C, Wang M, Becker LS, Sim D, Jarr K, Spear ET, Singh G, et al. Dysbiosis-Induced Secondary Bile Acid Deficiency Promotes Intestinal Inflammation. *Cell Host & Microbe*. 2020;**27**(4):659-670.e5. doi:10.1016/j.chom.2020.01.021
- [154] Hylemon PB, Zhou H, Pandak WM, Ren S, Gil G, Dent P. Bile acids as regulatory molecules. *Journal of Lipid Research*. 2009;**50**(8):1509–1520. doi:10.1194/jlr.R900007-JLR200
- [155] Li W, Hang S, Fang Y, Bae S, Zhang Y, Zhang M, Wang G, McCurry MD, Bae M, Paik D, et al. A bacterial bile acid metabolite modulates Treg activity through the nuclear hormone receptor NR4A1. *Cell Host & Microbe*. 2021;**29**(9):1366-1377.e9. doi:10.1016/j.chom.2021.07.013
- [156] Furusawa Y, Obata Y, Fukuda S, Endo TA, Nakato G, Takahashi D, Nakanishi Y, Uetake C, Kato K, Kato T, et al. Commensal microbe-derived butyrate induces the differentiation of colonic regulatory T cells. *Nature*. 2013;**504**(7480):446–450. doi:10.1038/nature12721

VI. References

- [157] Schrimpe-Rutledge AC, Codreanu SG, Sherrod SD, McLean JA. Untargeted Metabolomics Strategies—Challenges and Emerging Directions. *Journal of The American Society for Mass Spectrometry*. 2016;**27**(12):1897–1905. doi:10.1007/s13361-016-1469-y
- [158] Ganeshan K, Neilsen C V., Hadsaitong A, Schleimer RP, Luo X, Bryce PJ. Impairing oral tolerance promotes allergy and anaphylaxis: A new murine food allergy model. *Journal of Allergy and Clinical Immunology*. 2009;**123**(1):231-238.e4. doi:10.1016/j.jaci.2008.10.011
- [159] Schwarzer M, Hermanova P, Srutkova D, Golias J, Hudcovic T, Zwicker C, Sinkora M, Akgün J, Wiedermann U, Tuckova L, et al. Germ-free mice exhibit mast cells with impaired functionality and gut homing and do not develop food allergy. *Frontiers in Immunology*. 2019;**10**:205. doi:10.3389/fimmu.2019.00205
- [160] Coombes JL, Siddiqui KRR, Arancibia-Cárcamo C V., Hall J, Sun CM, Belkaid Y, Powrie F. A functionally specialized population of mucosal CD103+ DCs induces Foxp3+ regulatory T cells via a TGF- β -and retinoic acid-dependent mechanism. *Journal of Experimental Medicine*. 2007;**204**(8):1757–1764. doi:10.1084/jem.20070590
- [161] Zhang X, Li L, Butcher J, Stintzi A, Figeys D. Advancing functional and translational microbiome research using meta-omics approaches. *Microbiome*. 2019;**7**:154. doi:10.1186/s40168-019-0767-6
- [162] Geva-Zatorsky N, Sefik E, Kua L, Pisman L, Tan TG, Ortiz-Lopez A, Yanortsang TB, Yang L, Jupp R, Mathis D, et al. Mining the Human Gut Microbiota for Immunomodulatory Organisms. *Cell*. 2017;**168**(5):928–943. doi:10.1016/j.cell.2017.01.022
- [163] Hamadeh RM, Jarvis GA, Galili U, Mandrell RE, Zhou P, Griffiss JM. Human natural anti-Gal IgG regulates alternative complement pathway activation on bacterial surfaces. *Journal of Clinical Investigation*. 1992;**89**(4):1223–1235. doi:10.1172/JCI115706
- [164] Guo H, Yi W, Shao J, Lu Y, Zhang W, Song J, Wang PG. Molecular analysis of the O-antigen gene cluster of Escherichia coli O86:B7 and characterization of the chain length determinant gene (wzz). *Applied and Environmental Microbiology*. 2005;**71**(12):7995–8001. doi:10.1128/AEM.71.12.7995-8001.2005
- [165] Langley DB, Schofield P, Nevoltris D, Jackson J, Jackson KJL, Peters TJ, Burk M, Matthews JM, Basten A, Goodnow CC, et al. Genetic and structural basis of the human anti- α -galactosyl antibody response. *Proceedings of the National Academy of Sciences*. 2022;**119**(28):1–11. doi:10.1073/pnas.2123212119
- [166] Plum M, Michel Y, Wallach K, Raiber T, Blank S, Bantleon FI, Diethers A, Greunke K, Braren I, Hackl T, et al. Close-up of the immunogenic α 1,3-galactose epitope as defined by a monoclonal chimeric immunoglobulin E and human serum using Saturation Transfer Difference (STD) NMR. *Journal of Biological Chemistry*. 2011;**286**(50):43103–43111. doi:10.1074/jbc.M111.291823
- [167] Chen ZC, Radic MZ, Galili U. Genes coding evolutionary novel anti-carbohydrate antibodies: Studies on anti-Gal production in α 1,3galactosyltransferase knock out mice. *Molecular Immunology*. 2000;**37**(8):455–466. doi:10.1016/S0161-5890(00)00064-X
- [168] Galili U. Biosynthesis of α -Gal Epitopes (Gal α 1-3Gal β 1-4GlcNAc-R) and Their Unique Potential in Future α -Gal Therapies. *Frontiers in Molecular Biosciences*. 2021;**8**:746883. doi:10.3389/fmolb.2021.746883

VI. References

- [169] Montoya AL, Austin VM, Portillo S, Vinales I, Ashmus RA, Estevao I, Jankuru SR, Alraey Y, Al-Salem WS, Acosta-Serrano Á, et al. Reversed Immunoglycomics Identifies α -Galactosyl-Bearing Glycotopes Specific for *Leishmania major* Infection. *JACS Au*. 2021;**1**(8):1275–1287. doi:10.1021/jacsau.1c00201
- [170] Zamze SE, Ashford DA, Wooten EW, Rademacher TW, Dwek RA. Structural characterization of the asparagine-linked oligosaccharides from *Trypanosoma brucei* type II and type III variant surface glycoproteins. *Journal of Biological Chemistry*. 1991;**266**(30):20244–20261. doi:10.1016/S0021-9258(18)54916-4
- [171] Murangi T, Prakash P, Moreira BP, Basera W, Botha M, Cunningham S, Facey-Thomas H, Halajian A, Joshi L, Ramjith J, et al. *Ascaris lumbricoides* and ticks associated with sensitization to galactose α 1,3-galactose and elicitation of the alpha-gal syndrome. *Journal of Allergy and Clinical Immunology*. 2022;**149**(2):698-707.e3. doi:10.1016/j.jaci.2021.07.018
- [172] Palinauskas V, Mateos-Hernandez L, Wu-Chuang A, de la Fuente J, Aželytė J, Obregon D, Cabezas-Cruz A. Exploring the Ecological Implications of Microbiota Diversity in Birds: Natural Barriers Against Avian Malaria. *Frontiers in Immunology*. 2022;**13**:807682. doi:10.3389/fimmu.2022.807682
- [173] Crispell G, Commins SP, Archer-Hartman SA, Choudhary S, Dharmarajan G, Azadi P, Karim S. Discovery of alpha-gal-containing antigens in North American tick species believed to induce red meat allergy. *Frontiers in Immunology*. 2019;**10**:1056. doi:10.3389/fimmu.2019.01056
- [174] Fischer J, Riel S, Fehrenbacher B, Frank A, Schaller M, Biedermann T, Hilger C, Mackenstedt U. Spatial distribution of alpha-gal in *Ixodes ricinus* – A histological study. *Ticks and Tick-borne Diseases*. 2020;**11**(5):101506. doi:10.1016/j.ttbdis.2020.101506
- [175] Leviatan S, Vogl T, Klompus S, Kalka IN, Weinberger A, Segal E. Allergenic food protein consumption is associated with systemic IgG antibody responses in non-allergic individuals. *Immunity*. 2022;**55**:1–16. doi:10.1016/j.immuni.2022.11.004
- [176] Apostolovic D, Rodrigues R, Thomas P, Starkhammar M, Hamsten C, van Hage M. Immunoprofile of α -Gal- and B-antigen-specific responses differentiates red meat-allergic patients from healthy individuals. *Allergy*. 2018;**73**(7):1525–1531. doi:10.1111/all.13400